In vivo optical Measurements for Diagnostics and Monitoring of Treatment

ISBN: 90-9020593-4
Druk: PrintPartners Ipskamp
Cover and layout: Ward Glotzbach

In vivo optical Measurements for Diagnostics and Monitoring of Treatment

In vivo optische metingen voor diagnostiek en therapie monitoring

Proefschrift

ter verkrijging van de graad van doctor aan de
Erasmus Universiteit Rotterdam
op gezag van de rector magnificus

Prof.dr. S.W.J. Lamberts

en volgens besluit van het College voor Promoties.

De openbare verdediging zal plaatsvinden op
woensdag 7 juni 2006 om 13:45 uur

door
Robertus Leonardus Petrus van Veen
Geboren te Leidschendam

Promotiecommissie:

Promotor	Prof.dr. P.C. Levendag
Overige leden	Prof.dr. B.J. Heijmen Prof.dr. A.G.J.M. van Leeuwen Dr.ir. G.J. Puppels
Co-promotor	Dr.ir. H.J.C.M. Sterenborg

The projects were supported by:
The Dutch Cancer Society (NKB) grant NKI 97-1446
The European Commission Project LAIC (contract BMM4-CT-7-2030 1996)
The European Union Project Optimamm (contract QLG1-CT-2000-00690).
The European Union Network of excellence Medphot (Contract QLG1-2000-01464)
The Dutch Technology Foundation (STW), grant RNN 5316
The Dutch Technology Foundation (STW), grant RPG 6496

This thesis was financially supported by:
Biolitec AG, Jena, Germany and **OceanOptics,** Duiven,The Netherlands
Paranimfen: Fabio Bruna, Maurice Aalders

Contents

1.

General introduction and aim of the study

Introduction

The interaction of light with tissue and its use for medical purposes has been under investigation for centuries. Since the early nineteen sixties, the development of novel optical technology and advances in laser design/technology allowed a wide range of innovative applications in many fields of medicine. For the majority of light applications in medicine the distribution of light within tissue is of fundamental importance. The light distribution is determined by the optical properties of the tissue; scattering and absorption. This thesis focuses on two applications of light in medicine, photodynamic therapy (PDT) and optical diagnostics. For each application the effect of differences in and changes of tissue optical properties are investigated. The distribution of light within tissue is of vital importance in PDT and is strongly dependent on the *in vivo* optical properties. *In vivo* differences and variations in optical properties are also critically important for optical diagnostics. The hypothesis presented is that the underlying cause of the current limitations in clinical PDT and low sensitivity in optical diagnosis are due to the heterogeneous and dynamic nature of tissue optical properties. This thesis tests this hypothesis by investigating the spatial distribution, inter patient differences, and temporal behaviour of *in vivo* optical properties by means of *in vivo* light measurement.

Tissue Optical Properties

In tissue, light undergoes numerous scattering and absorption events. The relative magnitude of each of these processes determines the "optical properties" of the tissue. The distribution of light in tissue depends on the spatial distribution of these properties. These properties are of vital importance for PDT for they determine where and how much absorption occurs. The light that is not absorbed by the tissue chromophores will be diffusely re-emitted (reflectance) from the tissue surface, which in turn can be used for diagnostic proposes.

The scattering coefficient μ_s (m^{-1}) is defined as effective scattering cross section of the scattering particle times the volume density of the scattering constituents. The inverse is the mean free path length for a scattering event, whereas the absorption coefficient μ_a (m^{-1}) is defined as effective cross section of the absorbing particle times the concentration density of the absorbing constituents. The inverse is the mean free path length for an absorption event.

Absorption

The absorption of light in tissue, whether by endogenous chromophores or exogenous agents, can be used for spectroscopic analysis, imaging and has important implications for therapeutic applications such as PDT. In the visible and NIR wavelength region, water, lipid, oxy- and deoxy- hemoglobin are the predominant endogenous absorbers in tissue. Figure 1 shows the absorption spectra of water and lipids. In most soft tissue types an abundance of water is present, i.e. 70% or more. Water becomes a dominant absorber

above ~λ=900 nm with a peak around 980nm. Lipids on the other hand are dominantly present in adipose tissue. As seen in figure 1, lipid has a strong absorption band around 928nm. *In vivo* adipose tissue appears as yellowish; this is due to the presence of dissolved β-carotene in the lipids. Similar to water, lipid absorption in the visible region of the spectrum is negligible. In the visible and UV region, haemoglobin becomes the dominant absorber.

Haemoglobin (Hb), is the iron-containing oxygen-transport metallo-protein in the red blood cells. The molecule consists of globin, the apoprotein, and four heam groups, which are organic molecules with an iron atom in each. The iron molecule is located at the centre of each heam group, which is capable of binding oxygen. Oxygen bound to a haemoglobin molecule is referred to as oxy-haemoglobin or $Hb0_2$. When no oxygen molecules are bound to the haemoglobin molecule it is referred to as deoxy-haemoglobin or Hb.
Both spectra are depicted in figure 2. Haemoglobin has a strong absorption band in the UV at around 420nm, and 550 nm. The absorption spectra of oxy and deoxy-heamoglobin are clearly different over a wide range of the spectrum, this allows for the measurement of oxygenation.

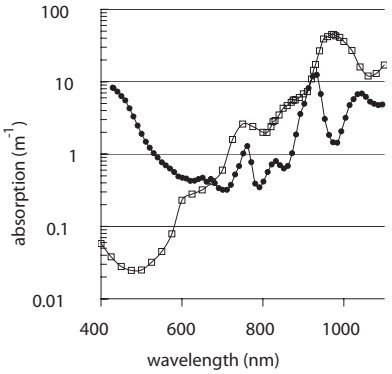

Figure 1 Absorption of pure water (□),and of mineral oil (•).

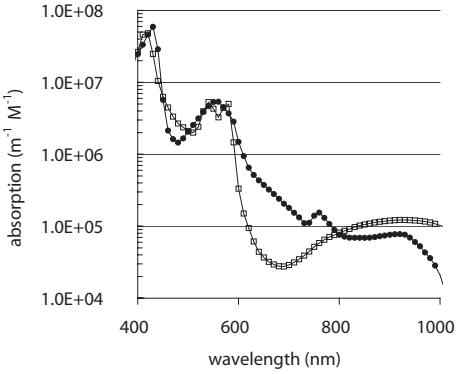

Figure 2 Absorption of Oxy-haemoglobin (□), and DeOxy-haemoglobin (•) from van Zijlstra et al[1].

The wavelength dependent absorption spectra of *in vivo* tissue is assumed to be the summation of the relative contribution to the total absorption of all chromophores present in the tissue, according to equation 1.

$$\mu_a(\lambda) = \sum_i c_i \cdot \varepsilon_i(\lambda) \qquad \text{Eq. 1}$$

Where c_i is the concentration, and ε_i the specific absorption coefficient of chromophore *i*. Therefore fitting the chromophore concentrations with the known specific absorption spectra yields absolute concentration quantities of the tissue constituents. Furthermore, the tissue oxygenation can be derived from the oxy- and deoxy-hemoglobin concentrations.

In PDT an exogenous absorbing agent i.e. photosensitiser is administered to the patient. The photosensitive molecules then accumulate in the tissue, after a certain time interval light with a wavelength that corresponds to an absorption band of the sensitiser is applied to the tumour tissue. This will induce the therapeutic effect. The tumour response depends on the total amount of light available for absorption, which depends on the optical properties of the tissue. Figure 3 shows an example of an absorption spectrum of a photosensitiser.

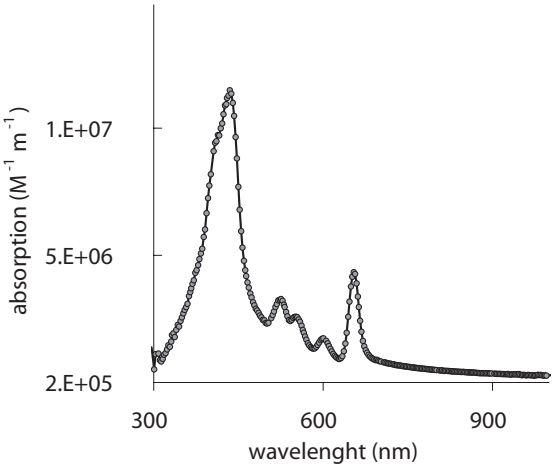

Figure 3. Absorption spectrum of the photosensitizer mTHPC (Foscan®)

Scattering

Most of the photons in tissue experience multiple scattering events, before they are absorbed, and have mean free paths in the range of ~50 up to 2000 micrometers. The highly scattering nature of tissue means that a relatively large portion of photons will be re-emitted from the surface of illuminated tissue. The re-emitted light has travelled a considerable distance through the tissue passing through various structures and contains spectral information on the tissue constituents that can be used for diagnostic purpose. The wavelength dependent scattering properties also determine the way that light is distributed in tissue, which is of great importance for PDT.

Scattering of light in tissue originates from the interaction of light with variations in the refractive index or small particles in the tissue, thus resulting in a refraction of the light in all directions. Tissue scattering structures extend from the cell membranes and membrane aggregates to collagen fibres to nuclei to cells.

After a scattering event a photon is redirected over a certain azimuthal (isotropically) and deflection angle to a different direction according to probability distribution function. The mean value of the cosine of this scattering angle is defined by the anisotropy factor g. Experimental work[2] has shown, that in tissue this factor varies between 0.7 and 0.99 illustrating the strongly forward directed nature of light scattering in tissue.

The reduced scattering coefficient μ_s' (m^{-1}) is commonly used for practical reasons. The reduced scattering coefficient combines the scattering coefficient with anisotropy factor g according to equation 2, and can be used in optical applications where multiple scattering occurs i.e. large detection volumes.

$$\mu_s' = (1-g)\cdot\mu_s \qquad \text{Eq. 2}$$

It has been experimentally demonstrated that scattering of light by structures on the same size scale as the photon wavelength can be approximated by Mie scattering according to equation 3. Figure 4 shows an example of the reduced scattering coefficient as function of wavelength.

$$\mu_s' = a\cdot\lambda^{-b} \qquad \text{Eq. 3}$$

Where a is measure for the amount of scatter locations, and b is a measure for the scatter size [3,4].

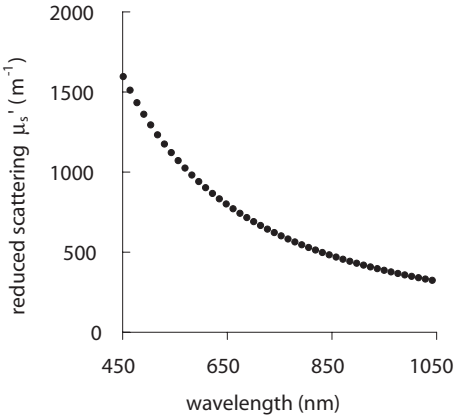

Figure 4. Reduced scattering as function of wavelength according to Eq. 3 of human breast skin.

Light Transport

In the last two decades, several analytical models capable of simulating light propagation through scattering media such as tissue have been developed. These analytical models require a priori knowledge on the absorbing and scattering properties and allow for the calculation of the light distribution in tissue. The measurement of light within or at the tissue surface can also be used to determine tissue optical properties. In this "inverse problem", the measured light from the tissue is used to deduce the optical properties from the tissue by fitting the analytical propagation model to the experimental data.

The light distribution in tissue is commonly expressed as the radiant energy fluence rate ψ in [W cm^{-2}]. The fluence rate $\psi(\mathbf{r})$ at position $\mathbf{r}$ is defined as equal to the integral of the radiance $\mathbf{L}(\mathbf{r},\mathbf{s})$ over all directions in space (4π sterradians) given by the unit vector $\mathbf{s}$.

$$\psi(r) = \int_{4\pi} L(r,s)\, d\Omega \qquad \text{Eq. 4}$$

The amount of photon energy absorbed per second at position $\mathbf{r}$ is given by $\mu_a(r) \bullet \psi(r)$.

Diffusion theory

Photon propagation in optically highly scattering media, such as biological tissues, can be described using the Boltzmann transport equation[5]. This equation requires the optical properties of the medium expressed in terms of the absorption coefficient μ_a, the scattering coefficient μ_s and the scattering phase function (g). A very useful approximation to this equation is called the diffusion approximation, where the scattering coefficient and the phase function are combined in one parameter according to Eq. 2.

The diffusion approximation to the transport equation with extrapolated boundary conditions has been adapted for spatial, time and frequency resolved reflectance or transmittance measurements[6-7] and improved by Kienle and Patterson[8]. Several authors have tested both solutions with tissue phantom experiments[9-10] and have obtained good results. Equation 5 describes the spatially resolved steady state diffuse reflectance[6] as function of μ_a, μ_s' and radial distance r. The approach of the extrapolated boundary conditions and virtual source is illustrated in figure 5. An example of a reflectance measurement on skin is depicted in figure 6.

$$R(r,\mu_a,\mu`_s) = \frac{1}{4\pi}\left[z_0 \left(\mu_{eff} + \frac{1}{r_1}\right)\frac{e^{-\mu_{eff} r_1}}{r_1^2} + (z_0 + 2AD)\left(\mu_{eff} + \frac{1}{r_2}\right)\frac{e^{-\mu_{eff} r_2}}{r_2^2}\right] \qquad \text{Eq. 5}$$

Where D is the diffusion constant $D=[3\{\mu_a+(1-g)\mu_s\}]^{-1}$ and b is depended on the Fresnel reflection coefficient and:

$$z_0 = \frac{1}{\mu_s`} \qquad \mu_{eff} = \sqrt{\frac{\mu_a}{D}} \qquad z_b \approx b z_0$$

$$r_1 = \sqrt{(z_0)^2 + r^2}$$

$$r_2 = \sqrt{(z_0 + 2z_b)^2 + r^2}$$

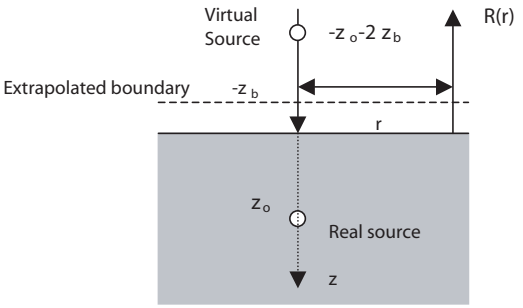

Figure 5. Schematic model of the diffusion theory for reflectance R(r) as function of radial distance r.
The model is based on an extrapolated boundary and virtual source.

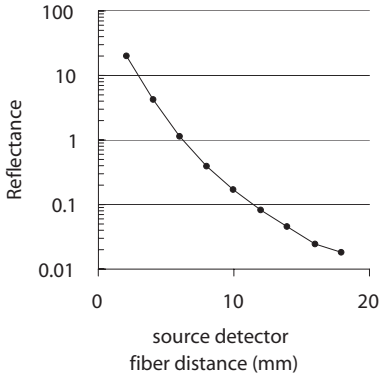

Figure 6. An example of diffuse reflectance R(r) as function of increasing distance between source and detection fibre at 800nm.

For the diffusion approximation to be valid, three important constraints are required.

- The measured light field is completely diffuse [6], this requires that the source-detector separation exceeds a distance larger than $1/\mu_s'$ e.g. > 2 mm for a μ_s'=500 m^{-1}.
- Scattering should dominate absorption[11-12], that is $\mu_a << \mu_s(1 - g)$.
- The tissue should be homogeneous and semi-infinite.

Fitting of the diffusion approximation model to the measured quantities yields the parameters μ_a, μ_s', at a chosen measurement wavelength at a given distance from the source.

Applications

As described earlier this thesis focuses on two applications of light measurement in medicine. The therapeutic application, photodynamic therapy is an emerging treatment modality for a range of primarily malignant conditions. The importance of light measurement and tissue optical properties in PDT is investigated. The measurement of the therapeutic light during treatment provides an insight into the spatial and dynamic behaviour of the tissue optical properties. The influence of spatial variations in optical properties due to tissue heterogeneity is investigated for the application of optical diagnostics. The re-emitted light from tissue contains spectral information on the tissue scattering and absorbing constituents. Two methods that employ the use of diffuse remitted light i.e. diffuse reflectance and differential path length spectroscopy, are used to investigate the *in vivo* spatial distribution of optical properties.

Photodynamic Therapy and Light Dosimetry

Photodynamic therapy (PDT) is an emerging treatment modality for the treatment of primarily malignant conditions[13-14]. In PDT an exogenous agent, the photosensitiser or its pre-cursor is administrated to the patient. After a certain time interval, the tumour site is illuminated superficially or interstitially with light of a specific wavelength that

corresponds to one of the absorption bands of the photosensitiser. A photochemical reaction is induced that leads to the destruction of the target tissue. The photosensitiser absorbs light and is excited from its ground singlet state to an excited singlet state. Through an intermediate triplet state, energy is transferred to molecular oxygen within tissue leading to the production of highly reactive singlet oxygen. Singlet oxygen causes damage to critical cellular structures such as membranes that induce direct cell death. A second mechanism is responsible for cell death for photosensitisers that preferentially accumulate in the endothelium of blood vessels. Damage to the tissue vasculature impedes tumour oxygen supply, which results in the destruction of the tumour. The "therapeutic" effect resulting from PDT depends on a combination of many parameters, such as drug dose, drug light interval, light delivery parameters. PDT response is strongly dependent on the rate at which the therapeutic light is delivered (fluence rate) and the total light dose (fluence)[15]. Many studies have demonstrated the importance of fluence rate in the response of tissue to PDT.

The fluence rate distribution in tissue is determined by the scattering coefficient (μ_s), the absorption coefficient (μ_a) and geometric properties of the illuminated treatment field/volume. For example, tissue structures with high scattering and absorption properties will have a limited light penetration depth. The *in vivo* fluence (rate) according to Eq. 4, can be measured by means of fibre optic isotropic detectors. These miniature diffuse light detectors measure the light from all directions[16].

The effect of light scattering in hollow organs

In tissue, light is scattered many times before its absorbed by either the exogenous molecule or endogenous tissue chromophore. A large proportion of the incident light however, is diffusely re-emitted at the tissue surface, and may re-enter somewhere else in case of hollow organs like the esophagus. The total amount of re-emitted (back scattered) light depends on the tissue optical properties[17-18]. The actual fluence rate at the surface of the tissue is therefore the sum of the incident light coming directly from the source and the scattered light, and is a measure for the amount of light available for photosensitiser absorption. In this thesis the build-up in fluence rate is referred to as the fluence rate build-up factor.

In vivo light dosimetry serves as a tool for delivering light to the treatment site in an optimal homogeneous manner, especially for complicated geometries. Furthermore *in vivo* light measurements provide information on intra- and inter-patient differences as well as PDT induced changes in optical properties.

Reflectance spectroscopy

In reflectance spectroscopy white light is coupled into an optical fibre and is directed onto the tissue at the site of investigation[19]. The intensity of the re-emitted light (reflectance) can be measured as a function of distance between the source and the detection fibre. The detected light contains spectral information on the scattering and

absorbing properties of the tissue. The use of multiple detection fibres at increasing distance from the source allows for the calculation of μ_a and μ_s' as a function of wavelength by fitting the diffusion approximation (Eq. 5) to the measured spectral intensities (e.g. shown in figure 6). The method averages out the optical properties over a large volume. The sampling volume for DRS, depends on the optical properties and source/detection fibre distance (e.g. ~2 cm^3 for an inter-fibre distance of 20 mm). However, these global averages over a large volume may present a problem, since small-scale inhomogeneities in tissue optical properties will not be detected. The extent to which this is a problem for optical diagnostics using DRS is investigated in this thesis. For the measurements of small lesions a method is needed that measures over a very small volume. Reducing the source-detection fibre distance decreases the interrogation volume, but violates diffusion theory constraints. Differential Path-length Spectroscopy [20-21] (DPS) is presented as a technique that overcomes this problem. DPS employs two adjacent fibres. The DPS method uses one fibre that serves as source as well as detection fibre, whereas the other fibre only detects. Subtraction of both fibre signals rejects the diffuse light component and yields only for photons that have travelled over a very small and constant photon path-length (only a few hundred microns). The photon path-length only depends on the fibre diameter. Hence, only scattering and absorption information over a small volume of tissue is obtained.

Aim of the study

The central aim of this thesis is to investigate the influence of spatial distribution and inter patient variations *in vivo* optical properties on light distribution in tissue by means of *in vivo* light measurements and the resulting consequences for PDT and optical diagnosis. For this purpose we have developed devices for *in vivo* light measurements, and performed clinical measurements during PDT, surgery and biopsy procedures. The results may contribute to further optimise photodynamic therapy and may improve methods and analysis for optical diagnostics.

Thesis outline

The thesis is divided into two sections: Chapters 2 to 6 focus on the influence of the spatial variations and temporal behaviour of *in vivo* optical properties on the light distribution during photodynamic therapy. Whereas in Chapters 7 to 10 the main focus is the measurement of intrinsic *in vivo* optical properties.

Chapter 2. Gives the results of *in vivo* therapeutic light measurements, during Photodynamic Therapy of Barrett's oesophagus with 5-aminolevulinic Acid. The origin of intra- and inter-patient differences in measured fluence rate for a fixed light output power, are identified and discussed.

Chapter 3. Describes the development of dedicated light applicator for photodynamic therapy of nasopharyngeal carcinomas. Prior to clinical use the applicators light

distribution was first determined in air, optical phantoms and in five healthy volunteers.

Chapter 4. Describes the *in vivo* light measurements during Foscan® mediated Photodynamic Therapy of nasopharyngeal cancer using a dedicated light applicator as described in chapter 3. Intra- and inter-patient variations and time dependence of the *in vivo* measured fluence rate the consequences for PDT are analysed and discussed.

Chapter 5. Describes the development of a wedge shaped applicator for additional light delivery and dosimetry in the diaphragmal sinus during Photodynamic Therapy for malignant pleural mesothelioma. The fluence rate distribution over the surface of the applicator for various tissue optical phantoms as well as the first clinical results are presented.

Chapter 6. Addresses the consequences of inter patient variations in measured fluence rate for a fixed source output power on the clinical outcome of PDT in Barrett's oesophagus.

Chapter 7. Describes a method that corrects for the inhomogeneous distribution of blood. This correction was incorporated into the analysis in order to expand and improve the validity of diffusion approximation for DRS and DPS measurements to a lower wavelength region and was evaluated on *in vivo* measurements.

Chapter 8. The objective of this study was the determination of a reliable absorption spectrum of mammalian lipid(s) for component analysis of *in vivo* absorption spectra derived from DRS. The VIS- NIR absorption coefficients of mammalian fat were determined, using time- and spatially- resolved diffuse reflectance and transmission spectroscopy.

Chapter 9. This chapter presents the results of intra-operatively assessed optical properties using spatially resolved DRS of malignant and healthy breast tissue. The validity of optical properties derived from DRS with respect to reproducibility and accuracy are evaluated in tissue optical phantoms and volunteers.

The DRS fitting algorithm as used in chapter 6-8 showed to be sensitive to tissue inhomogeneities. To overcome the problems encountered in chapter 8, a technique that measures more locally was required. Differential Path-length Spectroscopy is a minimally invasive technique able to determine intrinsic *in vivo* optical properties.

In *chapter 10,* the results of optical biopsy assessed optical properties using DPS of malignant and healthy breast tissue are given.

References:

1. Zijlstra WG, Buursma A and van Assendelft OW. Visible and Near Infrared Absorption Spectra of Human and Animal Haemoglobin. VSP Publishing, Utrecht, 2000.

2. van Gemert MJ, Jacques SL, Sterenborg HJ and Star WM. Skin optics. *IEEE Trans Biomed Eng.* 1989 **36(12)**: 1146-54.

3. Mourant JR, Fuselier T, Boyer J, Johnson TM and Bigio IJ. Predictions and measurements of scattering and absorption over broad wavelength ranges in tissue phantoms. *Appl Opt.* 1997 **36**: 949–57.

4. Nilsson AMK, Sturesson C, Liu DL and Andersson-Engels S. Changes in spectral shape of tissue optical properties in conjunction with laser-induced thermotherapy. *Appl Opt*. 1997 **37:** 1256–67.

5. Ishimaru A. Wave Propagation and Scattering in Random Media. (New York: Academic)1978

6. Farrell TJ, Patterson MS and Wilson BC.1992 A diffusion theory model of spatially resolved, steady state diffuse reflectance for the noninvasive determination of tissue properties *in vivo. Med Phys.* 1992 **19:** 879–88.

7. Haskell RC, Svaasand LO, Tsay T, Feng T, McAdams MS and Tromberg BJ. Boundary conditions for the diffusion equation in radiative transfer. *J Opt Soc Am A.* 1994 **11**: 2727–41.

8. Kienle A and Patterson MS. Improved solutions of the steady-state and the time-resolved diffusion equationsfor reflectance from a semi-infinite turbid medium. *J Opt Soc Am* A. 1997 **14**: 246–54.

9. Mourant JR, Fuselier T, Boyer J, Johnson TM and Bigio IJ. Predictions and measurements of scattering and absorption over broad wavelength ranges in tissue phantoms. *Appl Opt*. 1997 **36**: 949–57.

10. Nichols MG, Hull EL and Foster TH Design and testing of a white-light, steady state diffuse reflectance spectrometer for determination of optical properties of highly scattering systems. *Appl Opt.* 1997 **36**: 93–104.

11. Furutsu K. Diffusion equation derived from space-time transport equation. *J Opt Soc Am*. 1980 **70**: 360–6.

12. Hielscher AH, Alcouffe RE and Barbour RL. Comparison of finite-difference transport and diffusion calculations for photon migration in homogeneous and heterogeneous tissues. *Phys Med Biol*. 1998 **43**: 1285–302.

13. Dougherty TJ and Marcus SL. Photodynamic therapy. *Eur J Cancer.* 1992 **28(10)**: 1734-42.

14. Henderson BW and Dougherty TJ. How does photodynamic therapy work? *Photochem Photobiol.* 1992 **55(1)**: 145-57.

15. Robinson DJ, de Bruijn HS, van der Veen N, Stringer MR, Brown SB and Star WM. Fluorescence photobleaching of ALA-induced protoporphyrin IX during photodynamic therapy of normal hairless mouse skin: the effect of light dose and irradiance and the resulting biological effect. *Photochem Photobiol.* 1998 **67**: 141-149.

16. Marijnissen J, and Star WM. Calibration of isotropic light dosimetry probes based on scattering bulbs in clear media. *Phys Med Biol.* 1996 **41**(7): 1191-208.

17. van Staveren HJ, Beek JF, Ramaekers JW, Keijzer M and Star WM. Integrating sphere effect in whole bladder wall photodynamic therapy: λ=532 nm versus 630 nm optical irradiation. *Phys Med Biol*. 1994 **39**(**6**): 947-59.

18. Star WM. The relationship between integrating sphere and diffusion theory calculations of fluence rate at the wall of a spherical cavity. *Phys Med Biol.*1995 **40**(**1**): 1-8.

19. Doornbos RM, Lang R, Aalders MC, Cross FW and Sterenborg HJ. The determination of in vivo human tissue optical properties and absolute chromophore concentrations using spatially resolved steady-state diffuse reflectance spectroscopy. *Phys Med Biol*. 1999 **44**(**4**): 967-81.

20. Amelink A, Bard MP, Burgers SA and Sterenborg HJ. Single-scattering spectroscopy for the endoscopic analysis of particle size in superficial layers of turbid media. *Appl Opt*. 2003 **1;42**(**19**): 4095-101

21. Amelink A and Sterenborg HJ. Measurement of the local optical properties of turbid media by differential path-length spectroscopy. *Appl Opt.* 2004 **20;43**(**15**): 3048-54.

Suggested reading:

A.J. Welch, M.J.C. van Gemert eds. Optical-thermal response of laser-irradiated tissue. New York: Plenum

This book provides a comprehensive overview on light modelling in tissue, the measurements of optical properties and light delivery systems for PDT.

2.

In situ Light Dosimetry during Photodynamic Therapy of Barrett's Esophagus with 5-Aminolevulinic Acid

Adapted from:

R.L.P. van Veen, M.C. Aalders , K.L. Pasma, P.D. Siersema, J. Haringsma, W. van De Vrie, E.E. Gabeler, D.J. Robinson, H.J. Sterenborg. In situ light dosimetry during photodynamic therapy of Barrett's esophagus with 5-aminolevulinic acid. **Lasers Surg Med. 2002: 31(5): 299-304**

Abstract

Background and Objective: Previous studies with PhotoDynamic Therapy (PDT) in bladder and bronchi have shown that due to scattering and reflection, the actually delivered fluence rate on the surface in a hollow organ can be significantly higher than expected. In this pilot study we investigated the differences between the primary calculated and the actual measured fluence rate during PDT of Barrett's Esophagus (BE) using 23 independent clinical measurements in 15 patients.

Materials and methods: A KTP-dye module laser at 630 nm was used as light source. Light delivery was performed using a cylindrical light diffuser inserted in the center of an inflatable transparent balloon with a length corresponding to the length of the Barrett's epithelium. The total light output power of the cylindrical diffuser was calibrated using an integrating sphere to deliver a primary fluence rate of 100 mW cm^{-2}. Two fiber-optic pseudo sphere isotropic detectors were placed on the balloon and were used to measure fluence rate at the surface of the esophageal wall during PDT.

Results and conclusion: The actual fluence rate measured was 1.5-3.9 times higher than the primary fluence rate for 630 nm. In general the fluence rate amplification factor decreased with increasing redness of the tissue and was less for shorter diffusers. Fluence rate variations in time were observed which coincided with patients coughing, movement and esophageal spasms. These factors combined with inter patient variability of the fluence rate measured appears to justify the routine application of this technique in PDT of BE.

Introduction

Barrett's esophagus (BE) is a premalignant condition for which superficial ablation might be used to reduce the risk of malignant degeneration. The current therapy for high-grade dysplasia is still esophagectomy but this is comprised by a short-term morbidity of 30%. PDT using 5-aminolevulinic acid (ALA) as a pro-drug for the production of PpIX acting as photosensitiser has found world wide interest as a potential tool for treating early stage BE. ALA-PDT eliminates the epithelium of BE selectively without damaging the entire wall of the esophagus due to selective localisation of PpIX in the oesophageal mucosa rather than in the underlying stroma[1-3]. PDT for the superficial ablation of Barrett's mucosa might be superior to the existing therapies due to less morbidity and mortality compared to surgery.

For PDT the time interval between photosensitiser administration and illumination-scheme is important. More recently de Bruijn *et al* [4] suggested a two-fold illumination scheme for which a dramatic increase in tumour volume doubling time was demonstrated. Furthermore, light fluence rate and the fluence (also referred to as light dose) delivered to the tissue were demonstrated to strongly influence the severity of PDT-induced tissue damage[5]. In previous oesophageal PDT studies[1,6-11] light dosimetry was defined as either an estimation of the *primary fluence rate* (based on the total output power of a cylindrical diffuser divided by the area to be treated) or merely the light output power per length of diffuser. This approach assumes a radially emitting cylindrical diffuser and does not account for tissue light back scattering and reflection. In previous experiences with PDT in bladder and bronchi[12,13] we have shown that the actually delivered fluence rate in a hollow organ can be significantly higher than the primary fluence rate, due to back-scattering of light from the tissue and reflection at the tissue surface boundaries. The tissue optical and geometrical properties are different in each patient; consequently the actual fluence rate will vary, and thus may lead to either under-treatment or over-treatment. Measuring the actual fluence rate at the oesophageal surface can be expected to improve the correlation between treatment parameters and treatment effect and may ensure a safer illumination.

To evaluate the practical necessity of *in vivo* dosimetry we developed a balloon based light delivery system with integrated light detection system and performed measurements of the actual fluence rate during PDT in the esophagus of 15 patients. The purpose of the dosimetry study was a) to investigate the difference between the actual and primary fluence rate, b) to evaluate the necessity of performing such measurements on a routine basis and c) to investigate possible differences in fluence rate during the second session resulting from PDT effects of the first session of a two-fold illumination scheme. The dosimetric study described in this paper was performed during a clinical pilot experiment investigating a double illumination scheme for PDT of BE. The treatment was still based on the estimation of the primary fluence rate, hence measuring the true fluence rate was of no consequence for the treatment.

In this paper we present the results of *in situ* light dosimetry during PDT of 15 patients resulting in 23 independent measurements. From these results we have derived fluence rate amplification factors for all illuminations. All parameters that may contribute to this factor will be discussed.

Materials and Methods

Light dosimetry

A schematic representation of the inflatable balloon light delivery/dosimetry is depicted in figure 1.

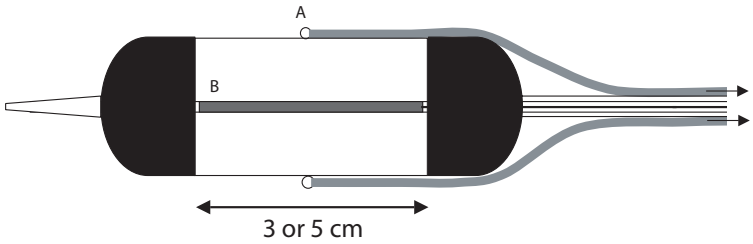

Figure 1. Light applicator with incorporated dosimetry for PDT of the barrett's esophagus consisting of an inflated windowed transparent balloon with (a) Two counter-opposite isotropic detectors taped in the middle, and (b) a channel for the cylindrical diffuser.

The aim was to deliver a primary fluence rate ($\phi_{primary}$) of 100 mW cm^{-2} to the esophageal surface based on a first order approximation of the primary fluence rate in absence of tissue according to equation (1).

$$\phi_{primary} = \frac{P_{out}}{\pi \cdot D_{ball} \cdot L_{dif}} \qquad \text{Eq. 1}$$

Where D_{ball} is the balloon diameter [cm], P_{out} the cylindrical diffuser total output power [mW], and L_{dif} length [cm] of the diffuser corresponding to the Barretts epithelium length[14]. In this approach the cylindrical diffuser is assumed to behave as a radially emitting line source with the output homogeneously distributed over the cylinder surface. Prior to BE PDT the total output power of the cylindrical diffuser was measured in an integrating sphere (Grasbery Optronics S370, Zevenaar, TeLintelo systems, The Netherlands) and was set to a value yielding a calculated fluence rate of 100 mW cm^{-2} for the 3 and 5 cm cylindrical diffusers respectively i.e. 3.9 Watts for a 5 cm diffuser in a 2.5 cm balloon diameter.

The fluence rate at the surface of the applicator was measured using a fiber (400 μm core diameter) with an outside diameter of 1 mm pseudo sphere isotropic detector at the distal end (Cardiofocus formerly known as Rare Earth Medical, West Yarmouth MA, USA), thus measuring the sum of the primary incident light from the cylindrical diffuser and the tissue remitted and reflected light. The response of the detectors was isotropic within 5%. A detailed description on isotropic detectors is given by van Staveren *et al*[15].

The isotropic probes were connected to an electronic device that enables real time fluence (rate) measurements. The electronic device was connected to a PC for storage and processing of the measured data. Calibration of the detectors was performed in a built-in integrating sphere that provides a well-defined diffuse calibration field. The dosimetry software applied a factor to correct for the difference in response of the detectors when measurements are performed at the air/tissue surface resulting from mismatch in refractive index[16]. Light delivery was performed using an inflatable transparent windowed balloon (Wizzard X-cell, Wilson-Cook Medical Inc, Winston-Salem, North Carolina, USA.)

The interior of the black non-transparent capped portions on both sides of the balloon is coated with a silver-grey reflective material[17]. Prior to PDT two probes were taped (transparent Scotch Magic tape, 3M) to the middle of the balloon opposite to each other. During PDT the two isotropic detectors recorded the fluence rate ($\phi_{1,2}$) every second at two positions at the BE surface. Balloon diameter was 2.5 cm with a transparent window length of either 3 or 5 cm. A KTP/532-dye laser module at 630 nm (Laserscope, San Jose, CA, USA) was used for light delivery. A Cylindrical diffuser (400 μm fibre core diameter) (CeramOptec, GmbH, Bonn, Germany) was aligned in the balloon prior to the procedure. The length of the balloon and cylindrical diffuser was chosen to be either 3 or 5 cm, corresponding to the estimated length of the Barrett's epithelium. This resulted in two different illumination geometries. Prior to PDT a white light endoscopic surveillance was performed and the guide-wire was positioned.The deflated balloon was positioned over the guide-wire and then inflated to a pressure of approximately 60 mmHg and its position endoscopically checked. After the guide-wire was removed the cylindrical diffuser was inserted. The output power of the cylindrical diffuser was checked prior and post PDT.

Data processing

The fluence rate was measured every second at two locations at the BE surface $\phi_1(t)$, $\phi_2(t)$. The mean of the actual measured fluence rate per illumination session was calculated according to equation (2).

$$\phi_{actual} = \frac{1}{T}\int_0^T \frac{\phi_1(t) + \phi_2(t)}{2}\, dt \qquad \text{Eq. 2}$$

Where T stands for the total illumination time in seconds. For each patient the fluence rate amplification factor F is determined which is the ratio of the actual fluence rate ϕ_{actual} and the first order approximation of the primary fluence rate in absence of tissue according to equation (3)[13].

$$F_{i,j} = \frac{\phi_{actual}}{\phi_{primary}} \qquad \text{Eq. 3}$$

For each patient (i) the fluence rate amplification factor for first and second illumination (j) were calculated. To investigate possible acute tissue response as result of the first illumination we have determined if there was a significant difference between $F_{i,1}$ and $F_{i.2}$ could be observed.

Patients

In this prospective study 15 patients with BE with estimated lengths varying from 2 to 5 cm, with low and high-grade dysplasia were randomly subdivided in various illumination schemes. After oral administration of 60 mg/kg 5-AminoLevulinic Acid (ALA) (Sigma Chemical Company, St. Louis, USA). PDT illumination schemes were: single illumination of 100 J cm^{-2} 4 hours after ALA administration, or fractionated: either 2 times 100 J cm^{-2} (4 and 5 hours after ALA administration) or 20 J cm^{-2} - 100 J cm^{-2} (1 and 4 hours after ALA administration). The patients were sedated with an intravenously injection of 5-10 mg midazolam (Dormicum, Roche Nederland B.V., Mijndrecht, the Netherlands).

Results

In Figure 2 and 3 examples of *in situ* fluence rate measurements during PDT are shown. Figure 2 illustrates the fluence rate versus treatment time of a patient receiving a two-fold illumination with a intended primary fluence of 20 and 100 J cm^{-2}, and $\phi_{primary}$ 100 mW cm^{-2} at 630 nm. The average fluence rates during the first illumination period were ϕ_1=152±7 mW cm^{-2} and ϕ_2=162±5 mW cm^{-2} and showed relatively small variations for the two detector positions 1 and 2 respectively. The average fluence rate delivered to the tissue during the second illumination period was ϕ_1=168±22 mW cm^{-2} and ϕ_2=173±25 mW cm^{-2} for the two detector positions respectively. The fluence rate amplification factors as calculated with eq. (3) were $F_{i,1}$=1.5 and $F_{i,2}$=1.7 for the first and second illumination period respectively.

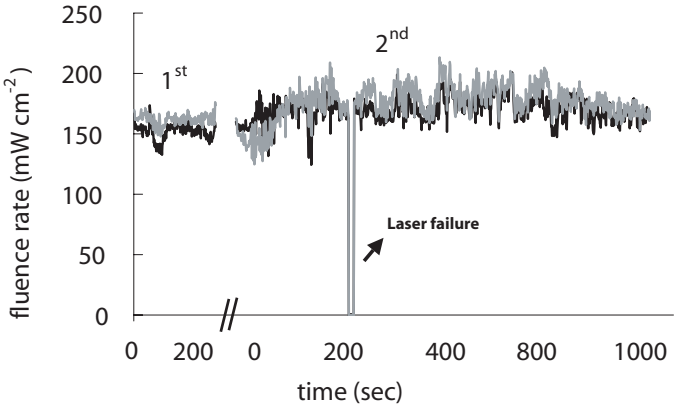

Figure 2. Fluence rate (mW cm^{-2}) measured in time (sec.) during a two-fold PDT illumination 630 nm of the Barrett's esophagus at two opposite positions (ϕ_1, ϕ_2 at 1 sample per sec.). The fluence rates amplification factors were 1.6 and 1.7 during the first and second illumination respectively (according to Eq.3). The desired calculated fluence was 20 and 100 J cm^{-2} using a fluence rate of 100 mW cm^{-2} (Eq.1). Diffuser length L_{diff} = 3 cm and the balloon diameter D_{ball} = 2.5 cm.

Figure 3 shows the fluence rate versus treatment time of a patient receiving a two-fold illumination with a intended primary fluence of two times 100 J cm^{-2}, $\phi_{primary}$ =100 mW cm^{-2} at 630 nm. Large variations in fluence rate were measured. During the first illumination period the difference in actual fluence rate between both locations was a factor 1.6. The fluence rate amplification factors $F_{i,1}$ and $F_{i,2}$ were 3.3 and 2.7 for the first and second illumination period.

Coughing, and spasm of the esophagus corresponded with large variations in fluence rate as recorded during PDT, smaller variations of the signal are possibly due to motion artefacts from respiration and heartbeat. The largest variation coincided with patient movement. Smaller variations were recorded when the patient was calm after additional administration of midazolam.

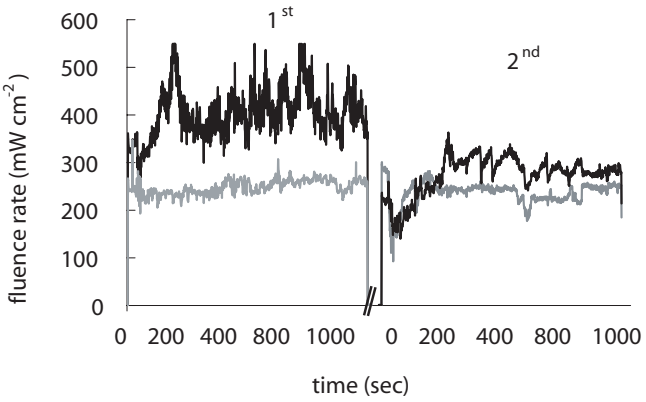

Figure 3. Fluence rate (mW cm^{-2}) measured in time (sec.) during a two-fold PDT illumination 630 nm of the Barrett's esophagus at two opposite positions (ϕ_1, ϕ_2 at 1 sample per sec.). The fluence rate amplification factors (Eq.3) were on average 3.3 and 2.7 during the first and second illumination respectively. The desired calculated fluence was 2 ×100 J cm^{-2} using a fluence rate of 100 mW cm^{-2} (Eq.1). Diffuser length L_{diff} = 5 cm and the balloon diameter D_{ball} = 2.5 cm.

In 8 patients the fluence rate amplification factor *F* was determined twice during a two-fold illumination. If the treatment would influence the optical properties of the tissue significantly, then the second *F* would always differ in the same manner for all patients. A paired t-test was used to test the hypothesis $F_{i,1} = F_{i,2}$. The t value was found to be –0.13321 at 12 degrees of freedom i.e. that at any reasonable significance level there is no significant difference between $F_{i,1}$, $F_{i,2}$ during the first and the second illumination in a single patient.

Figure 4 summarises the fluence rate amplification $F_{i,1}$ and $F_{i,2}$ factors during PDT for all patients as a function of illumination geometries i.e. ratio of diffuser length and balloon diameter (L_{dif}/D_{ball}). A students t-test revealed significant difference ($p<0.005$) between both geometries. The average fluence rate amplification factors *F* for both geometries were 1.8 (SD 0.5) and 2.8 (SD 0.5) respectively.

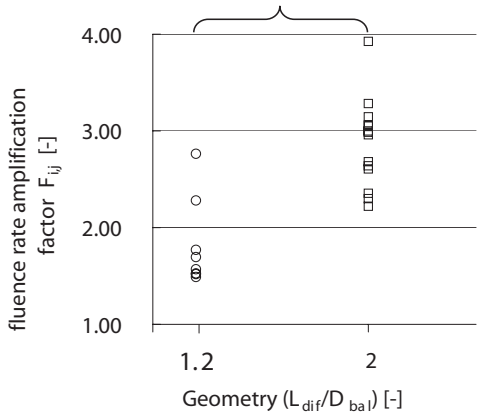

Figure 4 The fluence rate amplification factor Fi,j (measured i.e. scattered plus non scattered fluence rate, divided by the calculated fluence rate) as a functions of the illumination geometries used. Each point represents a patient F during the 1st. or 2nd illumination.

Conclusion

As seen in figure 3, the fluence rate can either increase at one measurement position while remaining stable at the other, or increase or decrease at both positions simultaneously. This gives a clue to the nature of these variations. When the patient coughs or an esophageal spasm occurs, muscles contract around the balloon. This squeezes blood out of the tissue, resulting in an increase in fluence rate build-up factor on both measurement locations simultaneously. The single sided variations should have a more local origin. Normal squamous epithelium often has a whitish colour whereas Barrett's columnar epithelium is more reddish-pink. Due to movement of the balloon, the position of the isotropic detectors at the mucosa surface will vary slightly. Thus when a detector is positioned in the vicinity of a clear junction between squamous and Barrett's epithelium local fluence rate variations may also occur. Although the fluence rate amplification is not a local effect, but mainly influenced by the optical properties of the whole esophageal wall, local colour variations will influence the actual fluence rate measured at that certain location.

The cylindrical diffuser was not fixed in the middle of the balloon but usually slightly bent, one probe was always located closer to the diffuser, thus measuring the highest primary fluence rate at the balloon surface. The large difference in fluence rate between both positions during the first illumination as seen in figure 3, may be attributed to an eccentric position of the cylindrical diffuser resulting from the patients spasms. Murrer *et al.* [18] investigated the influence of off-axis positioned cylindrical diffuser using Monte Carlo simulations in a trachea model and showed that central off-axis deviations may result in serious overdosing at the surface closest to the cylindrical diffuser. As seen in Figure 4, the fluence rate amplification factor depends on the illumination geometry. In case of small diffuser lengths relative more light is scattering isotropically into the absorbing part of the balloon (figure 1). Due to this, the contribution of back scattered light to the measured fluence rate at the tissue surface will be smaller. This may explain the difference in fluence

rate build-up factor between the 2 diffuser lengths. Panjehpour *et al.*[19,20] also measured the fluence (rate) in a normal canine esophagus model using isotropic detectors. They found relatively small variations of approximately ±12% between the (n=8) different animals. In that study the detectors were placed on three healthy tissue positions. From their data we have calculated a fluence rate amplification factor F = 0.64 according to equation (3). In a similar animal study by Overholt *et al.*[21], using a 180° windowed balloon (black coating over half the balloon window length) the measured fluence rate was shown to be less than with a 360° balloon. From their data we calculated an F of 0.43, which is much lower than what was measured in the present study. The explanation for this apparent discrepancy may be due to the illumination geometry and less back scattering from the balloon surface. Murrer *et al.*[18] described the cylindrical diffuser as the superposition of a series of isotropic point sources. This approach predicts a smaller fluence rate amplification factor for shorter diffusers due to axial loss of light. In addition, the effect of multiple reflections on the fluence rate amplification factor, not included in this analysis, will increase the losses for shorter diffuser lengths.

Van den Bergh *et al.*[22] highlighted the importance of standardising illumination devices and treatment procedures. They concluded that the comparison of the results between centres performing PDT in the esophagus would be much improved if procedures and light delivery devices we optimised and that this may also lead to improved treatment outcomes. Treatment outcome is also influenced by photosensitizer selectivity. Insufficient selectivity may result in stenosis or fistulas that could be compensated for to a certain extent with accurate light dosimetry as opposed by Bays *et al.*[23]. Furthermore they had measured the fluence rate distribution as a function of penetration depth in *ex-vivo* human esophagus tissue. From their data we have derived a fluence rate amplification factor at the esaphagus mucosa surface of approximately 2 and 1.7 for 630 nm and 514 nm respectively. Van den Boogert *et al.*[24] found similar results for *in vivo* measurement in an animal study; F=2.4 and F=1.3 for λ=633 nm and λ=532 nm respectively and found less epithelial damage at 523 nm which was attributed to differences in optical properties e.g. strong blood absorption and higher scattering resulting in a lower F. PDT of the BE using 514 nm (unpublished data) resulted in fluence rate amplification factors ranging from 0.8-1.8. The use of small isotropic detectors placed at the mucosa tissue surface will not result in under dosing underneath the detector surface, as light will be scattered around the isotropic detector[25].

In this study large variations were seen between the calculated and measured fluence rate, furthermore differences by a factor 2 to 3 in fluence rate were measured between the two opposite detectors, these variations may seriously alter the clinical response. For photosensitisers such as ALA induced PpIX risk of over-treatment is not very large, due to photobleaching. Insufficient treatment, however, may increase local recurrences, which has been observed frequently. With other photosensitises like mTHPC[26], or Photofrin[27] over-treatment may result in excessive PDT damage.

A large variability of the fluence rate was observed during PDT. Firstly, a major cause of variation was patient movement, coughing and esophageal spasm. Secondly, the fluence rate amplification factor varied in the range of 1.5-3.9 for 15 patients and appeared to depend on the redness of the BE. Thirdly, eccentric positioning of the cylindrical diffuser resulted in significant difference in fluence rate delivered to opposite sites of the BE esophagus. Finally the actual fluence rate delivered to the mucosal surface depended on the illumination geometry. All these factors appear to justify the routine application of in vivo dosimetry in PDT of BE especially for potent photosentisers such as HpD or m-THPC significant differences in fluence rate amplification were measured between the first and second illumination during a two-fold PDT.

References

1. Barr H, Shepherd NA, Dix A, Roberts DJ, Tan WC and Krasner N. Eradication of high-grade dysplasia in columnar-lined (Barrett's) esophagus by photodynamic therapy with endogenously generated protoporphyrin IX. *Lancet.* 1996 **348**: 584-585.

2. van den Boogert J, Houtsmuller AB, de Rooij FW, de Bruin RW, Siersema PD, van Hillegersberg and R. Kinetics, localization, and mechanism of 5-aminolevulinic acid-induced porphyrin accumulation in normal and Barrett's-like rat esophagus. *Lasers Surg Med.* 1999 **24**:3-13.

3. Ackroyd R, Brown N, Vernon D, Roberts D, Stephenson T, Marcus S, Stoddard C and Reed M. 5-Aminolevulinic acid photosensitization of dysplastic Barrett's esophagus: a pharmacokinetic study. *Photochem Photobiol.* 1999 **70**: 656-662.

4. de Bruijn HS, van der Veen N, Robinson DJ and Star WM. Improvement of 5-aminolevulinic acid based photodynamic therapy in vivo using light fractionation with 75 minute interval. *Cancer Res.* 1999 **59**: 901-904.

5. Robinson DJ, de Bruijn HS, van der Veen N, Stringer MR, Brown SB and Star WM. Fluorescence photobleaching of ALA-induced protoporphyrin IX during photodynamic therapy of normal hairless mouse skin: the effect of light dose and irradiance and the resulting biological effect. *Photochem. Photobiol.* 1998 **67**: 141-149.

6. Barr H 2000 Barrett's esophagus: treatment with 5-aminolevulinic acid photodynamic therapy. *Gastrointest Endosc Clin N Am.* 2000 **10:** 421-437.

7. Gossner L, May A, Sroka R, Stolte M, Hahn EG and Ell C. Photodynamic destruction of high grade dysplasia and early carcinoma of the esophagus after the oral administration of 5-aminolevulinic acid. *Cancer.* 1999 **86**: 1921-1928.

8. Tan WC, Fulljames C, Stone N, Dix AJ, Shepherd N, Roberts DJ, Brown SB, Krasner N and Barr H. Photodynamic therapy using 5-aminolaevulinic acid for oesophageal adenocarcinoma associated with Barrett's metaplasia. *J Photochem Photobiol B.* 1999; **53**: 75-80.

9. Regula J, MacRobert AJ, Gorchein A, Buonaccorsi GA, Thorpe SM, Spencer GM, Hatfield AR and Bown SG. Photosensitisation and photodynamic therapy of oesophageal, duodenal, and colorectal tumours using 5 aminolaevulinic acid induced protoporphyrin IX: a pilot study. *Gut.* 1995 **36**: 67-75.

10. Maier A, Tomaselli F, Gebhard F, Rehak P, Smolle J, Smolle-Juttner FM. Palliation of advanced esophageal carcinoma by photodynamic therapy and irradiation. *Ann Thorac Surg.* 2000 **69**: 1006-1009.

11. Ackroyd R, Brown NJ, Davis MF, Stephenson TJ, Marcus SL, Stoddard CJ, Johnson AG and Reed MW. Photodynamic therapy for dysplastic Barrett's esophagus: a prospective, double blind, randomised, placebo controlled trial. *Gut.* 2000 **47**: 612-619.

12. van Staveren HJ, Keijzer M, Keesmaat T, Jansen H, Kirkel WJ, Beek JF and Star WM. Integrating sphere effect in whole-bladder wall photodynamic therapy: III. Fluence multiplication, optical penetration and light distribution with an eccentric source for human bladder optical properties. *Phys Med Biol.* 1996 **41**: 579-590.

13. Murrer LHP, Marijnissen HPA, Baas P and Star WM. Applicator for light delivery and in situ light dosimetry during endobronchial photodynamic therapy: first measurements in humans. *Lasers Med Sci.* 1997 **12**: 253-259.

14. Murrer LHP, Marijnissen HPA and Star WM. *Ex vivo* light dosimetry and monte carlo simulations for endobronchial photodynamic therapy. *Phys Med Biol.* 1995 **40**: 1807-1817.

15. van Staveren HJ, Marijnissen HPA, Aalders MCG and Star WM. Construction, quality assurance and calibration of spherical isotropic fibre optic light diffusers. *Lasers Med Sci.* 1995 10:137-147.

16. Marijnissen HP and Star WM. Calibration of isotropic light dosimetry probes based on scattering bulbs in clear media. *Phys Med Biol.* 1996 **41**: 1191-1208.

17. Panjehpour M, Overholt BF and Haydek JM. Light sources and delivery devices for photodynamic therapy in the gastrointestinal tract. *Gastrointest Endosc Clin N Am.* 2000 **10**: 513-532.

18. Murrer LH, Marijnissen HP and Star WM. Monte Carlo simulations for EndoBronchial Photodynamic Therapy: the influence of variations in optical and geometrical properties and of realistic and eccentric light sources. *Lasers Surg Med.* 1998 **22**: 193-206.

19. Panjehpour M, Overholt BF, DeNovo RC, Sneed RE and Petersen MG. Centering balloon to improve esophageal photodynamic therapy. *Lasers Surg Med.* 1992 **12**: 631-638.

20. Panjehpour M, Overholt BF, DeNovo RC, Petersen MG and Sneed RE. Comparative study between pulsed and continuous wave lasers for Photofrin photodynamic therapy. *Lasers Surg Med.* 1993 **13**: 296-304.

21. Overholt BF, Panjehpour M, DeNovo RC, Petersen MG. Photodynamic therapy for esophageal cancer using a 180 degrees windowed esophageal balloon. *Lasers Surg Med.* 1994 **14**: 27-33.

22. van den Bergh H. On the evolution of some endoscopic light delivery systems for photodynamic therapy. *Endoscopy.* 1998 **30**: 392-407.

23. Bays R, Wagnieres GA, Robert D, Braichotte DR, Savary J-F, Monnier P, van den Bergh H. Light dosimetry for photodynamic therapy in the esophagus. *Lasers Surg Med* 1997 **20**: 290-303.

24. van den Boogert J, van Staveren HJ, de Bruin RW, Eikelaar JH, Siersema PD, van Hillegersberg R. Photodynamic therapy for esophageal lesions: selectivity depends on wavelength, power, and light dose. *Ann Thorac Surg.* 1999 **68**: 1763-1769.

25. Jode de ML. Monte Carlo simulations of the use of isotropic light dosimetry probes to monitor energy fluence in biological tissue. *Phys Med Biol* 1999 **44**: 3027-3037.

26. Gossner L, May A, Sroka R, Ell C. A new long-range through-the-scope balloon applicator for photodynamic therapy in the esophagus and cardia. *Endoscopy.* 1999 **31**: 370-376.

27. Panjehpour M, Overholt BF, Haydek JM and Lee SG. Results of photodynamic therapy for ablation of dysplasia and early cancer in Barrett's esophagus and effect of oral steroids on stricture formation. *Am J Gastroenterol.* 2000 **95**: 2177-2184.

3.

Performance of a dedicated light delivery and dosimetry device for photodynamic therapy of nasopharyngeal carcinomas: Phantoms and volunteers

Adapted from:

H. Nyst, R.L.P. van Veen, I,B. Tan, R. Peters, P.C. Levendag, H.J.C.M. Sterenborg and F.A. Stewart. Development of a dedicated light delivery and dosimetry device for photodynamic therapy of nasopharyngeal carcinomas: Phantom and volunteers. Ready for submission to **Lasers Surg Med.**

Abstract

The objective of this study was to develop and evaluate the performance of a dedicated light delivery and measurement device for PDT in the nasopharyngeal cavity that achieves an optimal homogeneous and reproducible fluence rate distribution to a target area and provides proper shielding of a predefined risk areas.

Material and Methods: A flexible silicone applicator with incorporated light delivery and dosimetry was developed. The applicator can be inserted through the mouth and fixed in the nasopharyngeal cavity. Tissue optical phantoms were prepared on the basis of optical properties measured *in vivo* using diffuse reflectance spectroscopy.. The fluence rate over the length of the applicator surface was measured in air, in phantoms and in five healthy volunteers.

Results: The fluence rate distribution over the applicator surface in air and tissue optical phantom was found to be homogeneous (SD/mean 3.8% and 18.3% respectively). However, the fluence rate distribution in five volunteers varied over the length of the applicator and was found to be significantly less homogeneous than in the tissue optical phantoms (SD/mean ranging from 19% up to 52%). The maximum observed fluence rate build-up varied between subjects and ranged from a factor of 4.1 to 6.9. Shielding of the risk area such as the soft palate and tongue was effective.

Conclusions: In air and in tissue optical phantoms the fluence rate distribution is highly homogeneous. The observed large inter-subject variations originated from average differences in optical properties and nasopharyngeal geometry, whereas significant intra-patient variations in fluence rate mainly reflect local differences in geometry and optical properties. Light delivery based on a single tissue surface measurement will not be adequate. For PDT in general, these observations should be taken in consideration when developing light applicators for PDT.

Introduction

We are investigating the use of photodynamic therapy (PDT) as an alternative or additional treatment modality for the treatment of nasopharyngeal carcinoma (NPC). The few published studies treating NPC using PDT all demonstrate variable clinical outcome. In all but one of these studies, light dosimetry was not employed and treatment parameters were varied considerably between patients[1-3]. In general, light delivery was based on manually positioning an optical fibre through an endoscope[4,5]. The only reference in the literature to a systematic approach to light delivery is from Lofgren *et al* [6]. They developed a rigid light delivery system for Photofrin-PDT that was inserted through the nose into the nasophanryngeal cavity. A beam deflector at the distal end of the system directed the light upward onto the nasopharynx. Five patients were treated, again with variable results. The variable outcome of tumour response most likely resulted in the cessation of all of the clinical studies.

The therapeutic effect during PDT depends on a combination of parameters that include drug dose, drug-light interval, and light fluence (rate). These parameters have been extensively investigated in pre-clinical models and a small number of stage I clinical trials optimising PDT. A homogeneous and reproducible fluence (rate) delivery during clinical PDT plays a vital role in preventing under- or over-treatment[7]. Previous attempts to perform PDT in the nasopharynx may in part have been hampered by inadequate and non-reproducible light delivery due to the difficulty of accessing the nasopharyngeal cavity and may be a reason for the unsatisfactory clinical response in the preliminary clinical studies.

In order to achieve optimal light delivery in the nasopharynx we have developed a flexible silicone applicator that facilitates a controllable and reproducible approach to the delivery and monitoring of light within the nasophanryngeal cavity. Monitoring of the *in vivo* fluence rate may prove to be important since in hollow organs the actual fluence rate in tissue is strongly increased due to multiple diffuse reflections from the tissue surface. This fluence rate build-up varies with the shape and tissue optical properties (scattering and absorption), and has been reported to be as high as a factor of 7.5 in the bladder[8]. In another study we have measured fluence rate variations during PDT of Barrett's oesophagus[9]. The results showed a dramatic variation between patients, with fluence rate build-up factors ranging from 1.5 up to 4, illustrating the importance of developing instrumentation for integrated light delivery and *in situ* light fluence rate measurement in PDT.

Prior to performing a clinical study of NPC-PDT the performance of the applicator was investigated. Here we report on the fluence rate distribution in the target area and shielding efficacy evaluated in air, tissue optical phantoms and in healthy volunteers. Inter- and intra– subject variations in fluence rate distribution are evaluated.

Materials and methods

The applicator

The applicator and its position with respect to the anatomical locations are schematically shown in figure 1b. The NPC-PDT applicator is made out of silicone (type 625, Wacker Chemie, Krommenie, The Netherlands) and consists of two 220 mm long silicone tubes. The inner diameter of the silicone tubing can accommodate standard flexible implant catheters (o.d. 6 mm, i.d. 4 mm, PB, Barendrecht, Holland) (o.d. 6F, Nucletron, Veenendaal, The Netherlands) for improved guidance of miniature (isotropic) fluence rate detectors. Both tubes are interconnected at the distal end of the applicator by a small silicone bridge, which abuts proximally to the nasal septum[10]. The bridge is perforated with two 5 mm holes to enhance flexibility. A removable flexible black silicon patch is applied as shown in figure 1a to protect the soft palate and prevents light from entering the oral cavity. In a pilot study we have investigated the influence of bending on the emission profile of cylindrical diffusers. In the tissue optical phantom and volunteers, a 30 mm long cylindrical diffuser demonstrated a highly in-homogeneous emission profile with a strong peak at the proximal position of the diffusing part.

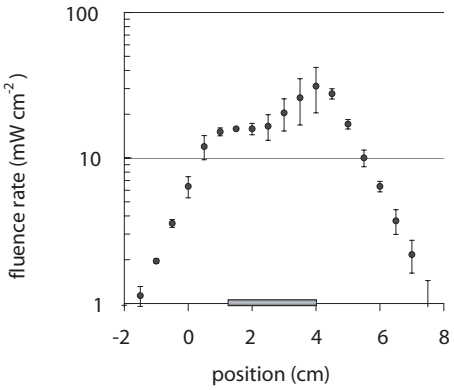

Figure 2. The fluence rate distribution over the length of the applicator surface for a 30mm long cylindrical diffuser immersed in a liquid optical phantom (μ_s'= 1500 m^{-1}, μ_a = 20 m^{-1}). The average fluence rate over the length of the diffuser is 20.2 mW cm^{-2} (S.D. 6.2) but demonstrates a peak of 32 mW cm^{-2} at the proximal position of the diffuser. The black squares represent the measurements on the tube that contained the diffuser.

This effect is the result from bending of the cylindrical diffuser. When the part, where the quartz fibre is connected to the flexible diffusely emitting material, is bent at a significant angle e.g. D=22 mm which is the radius of the bridge, the majority of the photons exit at the transition point. This results in a peak in fluence rate profile at the beginning of the diffuser as seen in figure 2. This phenomenon was not observed in phantoms for the 60 mm and longer diffuser, since the connection between fiber and diffuser is at the beginning of the bridges and is straight. To overcome the problem of the

inhomogeneous fluence rate distribution for short diffuser lengths e.g. < 30 mm, we have incorporated black catheters for guidance of 60 mm long cylindrical diffusers in both silicone tubes. As shown in figure 1 the black catheters end at the point where the bridge is in contact with the septum. This enables variable diffuser lengths (e.g. 10 up to 60 mm) by varying the insertion without adjustment of the laser output power and allows the effective diffuser length to be tailored to the patient's tumour dimensions. An additional benefit is the prevention of light entering the nasal cavity. In the current study a 652 nm 2 Watt diode laser (Ceralas PDT, Biolitec, Bonn, Germany) was used as light source.

In situ dosimetry

The fluence (rate) at the applicator surface was measured using isotropic light detectors (400 µm core diameter fibre pseudo sphere, 1 mm tip diameter, Cardiofocus, formerly Rare Earth Medical, West Yarmouth MA, USA). The detectors measure the sum total of both the incident light from the diffuser[10], and reflected and scattered (re-emitted) light, with an accuracy of ±10%. The isotropic probes were calibrated in air in a small integrating sphere, incorporated in the dosimetry device, illuminated via a flange by a small diode laser to ensures a homogeneous calibration field with known fluence rate. The dosimetry software applied a factor of 1.07 to correct for the difference in response of the detectors when measurements are performed at the air/tissue surface resulting from mismatch in refractive index between air and tissue[11]. Detector probes were connected to photodiodes with read-out electronics, which stores and displays the fluence (rate) at the tissue surface on a monitor.

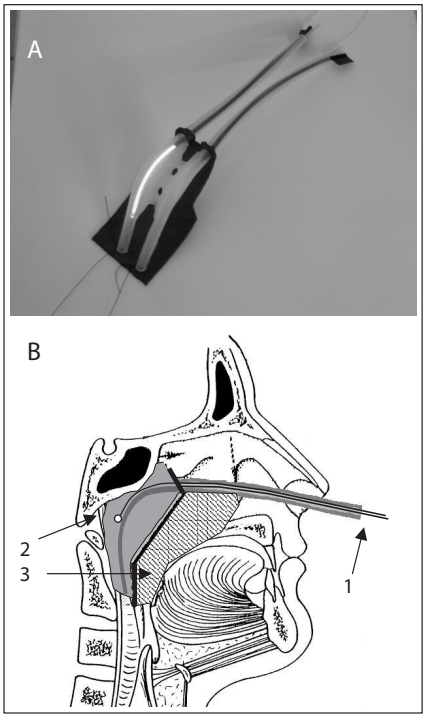

Figure 1.a) Basic shape of the NPC PDT applicator device and b) the position of the light application device with respect to the anatomical location. For the experiments, a cylindrical diffuser (1) that emits homogeneously over a 30 mm or 60 mm length was used. (1) The isotropic detector fibre. The NPC target area (2) is localised along the outer curve of the applicator. The white dot represents the isotropic detector bulb. The thick black line represents the black silicon patch intended to shield light from critical healthy areas like the soft palate (3).

Prior to the experiments, two isotropic detectors were inserted into the applicator, one situated in the same tube as the cylindrical diffuser and one in the parallel empty tube. During the illumination, two isotropic detectors recorded the fluence rate at two positions at the inner or outer surface of the applicator. Measurements were performed by scanning every 5 mm starting 10 mm before the start of the diffuser up to 10 mm past the distal end of the diffuser.

Phantom measurements

Prior to the phantom measurements the fluence rate distribution at the applicator surface was first determined in air. To investigate the influence of surrounding scattering and absorbing media on the fluence rate profile and build-up associated with the applicator, tissue optical phantoms were prepared. In order to determine a first order approximation of the reduced scattering and absorption coefficients of nasopharygeal mucosal (thickness 5 – 10 mm) with underlying bone tissue, we performed spatially resolved diffuse reflectance spectroscopy (DRS)[13]. Due to the dimensions of the head of our DRS detector it was not feasible to directly determine the optical properties of nasopharyngeal or any other mucosal tissue. Therefore DRS measurements were performed on comparable layered structures (bone and tissue) on the shin and the forehead. An average reduced scattering coefficient (μ_s') at 652 nm was determined to be 1500 m^{-1} and an absorption coefficient (μ_a) of 20 m^{-1}. Optical phantoms composed of saline, Intralipid and Evans Blue were formulated with these optical properties. The concentration of Intralipid determines the μ_s' of the phantom[15] and the concentration of Evans Blue determines the μ_a. A cylindrical diffuser was inserted into the NPC-PDT applicator and measurements were made using isotropic detectors in the guidance channel next to the diffuser, and in the empty silicon tube, as described before. After these measurements the cylindrical diffuser was switched to the empty tube and the measurements were repeated and the average and standard deviation were determent.

The applicator was completely immersed in the phantom and the fluence rate was determined every 5 mm for a 60 mm long cylindrical diffuser.

Volunteer measurements.

After decongestion (R/ Xylometazoline HCl 1%) and topical anaesthesia two tubes were inserted through the nose and collected in the oropharynx and trans-orally guided outwards. The applicator was then connected to the nose tubes and trans-orally introduced into the nasopharyngeal cavity by pulling the nose tubes[10]. The septum blocks and fixates the bridge in the nasopharyngeal cavity. Secured by a small silicone flange the applicator remained fixed in a stable position for the illumination period, during which the subjects were seated in an ENT chair. Fluence rate measurements were performed with two isotropic detectors; one in the tube that contained the diffuser and one in the empty tube. The measurements in the empty tube were performed to determine the magnitude of cross talk between illumination channels. Measurements were performed using a 60 mm long

cylindrical diffuser. In addition measurements were performed on the surface of the risk areas such as the soft palate, tongue and tonsils to investigate the efficacy of the shielding patch.

Results.

Phantoms

For the measurement in air, the diffuser output was set to 100 mW cm^{-1}. Figure 3 shows the results of a single fluence rate scan made over the outer surface of the silicon tube that contained the cylindrical diffuser, a second scan halfway between the two tubes, and finally a scan made at the surface of the empty tube. The average fluence rate over the length of the diffusers was 92 ± 3.5 mW cm^{-2} and represents a rather homogeneous fluence rate distribution. The average fluence rate halfway between the two tubes was 28 ± 7.4 mW cm^{-2}, whereas the average fluence rate over the surface of the empty tube of the applicator was 10.7 ± 3.2 mW cm^{-2}.

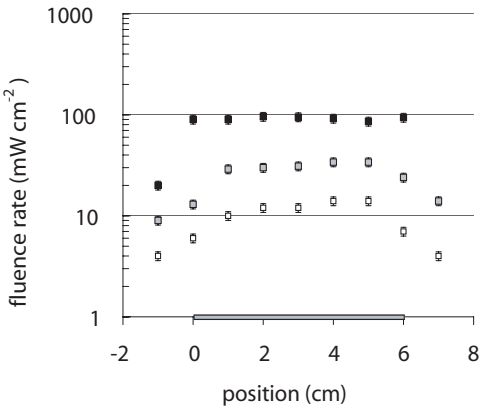

Figure 3. The fluence rate distribution over the length of the applicator surface for a 60 mm long cylindrical diffuser in air. The error bars represent the standard deviation of both left and right tube measurements. The black squares represent the measurements on the tube that contained the diffuser, the grey squares the measurements between the tubes and the white squares the measurements at the surface of the empty channel. The grey bar on the x-axe indicates the position of the cylindrical diffuser. The error bars represent the measurements accuracy of ±10%.

For the phantom measurements the diffuser output was set to 5 mW cm^{-1}. Prior to immersing the applicator into the phantom an additional air measurement was performed under identical conditions. Figure 4 shows the phantom results for a 60 mm cylindrical diffuser inserted in the applicator in combination with the measurements in air to demonstrate the influence of the optical properties of the phantom on the fluence rate build up and emission profile. The applicator again has a rather homogeneous fluence rate distribution, 17.5 ± 3.0 mW cm^{-2}, over the length of the NPC-PDT applicator. Figure 4 also illustrates the build up in fluence rate, due to scattering in the phantom, compared to the same output power in air. The average fluence rate build up over the length of the

diffuser was found to be 3.5 times higher than the incident light coming directly from the source. In addition, the profile of the fluence rate distribution extends significantly beyond the boundaries of the diffuser in particular at the distal end of the applicator.

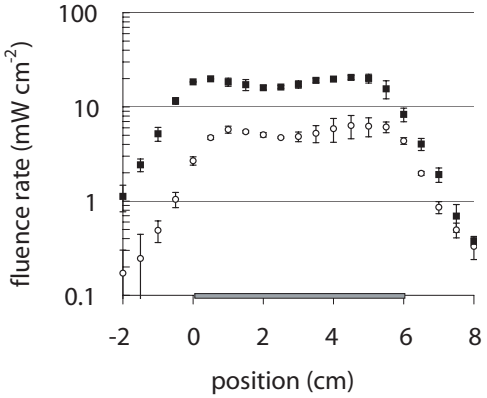

Figure 4. The fluence rate distribution over the length of the applicator surface for a 60mm long cylindrical diffuser immersed in a liquid optical phantom (black squares), and measured in air (empty squares). Both measurements were performed on the tube that contained the diffuser. The grey bar on the x-axe indicates the position of the cylindrical diffuser. The error bars represent the standard deviation of both left and right tube measurements.

Volunteers

In total five volunteers were recruited and *in vivo* fluence rate measurements were performed in both the applicator tube containing the 60 mm cylindrical diffuser and in the empty tube. Figure 5 shows the results of the five volunteer measurements for a 60 mm long diffuser. The diffuser output power was fixed at 600 mW, which corresponds to 100 mW cm^{-1} or ~100 mW cm^{-2} in absence of tissue at the tube surface (see figure 3). The error bars are not shown but are ±10% for each position. The fluence rate distribution was found to be significantly less homogeneous as compared to measurements in air and in phantoms. The fluence rate build up varied between subjects and over the length of the applicator within a single subject.

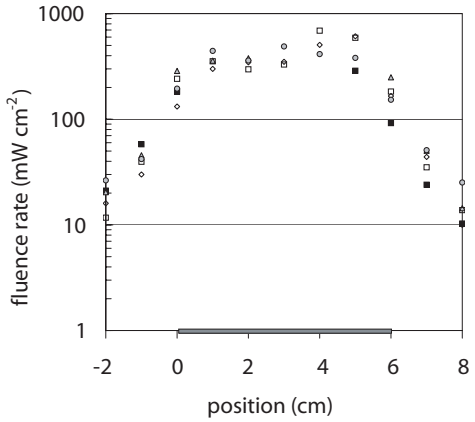

Figure 5. The fluence rate distribution scan over the length of the applicator surface for a 60 mm long cylindrical diffuser as measured in five healthy volunteers. Each symbol represents a volunteer. The output power per length of cylindrical diffuser corresponded to a value of 100 mW cm^{-1}.

The maximal observed fluence rate build-up was at the proximal diffuser location (position 4) and varied by a factor of 4.1 and 6.9. Table 1 summarises the average fluence rate, standard deviation, relative error and the average build-up factor over the length of the diffuser for each of the five subjects individually. The average relative error (SD/mean) i.e. variation within a subject was found to be 41%, with standard deviations ranging between 60 up to 186 mW cm^{-2}. Table 2 summarises the average fluence rate, standard deviation, relative error and build-up factor for different positions on the diffuser for all volunteers. The average relative variation between subjects for the same position and was found to be 24%. In the volunteer experiments, low fluence rates were measured at the surface of the shielded risk areas, with a maximum of 0.06 mW cm^{-2} at the surface of the tongue and a maximum of 4.8 mW cm^{-2} on the soft palate. This corresponds to a delivered fluence at the soft palate of less than 1 J cm^{-2} for a 200-second exposure at 100 mW cm^{-1}.

Table 1. Summarises the average fluence rate over the length of the diffuser (l_{diff}) for each volunteer for a fixed diffuser output power of 100 mW cm^{-1}.

Volunteer No.	Average fluence rate over L_{diff}	SD	Relative error (% SD/mean)	Build-up factor
1	188	98	52	1.9
2	318	60	19	3.2
3	344	171	50	3.4
4	384	186	49	3.8
5	348	127	36	3.5

Table 2. Summarises the average fluence rate for each measurement position on the diffuser for all volunteers for a fixed diffuser output power of 100 mW cm^{-1}.

Applicator position	Average per position of all volunteers	SD	Relative error (% SD/mean)
0	208	59	28
1	364	60	16
2	345	35	10
3	390	87	22
4	537	141	26
5	468	158	34
6	169	57	34

Discussion

We report on the development of a dedicated applicator for PDT in the nasopharyngeal cavity that enables the delivery of light using a cylindrical diffusing fibre and the measurement of *in situ* fluence rate profiles within the nasopharynx. Figures 4 and 5 illustrate that there is a significant build-up in fluence rate both in an optical phantom and in the nasopharyngeal cavity of volunteers. As shown in figure 4, the fluence rate profile also extends further towards the distal end of the applicator (~10 mm) than the geometric length of diffusing fibre. Clinically, this effect should be taken in consideration when tailoring the diffuser length for individual tumours and patients. If a dual illumination is considered i.e. illumination of both left and right tube to ensure full coverage of the NP cavity in case of large tumours, a significant delivered fluence between the tubes is desired. The measurements in air (figure 3) between the two tubes demonstrated that a significant fluence is delivered to the tissue between the two silicone tubes. Figure 5 also shows that there is a general increase in the average fluence rate measured in volunteers at the proximal end of the applicator. This is probably a result of the large integrating cavity effect over this length of the applicator compared to that around the black patch that protects the soft palate and oral cavity. In the vicinity of oropharynx the highly absorbing black patch covers half of the surface area of the cavity and thus results in a reduced fluence rate build up. In a future prototype this effect could be corrected for by whitening the inner surface of the shielding patch.

The optical properties of tissue structures similar to those of the nasopharynx were determined on volunteers using DRS and used to compose the phantoms. The average fluence rate build-up over the applicator surface in tissue optical phantoms was found to be 3.5 times higher then the incident light from the diffuser as seen in figure 4. The average build-up of all volunteers over the length of the applicator was found to be 3.14, thus indicating a reasonable estimate of the chosen optical properties of nasopharyngeal tissue.

The experiments in air and in optical phantoms both demonstrated the ability of the applicator to produce a homogeneous and reproducible light distribution. However, as shown in figure 5 measurements *in vivo* resulted in larger variations in fluence rate both within individual volunteers and between volunteers. This notwithstanding the black patch developed for shielding of the soft palate and oral cavity proved adequate.

The individual volunteers measurements demonstrated a significantly less homogeneous fluence rate distribution (SD/mean 19% up to 52%) over the length of the NPC-PDT applicator surface as compared to the phantom experiments (SD/mean 18.3%) and in air (SD/mean 3.8%). The average relative error i.e. average variation within a subject over the length of the diffuser was found to be 41% as compared to 24% between subjects on the same position. These findings are the result of local differences in optical properties e.g. local differences in vasculature, tissue oxygenation, scattering and of differences in nasopharyngeal geometry.

In addition to the intra-subject variations, the volunteer measurements demonstrated large inter-subject variations in average fluence rate build up (1.9 up to 3.8) over the applicators diffuser length as seen in table 1. These variations originate from differences in global optical properties and from differences in size and shape of the nasopharyngeal cavity of the volunteers. The relative contribution of both *in vivo* optical properties and geometry to these variations are difficult to de-couple, since the relative contributions from variations in optical properties and geometry are unknown.

In the majority of clinical studies using Foscan-PDT in head and neck cancer patients[16-19], dosimetry was based upon source output power and the treatment surface area, aiming to deliver an incident fluence rate of 100 mW cm^{-2} and a total fluence of 20 J cm^{-2}, without taking back scattering into account. Good long-term clinical response without significant side affects was observed in all these head and neck studies. In our prospective mTHPC mediated NPC-PDT study we will initially employ a similar approach, with the aim of delivering incident fluence of 20 J cm^{-2} for mTHPC and investigating the clinical consequences of intra- and inter patient variations in optical properties and geometry.

In vivo dosimetry illustrates that a significantly higher fluence is delivered to the tissue (38 J cm^{-2} up to 76 J cm^{-2}) based on the observed average build-up factors observed in the present study.

The consequences of these variations and substantial build-up in fluence rate on the clinical response and possible complications due to overdosing, of mTHPC (Foscan®) mediated PDT of NPC may prove to be limited. Critical tissue structures e.g. soft palate, are properly shielded whereas other vulnerable structures like the optic nerve are shielded by highly scattering bone. On the other hand under-dosing might most certainly lead to recurrence of the disease and an early death of the patient. Therefore, in this particular application aiming for overdosing may be the safest approach for the patient. *In vivo* light dosimetry for compensating inter-patient variations may be essential for limiting the overdose to acceptable levels.

The observed average intra patient variations are approximately twice as high as the variations between subjects. For PDT in general, light delivery based on *in situ* dosimetry in order to compensate for inter patient differences in optical properties and geometry, therefore demands for a different dosimetric approach, as it appears that measurements at the tissue surface mainly reflect local differences in optical properties and geometry. Due to these local variations, light delivery based on *in situ* dosimetry by a single point measurement at the surface will not be adequate. A dosimetric approach that either employs multiple surface measurements or a single/multiple fluence rate measurement at the centre of the cavity that averages out the local differences in optical properties is therefore required.

Conclusion

We have developed a dedicated light delivery and dosimetry device for PDT in the nasopharyngeal cavity that enables light delivery and measurements. In air and in tissue optical phantoms the fluence rate distribution is highly homogeneous, however in volunteers the emission profile demonstrated to be significantly less homogeneous. Large inter- and intra-patient variations were observed. These variations are attributed to variations in optical properties and geometry. For PDT in general, these observations should be taken in consideration when developing light applicators for PDT.

References

1. Stranadko EF, Garbuzov MI, Zenger VG, Nasedkin AN, Markichev NA, Riabov MV and Leskov IV. Photodynamic therapy of recurrent and residual oropharyngeal and laryngeal tumors. Vestn. *Otorinolaringol.* 2001 **3**: 36-39.

2. Schweitzer VG. Photodynamic therapy for treatment of head and neck cancer. Otolaryngol. *Head Neck Surg.* 1990 **102**: 225-232.

3. Sun ZQ. Photodynamic Therapy of nasopharyngeal carcinoma by argon or dye laser— an analysis of 137 cases. *Zhonghua Zhong Liu Za Zi.* 1992 **14**: 290-292.

4. Kulapaditharom B. and Boonkitticharoen V. Photodynamic therapy for residual or recurrent cancer of the nasopharynx. *J Med Assoc Thai.* 1999 **82**: 1111-1117.

5. Tong MC, Van Hasselt CA and Woo JK. Preliminary results of photodynamic therapy for recurrent nasopharyngeal carcinoma. *Eur Arch Otorhinolaryngol.* 1996 **253**: 189-192.

6. Lofgren LA, Hallgren S, Nilsson E, Westerborn A, Nilsson C and Reizenstein J. Photodynamic therapy for recurrent nasopharyngeal cancer. *Arch Otolaryngol Head Neck Surg*. 1995 **121**: 997-1002.

7. van Veen RL, Robinson DJ, Siersema PD and Sterenborg HJ. The importance of dosimetry during photodynamic therapy (submitted as a letter to *Gastrointestinal Endoscopy*).

8. Marijnissen HPA, Jansen H and Star WM. Treatment system for whole bladder wall photodynamic therapy with in vivo monitorring and control of light dose rate and dose. *J Urol.* 1989 **142**: 1351-1355.

9. Van Veen RL, Aalders MC, Pasma KL, Siersema PD, Haringsma J, Van De Vrie W, Gabeler EE, Robinson DJ and Sterenborg HJ. *In situ* light dosimetry during photodynamic therapy of Barrett's esophagus with 5-aminolevulinic acid. *Lasers Surg Med.* 2002 **31**: 299-304.

10. Levendag PC, Peters R, Meeuwis CA, Visch LL, Sipkema D, de Pan C and Schmitz PI. A new applicator design for endocavitary brachytherapy of cancer in the nasopharynx. *Rad Oncol.* 1997 **45(1)**: 95-8.

11. van Staveren HJ, Marijnissen HPA, Aalders MCG and Star WM. Construction, quality assurance and calibration of spherical isotropic fibre optic light diffusers. *Lasers Med Sci.* 1995 **10**: 137-147.

12. Marijnissen HP and Star WM. Calibration of isotropic light dosimetry probes based on scattering bulbs in clear media. *Phys Med Biol.* 1996 **41**: 1191-1208.

13. Doornbos RM, Lang R, Cross FW and Sterenborg HJ. The determination of *in vivo* human tissue optical properties and absolute chromophore concentrations using spatially resolved steady state diffuse reflectance spectroscopy. *Phys Med Biol.* 1999 **44**: 967-981.

14. Murrer LHP, Marijnissen HPA and Star WM. Ex vivo light dosimetry and monte carlo simulations for endobronchial photodynamic therapy. *Phys Med Biol*. 1995 **40**: 1807-1817.

15. van Staveren HJ, Moes CJM, van Marle J, Prahl SA and van Gemert MJC. Light scattering in Intralipid 10% in the wavelength region of 400-1100 nm. *Appl Opt.* 1991 **30**: 4507-4513.

16. Copper MP, Tan IB, Oppelaar H, Ruevekamp MC, and Stewart FA. Meta-tetra(hydroxyphenyl)chlorin photodynamic therapy in early-stage squamous cell carcinoma of the head and neck. *Arch Otolaryngol Head Neck Surg.* 2003 **129**(7): 709-11.

17. Hopper C, Kubler A, Lewis H, Tan IB, and Putnam G. mTHPC-mediated photodynamic therapy for early oral squamous cell carcinoma. *Int J Cancer.* 2004 **10;111**(**1**): 138-46.

18. D'Cruz AK, Robinson MH, and Biel MA. mTHPC-mediated photodynamic therapy in patients with advanced, incurable head and neck cancer: a multicenter study of 128 patients. *Head Neck.* 2004 **26**(**3**): 232-40 .

19. Fan KF, Hopper C, Speight PM, Buonaccorsi GA, and Bown SG.Photodynamic therapy using mTHPC for malignant disease in the oral cavity. *Int J Cancer.* 1997 **26;73**(**1**): 25-32.

4.

In vivo fluence rate measurements during Foscan® mediated Photodynamic Therapy of persistent and recurrent Nasopharyngeal Carcinomas using a dedicated light applicator

Adapted from:

R.L.P. van Veen, H. Nyst, S. Rai Indrasari, M. Adham Yudharto, D.J. Robinson, I.B. Tan, C. Meewis, R. Peters, S. Spaniol, F.A. Stewart, P.C. Levendag, H.J.C.M. Sterenborg. *In vivo* fluence rate measurements during Foscan® mediated Photodynamic Therapy of persistent and recurrent Nasopharyngeal Carcinomas using a dedicated light applicator, accepted for publication in **J Biomed Opt.**

Abstract

Objectives: The objective of this study was to evaluate the performance of a dedicated light applicator for light delivery and fluence rate monitoring during Foscan® mediated photodynamic therapy of nasopharyngeal carcinoma in a clinical phase I/II study.

Material and Methods: We have developed a flexible silicone applicator that can be inserted through the mouth and fixed in the nasopharyngeal cavity. Cylindrical diffusing fibres are then inserted to illuminate the left and right side of the cavity. Two individual illuminations were performed in order to deliver a total fluence of 20 J cm^{-1} over the entire nasopharyngeal cavity, at a calculated output power of 100 mW cm^{-1}. Three isotropic fibres, for measurements of the fluence (rate) during therapy, were located within the nasopharyngeal tumour target area and one was manually positioned to monitor structures at risk in the shielded area. A flexible black silicon patch, tailored to the patient's anatomy is attached to the applicator, to shield the soft palate and oral cavity from the 652 nm laser light.

Results: Fourteen patients were included in the study, resulting in 26 fluence rate measurements in the risk volume (2 failures). Very low fluence (rate) values were measured at the shielded risk areas, with a minimum of 0.013 J cm^{-2} (0.06 mW cm^{-2}) at the surface of the tongue and a maximum of 1.5 J cm^{-2} (7 mW cm^{-2}) in the oropharynx; no tissue damage was observed in the risk area. Measured fluence rates varied between 70 mW cm^{-2} and 440 mW cm^{-2}, with an average total fluence to the tumour target volume of 49 J cm^{-2}. We observed a systematic reduction in fluence rate during therapy in 20 out of 26 illuminations, which may be related to PDT induced increased blood content, decreased oxygenation or reduced scattering.

Conclusions: Our findings demonstrate that the applicator was easily inserted into the nasopharynx. The average light distribution in the target area was reasonably uniform (SD/mean 21%) over the length of the applicator, thus giving an acceptably homogenous illumination throughout the cavity. Shielding of the risk area was adequate. Large inter-patient variations in fluence rate, for a given incident fluence rate of 100 mW cm^{-1}, stress the need for in-vivo dosimetry. This enables corrections to be made for differences in optical properties and geometry resulting in comparable amounts of light available for Foscan® absorption.

Introduction

At present we are investigating the feasibility of using meta-tetrahydroxyphenyl chlorin (Foscan®) mediated photodynamic therapy (PDT) for nasophharyngeal carcinomas (NPC) as an alternative or additional treatment modality to current treatment protocols using combined chemo- radio and brachytherapy

The few published studies of PDT for nasopharyngeal cancer show a very variable clinical outcome. In studies where nasopharyngeal carcinomas were included in a larger series of head and neck cancers, light dosimetry was not systematically employed and treatment parameters varied per patient[1-3]. Other studies used manual positioning of the laser light through an endoscope[4,5]. The only example in the literature with a systematic approach to light delivery is from Lofgren et al[6] using the photosensitiser Photofrin. They used a specially developed rigid light delivery system, inserted through the nose into the nasophanryngeal cavity, with a beam deflector (mirror) at the distal end to direct light upwards. Results from five patients were reported with variable clinical results.
All published studies used the first-generation photosensitiser Photofrin or hematoporphyrin derivative (HpD). The side effect of long-term generalised photosensitisation induced by this drug, combined with the variable outcome of tumour response, resulted in cessation of these studies. We believe that the previous attempts to perform PDT in the nasopharynx were all hampered by inadequate light delivery due to the difficult accessibility of the nasopharynceal cavity. This seriously decreased the clinical effectiveness of these preliminary clinical experiments.

The nasopharyngeal cavity is located behind the septum and above the soft palate, and can be accessed through the nose or the oral cavity. Previously, we developed a flexible silicone device, the Rotterdam Nasopharynx Applicator[7], (RNA) to accurately position brachytherapy sources via the nose. Based upon this RNA concept, an applicator was developed to facilitate an accurate, controllable and reproducible approach to the delivery and monitoring of light in the nasopharyngeal cavity. The applicator was successfully evaluated in optical phantoms and volunteers (H. Nyst *et al* to be published).
Controlled light delivery is essential for local control of the tumour, while limiting PDT induced tissue damage to critical structures. In-vivo monitoring of fluence rate is also essential, since in hollow organs the actual fluence rate at the tissue surface is strongly increased due to reflections and backscattering from the tissue. This fluence rate amplification within a hollow cavity varies strongly with its shape and tissue optical properties, and has been reported to be as high as a factor of 7.5 for the bladder[8]. In situ fluence rate measurements in other PDT applications, such as the bladder, the oesophagus[9], the oral cavity[10], the thoracic cavity[11] and the trachea[12] emphasised the need for dedicated light delivery systems with an integrated in situ fluence rate measurement. Such an approach may contribute significantly to a standardisation of clinical response and a decrease in complications due to over-treatment. Furthermore fluence rate measurements can also reflect tissue changes in physiology as a direct result of PDT induced tissue

damage during treatment. Different fluence rates can also have a dramatic influence on the physiological response to PDT.

In this study, *in vivo* fluence rate measurements were conducted during a phase I/II study with the primary aim of lowering the drug dose and reducing the drug light interval, in order to reduce the duration of skin photo sensitisation and hospitalisation. Patients were divided into 2 Drug-Dose (DD) – Drug-Light-Interval (DLI) groups. Group 1: DD, 0.15 mg kg^{-1}; DLI, 96 hours; as recommended for the treatment of squamous cell carcinoma of the head and neck13-16. Group 2: DD of 0.10 mg kg^{-1} and a DLI of 48 hours to investigate PDT response and the time course of skin photosensitivity.These clinical data will be presented elsewhere.

Here we report on the effectiveness of shielding by the applicator in the risk areas such as the soft palate, tongue and tonsils. Secondly, we report on fluence rate measurements in the tumour target area, to investigate inter-patient variations, the fluence rate distribution in the nasopharyngeal cavity and PDT induced changes in fluence rate during Foscan® mediated PDT.

Materials and methods

Five patients were initially treated in a pilot study at the Netherlands Cancer Institute, with good clinical results. Due to the much higher incidence of NPC in Indonesia, the multi-center phase I/II study was subsequently carried out in Indonesia at the ENT departments of the Dr. Sardjito Hospital in Yogjakarta, and the Dr. Cipto Mangunkusumo Hospital in Jakarta.

Applicator

The applicator is depicted in figure1a on page 37, and the applicator with respect to anatomical locations is schematically shown in figure1b. The nasopharynx PDT applicator consists of two 220 mm long silicone tubes positioned through the nasal cavity, covering the nasopharynx up to the upper part of the oropharynx. Both tubes were interconnected at the distal end by a small silicone bridge, which abuts proximally to the nasal septum and that approximates the shape of the nasopharyngeal cavity [7]. The lateral distance between the tubes is 16 mm. The applicator-bridge is made out of medical grade silicone (Meprolastik, Biotool, Hengelo, The Netherlands) and remains *in situ* for the duration of the treatment (approximately 30 minutes). The bridge is perforated with two 5 mm holes to enhance flexibility. The inner diameter of the two silicone tubing (o.d.6 mm, i.d. 4 mm, PB, Barendrecht, The Netherlands) can accommodate a standard flexible implant tube (OD 6F, Nucletron, Veenendaal, The Netherlands) for improved guidance of the isotropic probes. Furthermore, both silicon tubes, house additional black tubes for guidance and shielding of the cylindrical diffusers, these shielding tubes end at the point where the bridge is in contact with the septum. This enables variable diffuser lengths to be used without adjustment of the laser output power; thus diffuser lengths are tailored to individual patients preventing light from entering the nasal cavity.

A removable flexible black silicon patch is applied to protect the whole soft palate and prevents light from entering the oral cavity. The black patch can also be tailored to fit the patient, depending on the oro-nasapharyngeal dimension. A 60 or 40 mm cylindrical diffuser (Biolitec, Bonn, Germany) connected to a single port 652 nm 2W diode laser (Ceralas PDT, Biolitec, Bonn, Germany) was used as the light source.

Dosimetry

The dosimetry device is constructed out of a 19 inch chassis with an universal AC power supply (PXI-1045 18-Slot 3U, National Instruments), with an 2.5 GHz embedded controller i.e. PC (PXI-8187 P4, National Instruments). Two 2-channel power measurement modules (PX2000-306-SS, BFI Optilas, Alphen aan de Rijn, The Netherlands) were used to detect the light from the isotropic detectors. The four isotropic detectors were connected via FC connectors to the power measurement modules and calibrated in an integrating sphere with a well-defined fluence rate. This calibration unit was incorporated into the chassis. LED's that generate the calibration fluence rate in the integrating sphere were controlled by a high-resolution analog output board (PXI-6704, National Instruments). The fluence rate in the integrating sphere was monitored by a digital multi meter unit (PXI-4070, National Instruments) connected to a photo-diode to ensure a constant and reproducible fluence rate. The fluence rate at the surface of the applicator was measured using a fibre-optic isotropic detector (model IP tip OD 0.85 mm, Medlight, Switzerland) that collects the sum of the primary incident light from the cylindrical diffuser and the tissue back-scattered light. All modules were simultaneously controlled by a single Labview™ program, which enables calibration, real time fluence and fluence rate measurements and data storage.

Prior to clinical application the NPC PDT applicator was first tested in the absence of tissue i.e. in optical tissue phantoms in air, and in five volunteers (data will be presented elsewhere). The fluence rate distribution over the applicator surface in air and tissue optical phantom was found to be homogeneous (SD/mean 3.8% and 18.3% respectively).

Patients

Fourteen patients were enrolled in the study complying with the following inclusion criteria: male or a non-pregnant, non-lactating female, at least 18 years of age and legally competent, a Karnofsky performance status of at least 70%, histologically confirmed recurrent nasopharyngeal carcinoma, type TI, II, III or IV; with a discrete tumour that was endoscopically visible and accessible for unrestricted surface illumination using a nasopharyngeal applicator, had exhausted all conventional treatment options. The procedure was performed according to a protocol approved by the local medical ethics committee and with the patient's written informed consent.

After decongestion (R/ Xylometazoline HCL1%) and topical anaesthesia, the applicator was introduced in the nose and nasopharynx trans-orally over 4 French guide tubes secured by a small silicone flange.

The applicator remained fixed in a stable position for the illumination period, during which the patient was seated in an ENT chair.

Previous studies using Foscan-PDT on early stage squamous cell carcinomas of the head and neck[13-15] demonstrated excellent clinical and cosmetic results using a fixed incident fluence rate of 100 mW cm^{-2} and a total fluence ("light dose") of 20 J cm^{-2}. Two separate illuminations were therefore performed in order to deliver a total fluence of 20 J per diffuser length (i.e. 20 J cm^{-1}) over the entire nasopharyngeal cavity at a fixed diffuser output power of 100mW cm^{-1}. The latter corresponds to a fluence rate at the surface of the applicator of approximately ~100mW cm^{-2} as measured in air. Fluence rate measurements were performed using four isotropic detectors, three located inside the nasopharyngeal cavity, and one manually held detector to measure the fluence rate on the critical structures i.e. soft palate, hard palate, tongue, tonsil left and right, oropharynx near the distal end of the PDT applicator PDT. As seen in figure 2, two isotropic detectors were placed in the tube adjacent to the cylindrical diffuser i.e. one in the middle and one at the end of the diffuser, a third detector was positioned in the empty tube.
Phantom experiments showed that approximately 5% of the maximum fluence was delivered to the empty tube located at 16 mm from the diffuser. To investigate the extent of this cross talk between illumination channels the third detector was moved during treatment progressively from the distal to the proximal end of the empty channel.

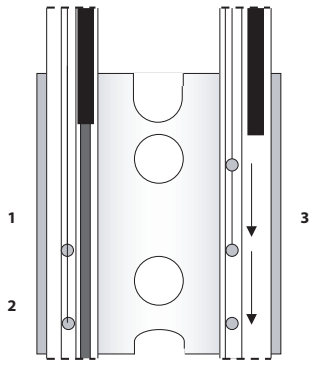

Figure 2. Schematic diagram of the position of the isotropic detectors as placed in the NPC PDT applicator. The silicon-bridge connecting both tubes is seen from above. Position 1 and 2 indicate the location of the two isotropic detectors that remained fixed in position next to the diffuser during PDT. Position 3 indicates the location of the third isotropic detector that is repositioned from the beginning, to the middle and finally to the end of the applicator. The first illumination was always on the left side after which the diffuser plus detectors were switched from tube.

Results

All patients received two illuminations i.e. left and right tube. For each illumination the cylindrical diffuser output power was fixed at 100 mW cm^{-1}, and a calculated total fluence of 20 J cm^{-1} was delivered for each tube.

Table 1 shows the average fluence of the first group of patients (n=7), delivered to the risk area locations i.e. soft palate, hard palate, tongue, tonsil left and right, oropharynx near the distal end of NPC PDT applicator. The fluence rate was calculated by multiplying the measured fluence rate by the exposure time, without taking into account possible changes in fluence rate during PDT. No PDT induced tissue damage was seen in any of the risk areas up to the three months follow-up.

Table 1. Average delivered fluence to the risk areas.

Anatomical Location	Average fluence (J cm^{-2})	SD
Soft palate	0.068	0.041
Hard palate	0.049	0.032
Tongue	0.013	0.017
Tonsil right	0.67	0.84
Tonsil left	0.66	0.74
Oropharynx	1.51	1.29

Probe 1 and 2 located in the same channel as the diffuser, measured the fluence rate during the two sided illumination in 14 patients, two software data storage failures occurred during the first illumination, thus resulting in a total of 52 measurements. The histogram in figure 3 shows the distribution of the initial fluence rate (average of the first 4 seconds) measured during the start of each of the two illuminations for all patients at the middle of the diffuser. The average fluence rate recorded by probe 1 was 245 mW cm^{-2} ranging from a minimum of 70 mW cm^{-2} up to a maximum of 440 mW cm^{-2}. This results in an average fluence at the tissue surface of 49 J cm^{-2}. A similar trend was observed for probe two, however the fluence rate at the distal location of the diffuser was significantly lower (23%) (t-test $p < 0.05$) than the average initial fluence rate at the middle of the diffuser. The average fluence rate recorded by probe 2 was 188 mW cm^{-2} (SD 63 mW cm^{-2}), with a maximum of 375 mW $cm^{-2}$and minimum of 51 mW cm^{-2}. The average fluence rate distribution over the applicator surface, was less homogeneous as compared to the measurements in air and in phantoms and was found to be 21% i.e. SD/mean (range 1.2% up to 56.0%).

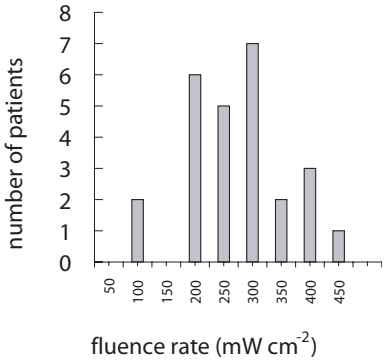

Figure 3. Histogram of the fluence rate as measured in 14 patients (n = 52 measurements), with an average of 243.4 mW cm^{-2}.

Figure 4a shows the fluence rate as a function of exposure time of a 61 years old male patient with an undifferentiated persistent NPC (T2a N1 M0). The average fluence rates at the middle and end of the diffuser (L_{dif} 40mm) were 165.6 mW cm^{-2} and 158.2 mW cm^{-2}, respectively, and varied little during treatment time. Figure 4b shows the fluence rate as a function of exposure time of a 45 years old female patient with an undifferentiated persistent NPC (T4 N2 M0). In this patient a strong decrease in fluence rate was observed over the 200 seconds exposure time. The initial fluence rates dropped by 33% and 35% respectively for probes 1 and 2. A similar pattern was observed during the second illumination. The small, transient dips in fluence rate coincide with the patient's swallowing and regurgitative spasm.

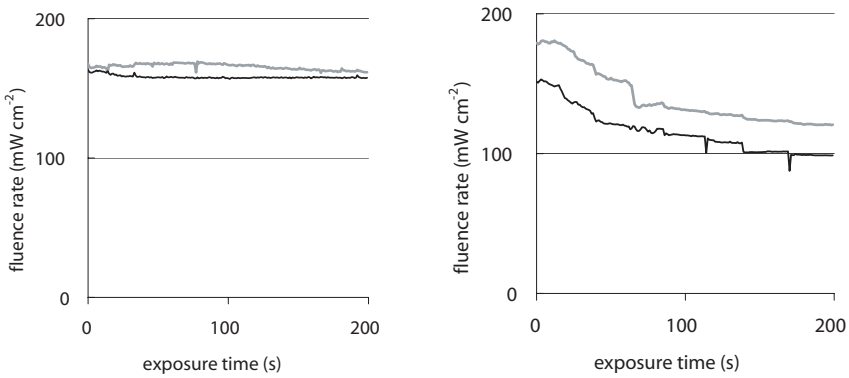

Figure 4. An example of the fluence rate as measured by detector one and two as a function of exposure time, during 200 seconds of the first illumination (left side), for two different patients a and b. The grey and black lines represent the fluence rate as measured by probe 1 and 2 respectively.

Figure 5 shows the change in fluence rate during PDT of all subjects and both illuminations as a function of the initial fluence rate i.e. the average over the first 4 seconds. No correlation between these parameters was observed (n=52, spearman's coefficient r = -0.255, P=0.0715, 95% confidence Interval for r = -0.496 to 0.022), furthermore no significant differences between both drug dose-light interval groups were observed.

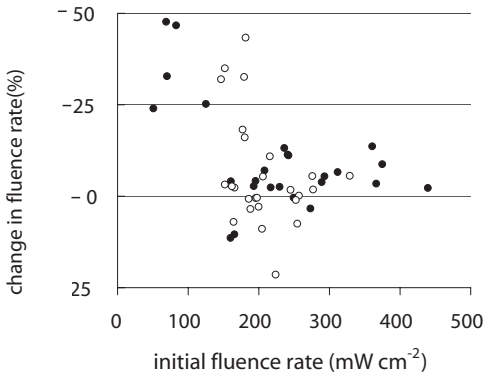

Figure 5. PDT induced change in fluence rate during treatment of all patients. A decrease in fluence rate during illumination corresponds to a negative percentage. Closed circles represent the 7 patients from group 1, DD, 0.15 mg kg^{-1}; DLI, 96 hours, and the open circles group 2 i.e. DD, 0.10 mg kg^{-1}, DLI, 48 hours

Figure 6 shows the results of the average of all fluence rate cross talk measurements of all patients. On average, a fluence rate (for the middle location) of 10.4 mW cm^{-2} is delivered contra lateral to the illumination tube to the empty tube. This corresponds to an additional fluence of ~ 2 J cm^{-2} i.e. 4% of the average 49 J cm^{-2}.

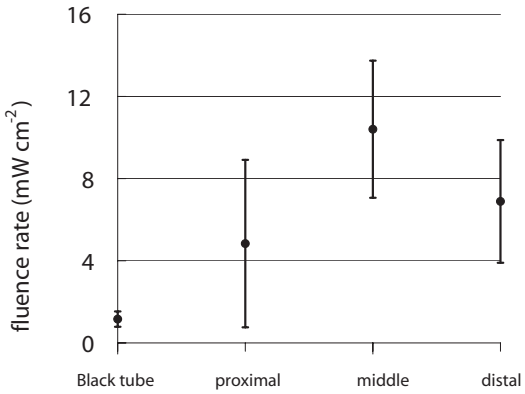

Figure 6. Fluence rate cross talk from the illumination tube to the empty tube.

Discussion

In this study, fluence rate measurements were performed in risk and target areas during Foscan® mediated NPC PDT, using a novel light applicator with incorporated isotropic detectors at strategic locations in the nasopharyngeal cavity. In the majority of clinical studies using Foscan-PDT in head and neck cancer patients, dosimetry was based upon microlense total output power and the treatment surface area, aiming to deliver an incident fluence rate of 100 mW cm^{-2} and a total fluence of 20 J cm^{-2}, without taking back scattering into account[13-16]. Only one study[10] measured the tissue surface fluence rate by means of isotropic detectors placed at the tumour centre and periphery during illumination. This study demonstrated that the fluences delivered to the oral cavity were 133% to 545% of the incident fluence. Good clinical responses without long-term side affects of the PDT were observed in all these head and neck studies. It is therefore evident that the fluence rates used result in sufficient PDT efficacy and can be safely employed in the oral cavity. However, the wide variation in the total delivered fluence for a given prescribed incident fluence, as shown by Tan *et al* [10], suggests that many patients treated with this protocol received much higher light dose than would be required for tumour control. This could be a severe drawback for PDT in areas where critical normal tissues are involved, and tissue regeneration may not be so complete as in the oral cavity.

To ensure maximal ablation of NPC with minimal normal tissue damage, it was therefore decided to include dosimetric parameters in PDT protocols for NPC.
Our measurements demonstrated a wide range of total tissue fluence rated for a given incident fluence rate, as was previously seen in the oral cavity[10]. We note that while the dosimetric parameters used in the present study were similar to those used previously in the oral cavity, the average measured fluence (rates) in the nasopharynx were relatively high (49 J cm^{-2}, 245 mW cm^{-2}). Despite the variation in tissue surface fluences between NPC patients, significant necrotic slough over the entire illuminated cavity was seen in all patients, without major complications. This may be explained by the fact that the underlying structures in the nasopharyngeal cavity is highly scattering bone which protects the deeper structures e.g. blood vessels, nerves (optic nerve) or brain tissue from PDT induced tissue damage.

We note that while the dosimetric parameters used in the present study are similar to those used previously in the oral cavity, the average measured fluence rate and fluence are relatively high (49 J cm^{-2}, 245 mW cm^{-2}). Other organs that lack an underlying bone structure, such as the oesophagus and the bronchus are more prone to PDT complications like fistulas[18-21].

Several studies have shown that the efficacy of Foscan-PDT can be optimised by lowering the fluence rate in order to reduce the rate and extent of oxygen depletion during PDT[22-24].

While it is difficult to directly translate these pre-clinical findings into the clinic, the use of a lower fluence rate may be a way of further enhancing the response of tissue to PDT. We note that high fluence rates have generally been used in clinical Foscan®-PDT of the nasophrangeal and the oral cavity. Results could potentially be improved by lowering the fluence rate. A larger randomised trial may benefit from standardisation of the low fluence rate during the illumination period.

The inter-patient variations in fluence rate originate from differences in tissue optical properties and anatomic geometry. Absorbing properties of tissues can vary according to differences in blood flow and tissue oxygenation. Large variations between patients were also seen in the dimensions of the oro- nasopharynx. In some cases the applicator bridge had to be reduced in size in order to insert the applicator properly. In phantom measurements in air, the fluence rate remained constant over the length of the diffuser but in vivo the fluence rate at the distal end of the diffuser was 23% lower than the average fluence rate at the middle of the diffuser. Despite these low fluence rates, substantial necrosis was still observed to 5mm beyond the diffuser tip. We believe that this decrease can be explained by integrating cavity theory. In the nasopharyngeal cavity approximately 75% of the surface consists of scattering tissue and only 25% comprises the highly absorbing black patch protecting the soft pallet, whereas towards the orophanrynx the ratio between the scattering tissue and the patch is more likely to be 1; resulting in a lower fluence rate. To improve the light distribution profile we are currently developing patches that are highly scattering on the inside, and black on the side of the nasopharynx.

A number of factors influence the variation in fluence rate that we observe during illumination. These include increased tissue haemoglobin content, changes in tissue oxygenation due to oxygen consumption during PDT, changes in perfusion or, to a lesser extent decreased scattering[25]. These parameters were not measured directly in the present study but they may also play a role in the PDT induced clinical response. For example, the absorption contrast between oxy- and deoxy haemoglobin reaches it maximum at around 650 nm. A 50% drop in oxygenation during illumination would increase the absorption coefficient by a factor of 3.4; clearly altering the cavities optical properties since blood is the major absorber at this wavelength.

No PDT induced tissue damage in any of risk areas was observed, demonstrating sufficient shielding. However delayed regeneration of normal oropharyngeal mucosal was observed in 5 out of 6 patients in group I. In this group all patient where treated with diffuser lengths of 5 - 6 cm. It was therefore decided to use 4 cm diffuser lengths for the second group of patients, to ensure full closure of the soft palate and the oropharynx. The drawback of using shorter diffuser lengths is the risk of insufficient coverage of tumour margins. Prior knowledge, based on CT and MRI, on how far the tumour extends into the oropharynx, would further improve treatment planning with respect to the optimal cylindrical diffuser length. Another treatment planning aspect that should be taken into consideration is that, due to tissue backscattering, the fluence rate profile

broadens along the length of the diffusers. Based on phantom measurements (Nyst et al to be published), it is estimated that an additional 5-10mm of necrosis can be expected at the distal end of the diffuser.

Measuring the fluence rate at the risk areas required use of a tongue spatula to expose the region of interest. In combination with the inserted NPC applicator, this induced stress and regurgitative spasm to the patients. Since the initial measurements demonstrated only low fluence rates in shielded areas, these measurements were discontinued for the second group of patients.

Conclusion

In conclusion, our findings demonstrate that the applicator is easily inserted and enables for the delivery of a reasonably homogeneous light distribution (i.e. SD/mean 34%) in the target area, with adequate shielding of the risk area. Inter-patient variations in fluence rate stress the need for in-vivo dosimetry, to allow for correction of differences in optical properties and anatomic geometry between patients and thus deliver a comparable amount of light available for Foscan® absorption. Eleven out of 13 patients seen three months after PDT were biopsy proven tumor free.

In a future planned randomised phase III study, dosimetry will be further fine-tuned and based upon in vivo real-time fluence measurements and delivering a standardised fluence to the tissue surface. Furthermore the use of lower fluence and fluence rate may further improve the complete response rate.

References

1. Stranadko EF, Garbuzov MI, Zenger VG, Nasedkin AN, Markichev NA, Riabov MV and Leskov IV. Photodynamic therapy of recurrent and residual oropharyngeal and laryngeal tumors. *Vest Otorinolaringol*. 2001 **3:** 36-39.

2. Schweitzer VG. Photodynamic therapy for treatment of head and neck cancer. *Otolaryngol Head Neck Surg*. 1990 **102:** 225-232.

3. Sun ZQ. Photodynamic Therapy of nasopharyngeal carcinoma by argon or dye laser, an analysis of 137 cases. *Zhonghua Zhong Liu Za Zi.* 1992 **14:** 290-292.

4. Kulapaditharom, B. and Boonkitticharoen V. Photodynamic therapy for residual or recurrent cancer of the nasopharynx. *J Med Assoc. Thai.* 1999 **82:** 1111-1117.

5. Tong MC, van Hasselt CA and Woo JK. Preliminary results of photodynamic therapy for recurrent nasopharyngeal carcinoma. *Eur Arch Otorhinolaryngol.* 1996 **253:** 189-192.

6. Lofgren LA, Hallgren S, Nilsson E, Westerborn A, Nilsson C and Reizenstein J. Photodynamic therapy for recurrent nasopharyngeal cancer. *Arch Otolaryngol Head Neck Surg.* 1995 **121:** 997-1002.

7. Levendag PC, Peters R, Meeuwis CA, Visch LL, Sipkema D, de Pan C and Schmitz PI. A new applicator design for endocavitary brachytherapy of cancer in the nasopharynx. *Radiother Oncol.* 1997 **45(1):** 95-8.

8. Marijnissen HPA, Jansen H and Star WM. Treatment system for whole bladder wall photodynamic therapy with in vivo monitorring and control of light dose rate and dose. *J Urol.* 1989 **142:** 1351-1355.

9. Van Veen RL, Aalders MC, Pasma KL, Siersema PD, Haringsma J, van De Vrie W, Gabeler EE, Robinson DJ and Sterenborg HJ. In situ light dosimetry during photodynamic therapy of Barrett's esophagus with 5-aminolevulinic acid. *Lasers Surg Med.* 2002 **31:** 299-304.

10. Tan IB, Oppelaar H, Ruevekamp MC, Veenhuizen RB, Timmers A, and Stewart FA. The importance of in situ light dosimetry for photodynamic therapy of oral cavity tumors. *Head Neck.* 1999 **21:** 434-441.

11. Baas P, Murrer L, Zoetmulder FA. Stewart FA, Ris HB, van Zandwijk N, Peterse JL and Rutgers EJ. Photodynamic therapy as adjuvant therapy in surgically treated pleural malignancies. *Br J Cancer.* 1997 **76:** 819-826.

12. Murrer LHP, Marijnissen HPA, Baas P and Star WM. Applicator for light delivery and in situ light dosimetry during endobronchial photodynamic therapy: first measurements in humans. *Lasers Med Sci.* 1997 **12:** 253-259.

13. Copper MP, Tan IB, Oppelaar H, Ruevekamp MC and Stewart FA. Meta-tetra(hydroxyphenyl)chlorin photodynamic therapy in early-stage squamous cell carcinoma of the head and neck. *Arch Otolaryngol Head Neck Surg.* 2003 **129(7):** 709-11.

14. Hopper C, Kubler A, Lewis H, Tan IB and Putnam G. mTHPC-mediated photodynamic therapy for early oral squamous cell carcinoma. *Int J Cancer.* 2004 **10;111(1):** 138-46.

15. D'Cruz AK, Robinson MH and Biel MA. mTHPC-mediated photodynamic therapy in patients with advanced, incurable head and neck cancer: a multicenter study of 128 patients. *Head Neck.* 2004 **26(3):** 232-40.

16. Fan KF, Hopper C, Speight PM, Buonaccorsi GA and Bown SG. Photodynamic therapy using mTHPC for malignant disease in the oral cavity. *Int J Cancer.* 1997 **26;73(1):** 25-32.

17. Kubler AC, Stenzel W, Ruhling M, Meul B and Fischer JH. Experimental evaluation of possible side effects of intra-operative photodynamic therapy on rabbit blood vessels and nerves. *Lasers Surg Med.* 2003 **33(4):** 247-55.

18. Etienne J, Dorme N, Bourg-Heckly G, Raimbert and, Flejou JF. Photodynamic therapy with green light and m-tetrahydroxyphenyl chlorin for intramucosal adenocarcinoma and high-grade dysplasia in Barrett's esophagus. *Gastrointest Endosc.* 2004 **59(7):** 880-9.

19. Andrejevic Blant S, Grosjean P, Ballini JP, Wagnieres G, van den Bergh H, Fontolliet C and Monnier P. Localization of tetra(m-hydroxyphenyl)chlorin (Foscan) in human healthy tissues and squamous cell carcinomas of the upper aero-digestive tract, the esophagus and the bronchi: a fluorescence microscopy study. *J Photochem Photobiol B.* 2001 **15;61(1-2):** 1-9.

20. Savary JF, Monnier P, Fontolliet C, Mizeret J, Wagnieres G, Braichotte D and van den Bergh H. Photodynamic therapy for early squamous cell carcinomas of the esophagus, bronchi, and mouth with m-tetra (hydroxyphenyl) chlorin. *Arch Otolaryngol Head Neck Surg.* 1997 **123(2):** 162-8.

21. Murrer LH, Hebeda KM, Marijnissen JP and Star WM. Short- and long-term normal tissue damage with photodynamic therapy in pig trachea: a fluence-response pilot study comparing Photofrin and mTHPC. *Br J Cancer.* 1999 **80(5-6):** 744-55.

22. Coutier S, Bezdetnaya LN, Foster TH, Parache RM and Guillemin F. Effect of irradiation fluence rate on the efficacy of photodynamic therapy and tumor oxygenation in meta-tetra (hydroxyphenyl) chlorin (mTHPC)-sensitized HT29 xenografts in nude mice. *Radiat Res.* 2003 **158(3):** 339-45.

23. Tsutsui H, MacRobert AJ, Curnow A, Rogowska A, Buonaccorsi G, Kato H and Bown SG. Optimisation of illumination for photodynamic therapy with mTHPC on normal colon and a transplantable tumour in rats. *Lasers Med Sci.* 2002 **17(2):** 101-109 .

24. Coutier S, Mitra S, Bezdetnaya LN, Parache RM, Georgakoudi I, Foster TH and Guillemin F. Effects of fluence rate on cell survival and photobleaching in meta-tetra-(hydroxyphenyl)chlorin-photosensitized Colo 26 multicell tumor spheroids. *Photochem Photobiol.* 2001 **73(3):** 297-303.

25. Amelink A, van der Ploeg van den Heuvel A, de Wolf WJ, Robinson DJ and Sterenborg HJ. Monitoring PDT by means of superficial reflectance spectroscopy. *J Photochem Photobiol B.* 2005 **9(3):** 243-251.

5.

Wedge shaped applicator for additional light delivery and dosimetry in the diaphragmal sinus during Photodynamic Therapy for Malignant Pleural Mesothelioma

Adapted from:

R.L.P. van Veen, J.H. Schouwink, W.M. Star, H.J. Sterenborg, J.R. van der Sijp, F.A. Stewart, P. Baas. Wedge-shaped applicator for additional light delivery and dosimetry in the diaphragmal sinus during photodynamic therapy for malignant pleural mesothelioma. **Phys Med Biol. 2001: 46**(7)**: 1873-83.**

Abstract

In situ light dosimetry during Photodynamic Therapy (PDT) of Malignant Pleural Mesothelioma (MPM) after tumor resection facilitates the delivery of a controlled light distribution to the inner thoracic surface. Illumination of the diaphragm-induced sinus, however, remains difficult. Our aim was to develop a wedge shaped light applicator with incorporated light dosimetry to deliver an additional fluence limited to the sinus. The wedge shaped applicator contains a cylindrical diffuser for light delivery and two isotropic detectors for simultaneous light dosimetry. These detectors were placed at strategic positions where the fluence rate is maximal or minimal (middle and edge). Prior to its clinical use, the performance of the sinus-light applicator was tested in several optical tissue phantoms with different optical properties. The fluence rate distribution over the surface of the applicator showed little change when the wedge was submerged in four different optical phantoms. During clinical PDT of MPM the applicator had to be re-located manually 4 times in order to give an additional fluence of approximately 2 J cm^{-2} to the entire sinus. The light applicator enables dosimetry-controlled light delivery for additional illumination of the sinus region that is often under- illuminated during thoracic integral illumination of MPM.

1. Introduction

Malignant Pleural Mesothelioma (MPM) is a diffuse growing tumor of the pleura that is closely related to asbestos exposure. General prognosis for MPM is poor, with a median survival of approximately 1-year. Surgical resection alone or with adjuvant radiotherapy (Hilaris *et al* 1984) or chemotherapy (Sugarbaker *et al* 1991, Baas *et al* 1998) does not significantly improve life expectancy. Several investigators have studied the feasibility of photodynamic therapy (PDT) of the whole thoracic cavity wall as an adjuvant to surgical debulking for the treatment of MPM (Lofgren *et al* 1991, Pass *et al* 1994, Baas *et al* 1997, Ris *et al* 1996 , Moskal *et al* 1998). In some of these studies the fluence (rate) was defined by the total output power of an optical bare fiber or diffuser and the tissue surface area being treated. The complex illumination geometry and tissue light- backscattering were not taken into account and this may result in an inhomogeneous light distribution.
The complexity of the geometry is mainly due to the absence of lung mass after surgical resection. As a result the diaphragm folds upwards into the thoracic cavity and forms a region (sinus), also referred to as diaphragmatic gutter (Pass *et al* 1994), which is partially shielded from the integral illumination. We believe that accurate real time light dosimetry is essential to achieve a homogeneously distributed fluence over the entire hemithoracic surface, in order to prevent under/overdosing. In our ongoing Phase II study (Baas *et al* 1997, Klaase *et al* 2000, Schouwink *et al* 2001 in press), *in situ* light dosimetry with four isotropic detectors was performed in 25 patients in total. Four isotropic detectors were placed on the treated surfaces measuring both the direct incident light from the spherical diffuser and the tissue-backscattered light. Probes were usually placed in the diaphragmal sinus and at the apex of the lung. The two remaining probes were placed at tissue structures that are more prone to complications as a result of PDT induced tissue damage like the oesophagus, pericardium, bronchial stump and the at entrance site (scar). In order to improve the illumination geometry a plastic transparent sterile stomach bag was placed inside the thoracic cavity prior to PDT and filled with saline to push the diaphragm back towards the abdominal cavity. In our clinical studies we showed that illumination of the sinus remained difficult in 11 out of 25 patients despite this approach. Similar problems were also reported by Pass *et al* (1995). In these cases, the saline filled stomach bag was removed and one or more additional illuminations were performed in the sinus using either a microlens or a spherical diffuser and exposing the sinus by manually pressing down the diaphragm. This however results in overlapping light fields and uncontrolled light dosage. In some cases this approach also led to an additional fluence of approximately 2 J cm^{-2} being delivered to regions that had already received the desired fluence; these areas consequently may have been overdosed. In order to improve the additional illumination to the sinus in a controlled way, a light applicator was developed. The applicator is wedge shaped, separating the diaphragm from the thorax wall with minimal force and exposing the sinus. Since minimal force is applied to the tissue the applicator is assumed not to intervene with the blood (oxygen) supply which is considered to be of vital importance for

PDT effectiveness. The applicator includes two isotropic detectors that enabled us to measure the fluence (rate) in the sinus at positions where the fluence rate is maximal and minimal. In the present paper we present the technique of constructing the applicator as well as the results of measurements performed in liquid optical phantoms having different scattering and absorption coefficients in order to asses the fluence rate distribution at relevant positions at the surface of the applicator. Based on these results we have designed an illumination procedure for an optimally distributed fluence to be delivered to the sinus only. Furthermore we present the light dosimetry results of the applicator applied clinically in one patient to demonstrate the practical feasibility of the procedure.

2. Materials and Methods

2.1. Light applicator

The wedge- shaped light applicator was constructed using a flexible silicone polymer (Biotool, Hengelo, The Netherlands). The material is partially transparent with low diffusing properties. First a Styrofoam model of the wedge was made and used to create a plaster mould. The plaster mould contained three prefixed catheters (Transfusion Set, CODAN, Germany). One catheter, for the cylindrical diffuser was positioned in the centre at the bottom of the applicator. Two catheters for the isotropic detectors were positioned in the middle and at the bottom edge of the applicator 0.5-mm beneath the surface.
The silicone was poured (not polymerized yet) into the plaster mould and left to harden. A vacuum chamber was used to prevent the formation of air bubbles (Bays *et al* 1997). The shape of the applicator (locations 1–11, Figure 1) follows the curvature of the diaphragm.

The side indicated by location 11-23 (Figure 1) is pressed against the mediastinum or thorax wall. The cylinder at the bottom indicates the position of the catheter for the cylindrical diffuser. The length (z) and the height of the applicator (locations 11-23) were 100mm and 75mm respectively. The total length of the catheters was 1.5 m.

2.2. Fluence rate distribution

The influence of the medium surrounding the applicator on the fluence rate distribution at the surface of the sinus-light applicator was determined in tissue optical phantoms with different optical properties. The phantoms were composed of Intralipid (Pharmacia & Upjohn BV, Netherlands), Evans blue (Janssen Chimica, Belgium) and saline (van Staveren *et al* 1991). The optical properties of the four phantoms used are given Table 1. The in-vivo reduced scattering and absorption coefficients of human diaphragm are assumed to be in the range between phantom 1 and 2. Measurements were performed in a tank (20×20×20 cm) with the sinus- light applicator completely submerged (Figure 2).

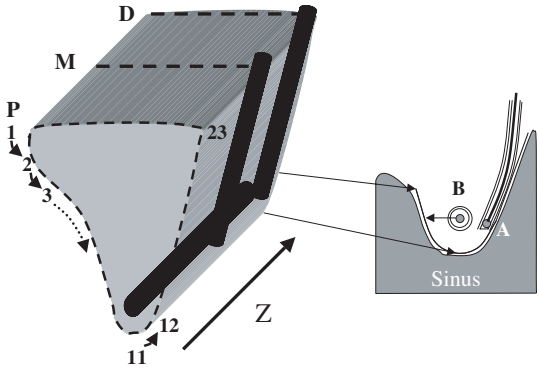

Figure 1. Schematic representation of the silicone sinus light applicator. The two vertical cylinders represent the position of the catheters for the isotropic detectors. The cylinder at the bottom is where the cylindrical diffuser is positioned. P, M and D indicate the proximal, mid and distal measurement planes on the applicator. Z is the total length (100 mm). The numbers 1 to 23 indicate the measurement positions. On the right a cross-section of the bottom of the wedge placed in the sinus. (A) The isotropic detectors inside the catheter are approximately 1 mm from thorax wall, (B) the cylindrical diffuser is centrally positioned at the bottom (sinus) of the wedge.

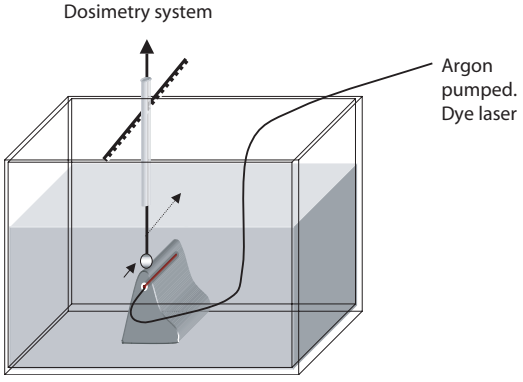

Figure 2. Set-up for measuring fluence rate distribution. Measurements were performed with an isotropic detector (1), and were taken every 5 mm over the total length of the bottom of the wedge (2) (locations P11-D11 as depicted in figure 1). Three tracks at the proximal, mid and distal end of the wedge were also measured. The latter was performed in 23 steps with approximately 7 mm spacing between each measurement location.

The fluence rate at the surface of the applicator was measured using a fibre-optic isotropic detector (400 µm core diameter fibre Pseudo Sphere, 1mm tip diameter, Cardiofocus, formerly Rare Earth Medical, West Yarmouth MA, USA), measuring the sum of the primary incident light and the scattered light. The response of the detectors was isotropic within ±5% (van Staveren *et al* 1995). The isotropic probes were connected to an electronic device that enables

real time fluence (rate) measurements. The electronic device was connected to a PC for storage and processing of the measured data. Calibration of the detectors was performed in a built-in integrating sphere that provides a well-defined diffuse calibration field. The dosimetry software uses a factor to correct for the difference in response of the detectors when measurements are performed in water, relative to air (Marijnissen *et al* 1996). A 50 mm long cylindrical diffuser (600 μm fiber core diameter, Cardiofocus, West Yarmouth, MA, USA) was inserted through a saline filled catheter into the applicator and aligned in the centre. Light sources used were an Argon pumped dye laser (Spectra Physics model 2040E / 375B) for the phantom experiments and a 652 nm diode laser (Applied Optronics 6W, South Plainfield, NJ, USA) for PDT.
An aluminium strip was folded into the shape of the wedge and was used to press the fiber of the isotropic detector gently against the surface of the sinus-light applicator. The distance between the actual detection tip and the strip was 15 mm. The strip was marked to indicate the measurement positions on the applicator. The distance between each marking was 7 mm, resulting in 23 measurement positions per plane (Figure. 1). Measurements were performed at the mid plane (*M*, z=50mm), the proximal plane (*P*, z=5 mm) and distal planes (*D*, z = 95mm) from locations P,M,D, 1-23, Figure 1 of the applicator. The fluence rate distribution at the bottom (Locations P11-D11, Figure 1) was measured by scanning the isotropic detector every 5mm over the total length (z) of the applicator as depicted in Figure 2.

The total perimeter length of the sinus is larger than the length of the applicator. Therefore, several sequential illuminations are necessary in order to illuminate the entire sinus i.e. the applicator has to be repositioned (shifted) in the sinus over a certain curvature length (L). Based on the results of the fluence rate distribution at the bottom of the wedge, (P11-D11, figure 1) we calculated the cumulative fluence rate distribution as a result of two illuminations, the first at position x and the second at position (x + L). The applicator's maximum and minimum shift (L) with a tolerance of ±15% of the desired fluence rate was calculated for phantoms 1,2 and 3.

2.3. Clinical procedure

A 67-year-old man was referred to the Daniel Den Hoed Cancer Center for the treatment of MPM. After surgery the PDT procedure was performed according to a protocol approved by the medical ethics committee and with the patient's written informed consent. The PDT procedure was as follows: Four days prior to illumination, 0.1 mg/kg mTHPC (Scotia Pharmaceuticals, Stirling, Scotland) was i.v. administered to the patient. For the last patient in this phase II study we had two dosimetry devices at our disposal. After a pleuropneunonectomy and tumor debulking, six isotropic probes were positioned at the surface of the thoracic cavity to monitor the fluence-rate (incident plus scattered) distribution using two 4-channel dosimetry devices developed in our group and described elsewhere (Baas *et al* 1997). The probes were inserted in sterile catheters (Transfusion Set, CODAN, Germany) filled with saline so that the refractive index of the surrounding medium matched (Marijnissen *et al* 1996). Two detectors were positioned in the sinus (ventral and dorsal). Four detectors were placed on the following positions: one

the oesophagus, one near the pericardium, one at the apex and one at the ventral thorax. The remaining two detectors were reserved for the sinus- light applicator. Prior to illumination, a sterile transparent stomach bag (Steri-Drape, 3M) was placed inside the thorax cavity and filled with saline (3-4 liters at body temperature) to optimize the illumination geometry by pressing diaphragm back towards the abdominal cavity. Light from a 652nm diode laser was delivered by a 600 μm core fiber spherical diffuser (Cardiofocus, West Yarmouth, MA, USA) which was positioned manually so that a total fluence of 10 J cm^{-2} was distributed approximately uniformly over the hemithoracic surface. Prior to PDT the two probes and the cylindrical diffuser were positioned inside the sinus applicator. The applicator was then placed in a sterile transparent cover (Video Camera Cover, International Medical Products B.V., Netherlands). After the first integral illumination, the stomach bag was removed and all six probes remained in position. The sinus- light applicator was positioned manually into the sinus and a total of four sequential illuminations were given each with a maximal fluence of 2 J cm^{-2}.

3.Results

3.1. Phantom model

The position codes of Figure 1 are used as reference. The fluence rate distribution over proximal, mid and distal plane was determined. Figure 3 shows the normalized (to the maximum at location M11) fluence rate distribution over the mid (M1-M23) plane for 4 different optical phantoms.

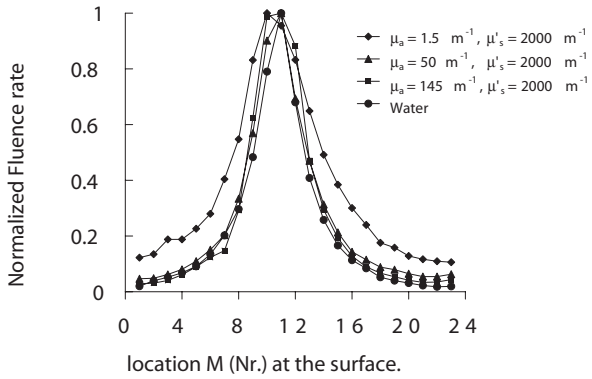

Figure 3. Normalized Fluence rate distribution over the middle cross section (M) of the applicator for 4 different optical phantoms. A total number (Nr) of 23 fluence rate measurements were performed from M1 to M23 (see Figure 1).

The fluence rate distribution for the proximal (P1-P23) and distal (D1-D23) planes showed a similar bell-shape curvature as the mid plane. The average fluence rate on top of the applicator (P1+P23+M1+M23+D1+D23)/6 were 12%, 5%, 2%, and 3% of the maximum fluence rate at position M11 for phantoms 1, 2, 3, and 4 respectively (Table 1).

Table 1. Optical properties of all four phantoms

λ = 652 nm	μ_a (m^{-1})	μ_s' (m^{-1})
1 Intralipid*	1.49	2000
2 Intralipid /Evans Blue	50	2000
3 Intralipid /Evans Blue	145	2000
4 Water	<0.010	<0.010

** van Staveren H. et al 1991*

Figure 4 shows the normalized fluence rate distribution over the entire length (z) where measurements were taken every 5 mm from (positions P11 –D11) over the bottom of the applicator for all four phantoms. The average fluence rate (P11+D11)/2 at the bottom edges were 26 %, 12 %, 9%, and 6% of the maximum fluence rate at position M11 for phantoms 1, 2, 3, and 4 respectively.

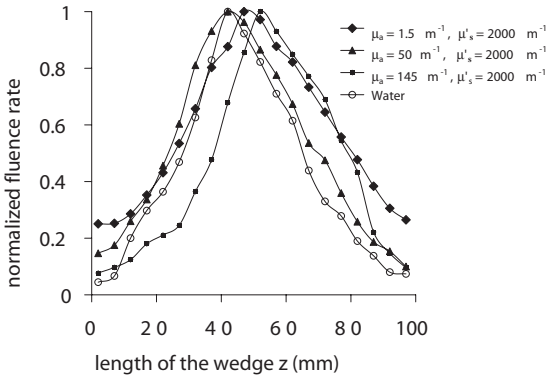

Figure 4. Normalized Fluence rate distribution over the bottom plane (P11-D11 as depicted in figure 1) of the applicator for 4 different optical phantoms.

For clinical use the sinus applicator has to be repositioned (shifted) over a length, L, in order to deliver an approximately homogeneous fluence to the entire sinus. Figure 5 shows an example of the cumulative fluence as result of n=4 sequential illuminations. For these calculations the applicator was shifted 3 times over a length L of 52 mm. These calculations were based on the fluence rate distribution at P11, D11 for phantom 2.

If illumination 4 (Figure 5) overlaps illumination 1 by L = 52mm a homogeneous fluence with a tolerance of ±15% of the desired fluence is delivered to a total sinus perimeter length of 208 mm (n◊L). Table 2 shows the maximal and minimal shifts (± 15% of the desired fluence) for three different phantoms. The tissue optical properties of the diaphragm and underlying tissue are assumed to be in the range between phantom number 1 and 2. Based on this assumption a shift L of 50mm ± 10mm can be expected in a clinical setting.

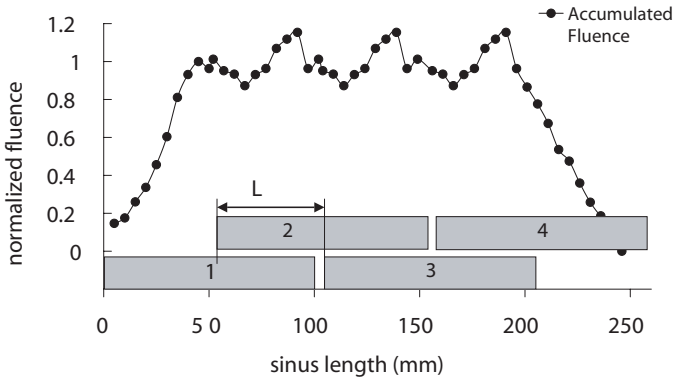

Figure 5.Example of the cumulative fluence distribution (solid circles) for four sequential illuminations in the diaphragmal sinus. The sinus light applicator is shifted in the z-direction over (L = 52 mm) in the sinus after each illumination. In this manner an optimally homogeneous fluence distribution (within +/- 15 % of the desired fluence) is delivered to the sinus over a total length of 208 mm.

3.2. Clinical light delivery and dosimetry

The oesophagus is potentially at risk for PDT damage due to its thin walled nature. After extensive tumor resection the thickness of the remaining oesophageal wall was approximately 3 mm. To avoid the risk of an oesophageal perforation this was covered with green cloth to shield it from illumination. An isotropic detector was placed below the cloth at the surface of the tissue to monitor possible exposure. Figure 6 shows that this reduced the fluence to this critical site to 0.24 J cm^{-2}, whereas total fluences of 5 to 12 J cm^{-2} were delivered to the non-shielded part of the thoracic cavity during the first illumination with a 4 W output spherical diffuser. The diaphragmal sinus was underdosed relative to the rest of the thoracic cavity. The fluence delivered in dorsal and ventral sinus during the integral illumination was 5.4 J cm^{-2} and 6.3 J cm^{-2} respectively.

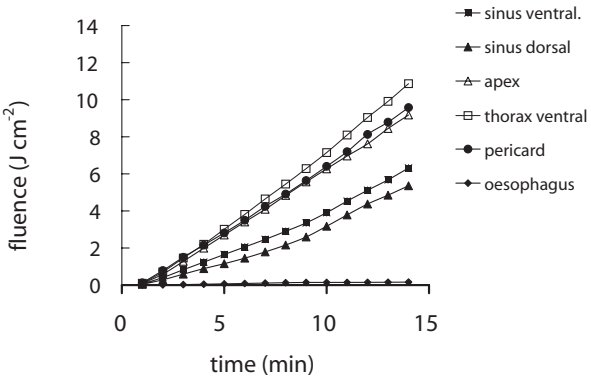

Figure 6. Fluence (J cm^{-2}) versus time (min) delivered at six detector positions in the thoracic cavity. Desired total fluence of 10 J cm^{-2} for all six positions. First illumination performed with a spherical diffuser and the second illumination with the sinus- light applicator. The apex, thorax ventral and pericardium received approximately 10 J cm^{-2}, sinus ventral, sinus dorsal received 5.4 J cm^{-2} and 6.3 J cm^{-2} respectively. Oesophagus was protected with green cloth and received a total fluence of 0.24 J cm^{-2} over both sessions.

Table 2. The minimal and maximal length (L) over which the applicator can be shifted in order to stay within +/- 15% of the desired fluence in the region were the applicator overlaps.

Phantom	μ_a (m^{-1})	μ_s' (m^{-1})	Minimal shift L (mm)	Maximal shift L (mm)
3	145	2000	42	47
2	50	2000	47	57
1	1 .49	2000	57	67

The sinus was then given a second illumination (consisting of four separate sequential illuminations) using the sinus-light applicator. The total additional illumination time of the entire sinus was 8 min. Since this was the first experimental clinical trial of the applicator and no previous experience was available, we decided to deliver low fluences to the sinus region (2 J cm^{-2}) and an extra low fluence of 1 J cm^{-2} to the mediastinum. Four sequential illuminations were applied to cover the complete sinus. First the applicator was gently positioned in the vicinity of the ventral sinus and a fluence of 2.9 J cm^{-2} was delivered, after which the applicator was shifted towards the lateral sinus over a length (L) of approximately 60mm where a fluence of 2 J cm^{-2} was delivered.

Table 3. Fluence (rate) delivered to the diaphragm-induced sinus by the applicator given as the mean and standard deviation.

Position Sinus	Fluence rate mW cm^{-2}		Fluence J cm^{-2}	
	M*	D*	M	D
Ventra l	124 (9)	40 (3)	2.9	0.9
Lateral	69 (7)	26 (3)	2.0	0.8
Dorsal	70 (6)	29 (3)	2.2	0.9
Mediastinum	81 (14)	18 (4)	1.2	0.3

**M middle, D distal end of the applicator*

This was repeated for the dorsal and mediastinum sinus thus covering a total sinus length of approximately 210mm. More details of the extra fluence (rate) at the surface of the sinus for each position are given in table 1. The fluence rate at the distal side (location D 11) was on average 33% (SD 9%) of the maximum fluence rate measured in the middle of the wedge (location M11).

4. Discussion and Conclusions

The fluence rate distribution over the surface of the applicator did not strongly depend on the tissue optical properties as seen in Figure 3, and 4. Our aim was to develop a light applicator that would deliver a fluence to the sinus with minimal radiance emitting from the top of the applicator, that is in the direction of the pre-illuminated thoracic cavity. The phantom model results show that 2 to12 % of the maximal fluence rate (location M11) is emitted in the direction of thoracic cavity. The latter was confirmed by our clinical measurements since the fixed probes (apex, thorax ventral, pericardium and oesophagus) measured a only minor additional fluence as result of the four sequential wedge illuminations. During clinical MPM PDT the fluence rate at the distal side of the applicator was 33% (SD 9%) of the maximal fluence rate in the middle of the applicator. This is higher than measured in phantom models 1,2 and 3 respectively, which can be explained by the fact that the proximal and distal sides were not pressed against the tissue but were in contact with air resulting in a mismatch in refractive index whereas in the phantom model the applicator was completely submerged. The mismatch in refractive index causes an increased build up in fluence rate due to a higher internal diffuse reflectance coefficient.

The results shown in Figure 5 were based on 4 sequential illuminations with the applicator shifted over a length L = 52mm and resulted in a homogeneously distributed fluence delivered to a sinus length of 208mm. In a clinical setting however, the total sinus perimeter length differs between individuals, and therefore the number of illuminations (n) times the optimal shift length L (n◊L) is not always in agreement with the actual sinus perimeter length. This could result in under-dosing over a short length of the sinus.

In other MPM-PDT studies only the total output power and spot-size of a bare optical fiber defined the light dosimetry. This may have led to inaccurate light dosing as results of spot-size uncertainties due to the complexity of the illumination geometry (Ris *et al* 1991, 1996). Pass *et al* (1994, 1995) measured *in situ* the incident irradiance at the tissue surface during MPM- PDT with flat photodiodes mounted at strategic positions in the thoracic cavity. This can result in under dosing underneath the surface of photodiode leaving tumor cells untreated. This effect is negligible for small isotropic detectors (de Jode *et al* 1999). Furthermore, these photodiodes are insensitive to back scattered light from the tissue and therefore underestimate the true fluence rate (Vulcan *et al* 2000). Takita *et al* (1994, 1995) and Moskal *et al* (1998) based their dosimetry on the calculation of the total area of the thoracic surface from full scale CT scans and the total light output power, without taking into account the formation of the sinus in the absence of the lung mass.

The use of isotropic detectors placed at strategic positions in combination with a spherical diffuser enables an optimal integral illumination of the thoracic cavity. The use of six instead four isotropic detectors (Baas *et al* 1997) results in a more accurate light distribution and allows two probes to be placed on structures that are sensitive to complications e.g. myocardial infarction, oesophageal perforations and bronchopleural

fistulas (Luketich *et al* 1996). The isotropic detectors are normally placed at least 10 mm above the actual sinus since suturing the sterile catheters containing the detectors is difficult in this narrow region, and this would imply that the total fluence in the actual sinus could be even lower than measured. The need for optimal light distribution during PDT has been recognized in many studies and specific light applicators have been developed e.g. for the oral cavity (Benthum *et al* 1997).

In the majority patients with MPM the tumor is concentrated in the lower part of the thoracic cavity and in the diaphragmal sinus which emphasizes the necessity for a uniform and controlled illumination in this region. For this purpose a flexible silicon based light delivery applicator with incorporated light dosimetry was developed and the fluence rate distribution over the surface of the applicator was quantified in several optical phantoms. Since the fluence rate distribution is known, by measuring the fluence rate at two critical positions we can use the advantage of overlapping surfaces to avoid under/over dosing and to optimize light delivery. In clinical use, the applicator is easy handled and enables an optimal controlled administration of an additional fluence in the diaphragmal sinus.

References

- Baas P, Murrer L, Zoetmulder FAN, Stewart FA, Ris HB, Zandwijk van N, Peterse JL and Rutgers EJTh. Photodynamic therapy as adjuvant therapy in surgically treated pleural malignancies. *Br J Cancer.* 1997 **76**: 819-826.
- Baas P, Schouwink H and Zoetmulder FA. Malignant pleural mesothelioma. *Ann. Oncol*. 1998 **9**: 139-49.
- Bays R, Wagnières G, Robert D, Theuman JF, Vitkin A, Savry JF, Monnier P and van den Berg H. Three-dimensional optical phantom and its application in photodynamic therapy. *Lasers Surg Med.* 1997 **21**: 227-234.
- Benthum van HE, Sterenborg HJCM, Meulen van der FW and Gemert van MJC. Performance of a light applicator for photodynamic therapy in the oral cavity: calculations and measurements. *Phys Med Biol.* 1997 **42**: 1689-1700.
- Hilaris BS, Nori D, Kwong E, Kutcher GJ and Martini N. Pleurectomy and intraoperative brachytherapy and postoperative radiation in the management of malignant pleural mesothelioma. *Int J Radiat Oncol Biol Phys.* 1984 **8**: 19-25.
- Jode de ML. Monte Carlo simulations of the use of isotropic light dosimetry probes to monitor energy fluence in biological tissue. *Phys Med Biol.* 1999 **44**: 3027-3037.
- Klaase JM, Swaanenburg JCJM, Schouwink H, Sosef MN, Bonfrer JMG, Zoetmulder FAN, Rutgers EJTh, and Baas P. Monitoring of impending myocardial damage after pleuropneumonectomy and intraoperative photodynamic therapy for malignant pleural mesothelioma using biochemical markers. *Photochem Photobiol*. 2000 **71**: 351-354.
- Löfgren L, Larsson M, Thaning L and Hallgren S. Transthoracic endoscopic photodynamic therapy for malignant mesothelioma. *Lancet.* 1991 337 359.
- Luketich JD, Westkaemper J, Sommers EK, Ferson PF, Keenan RJ and Landreneau RJ. Bronchoesophagoplueral fistula after photodynamic therapy for malignant mesothelioma. *Ann Thorac Surg.* 1996 **62**: 283-284.
- Marijnissen JPA and Star WM. Calibration of isotropic light dosimetry detectors based on scattering bulbs in clear media. *Phys Med Biol.* 1996 **41**: 1091-1208.
- Moskal TL, Dougherty TJ, Urschel JD, Antkowiak JG, Regal AM, Driscoll DL and Takita H. Operation and photodynamic therapy for pleural mesothelioma: 6-year follow-up. *Ann Thorac Surg.* 1998 **66**: 1128-1133.
- Pass HI, DeLaney TF, Tochner Z, Smith PE, Temeck BK, Pogrebniak HW, Kranda KC, Russo A, Friauf WS, Cole JW, Mitchel JB and Thomas G. Intrapleural photodynamic therapy: Results of a Phase I trial. *Ann Surg Oncol.* 1994 **1**: 28-37.
- Pass HI and Donington JS. Use of photodynamic therapy for the management of pleural malignancies. *Semin Surg Oncol.* 1995 **11**: 360-367.

- Ris HB, Altermatt HJ, Nachbur B, Stewart JM, Wang Q, Lim CK, Bonnett R and Althaus U. Intraoperative photodynamic therapy with m-Tetrahydroxyphenylchlorin for chest malignancies. *Lasers Surg Med.* 1996 **18**: 39-45.
- Ris HB, Altermatt HJ, Inderbitzi R, Hess R, Nachbur B, Stewart JCM, Wang Q, Lim CK, Bonnett R, Berenbaum MC and Althaus U. Photodynamic therapy with chlorins for diffuse malignant mesothelioma: initial clinical results. *Br J Cancer.* 1991 **64**: 1116-1120.
- Schouwink JH, Rutgers Eth, Sijp van der J, Oppelaar H, Zandwijk van N, Veen van RLP, Burgers S, Steward FA, Zoetmulder F and Baas P. Intra-operative photodynamic therapy after pleuropneumonectomy in patients with malignant pleural mesothelioma: dose finding and toxicity results. *Chest* in press.
- van Staveren H, Marijnissen JPA, Aalders MCG and Star WM. Construction, quality assurance and calibration of spherical isotropic fibre optic light diffusers. *Lasers Med Sci.* 1995 **10** 137-147.
- van Staveren H, Moes HJ, van Marle CJM, Prahl SA and van Gemert MJC. Light scattering of intralipid-10% in the wavelenght range of 400-1100 nm. *Appl Opt.* 1991 **30**: 4507-4517.
- Sugarbaker DJ, Heher EC, Lee TH, Couper G, Mentzer S, Corson JM, Collins JJ, Shemin R, Pugatch R, WeissmanL and Antman KH. Extrapleural pneumonectomy, chemotherapy and radiotherapy in the treatment of diffuse malignant pleural mesothelioma. *J Thorac Cardiovasc Surg.* 1991 **102**: 10- 15.
- Takita H and Dougherty T. Intracavitary photodynamic therapy for malignant pleural mesothelioma. *Semin Surg Oncol.* 1995 **11**: 368-371.
- Takita H, Mang TS, Loewen GM, Antkowiak JG, Raghavan D, Grajek JR and Dougherty TJ. Operation and intracavitary photodynamic therapy for malignant pleural mesothelioma: a phase II study. *Ann Thorac Surg* 1994 **58**: 995-998.
- Vulcan TG, Zhu TC, Rodrigues EC, His A, Fraker DL, Baas P, Murrer LHP, Star WM, Glatstein E, Yodh AG and Hahn SM. Comparison between isotropic and nonisotropic dosimetry systems during intraperitoneal photodynamic therapy. *Lasers Surg Med.* 2000 **26**: 292-301.

6.

On the importance of *in situ* dosimetry during photodynamic therapy of Barrett's oesophagus

Adapted from:

R. L. P. van Veen, D. J. Robinson and H. J. C. M. Sterenborg. Letter: On the importance of *in situ* dosimetry during photodynamic therapy of Barrett's oesophagus. submitted as a letter to **Gastrointestinal Endoscopy**

Photodynamic therapy (PDT) is an emerging treatment modality for a range of primarily malignant conditions. It is under investigation for the treatment of cancers of head and neck, bladder, lung, prostate, esophagus, brain, and skin and several non-malignant indications. So far, except for the treatment of wet-type age related macular degeneration (AMD), the break-through of PDT has proved to be challenging; many clinical applications of PDT have led to either insufficient tumor response or clinically unacceptable complications. This has led to premature cessation of many clinical studies without a full understanding of the mechanism(s) behind the variable response or the incidence of complications.

This problem is particularly evident in the application of PDT for Barrett's esophagus (BE). Despite the fact that the management of BE remains an issue of significant debate[1, 2], several clinical studies investigating PDT for BE have been performed.
Initial investigations with Photofrin[3] were followed by the use of the photosensitiser precursor aminolevulinic acid (ALA)[4] and more recently meso-tetrahydroxyphenylchlorin (mTHPC). To date four randomized clinical trials have been published on PDT of BE, three using ALA[5-8] and one using Photofrin[9]. The general response of BE to PDT reported in these studies is difficult to compare due to the use of different photosensitisers and widely varying treatment parameters. Overholt *et al* [9] used systemically administered Photofrin, whereas Ackroyd *et al* [5], Kelty *et al* [6,7] and Hage *et al* [8] used ALA but with different drug doses and light treatment regimes.

Siersema[2] recently reviewed the current status of PDT for the treatment of BE and concluded that PDT results in complete ablation in approximately 77% of patients receiving Photofrin-PDT[9] for high-grade dysplasia and between 50 - 82% using ALA-PDT. Besides skin photosensitivity, complications such as strictures do not occur in ALA-PDT but are a significant issue following Photofrin-PDT. More severe complication have been reported with mTHPC-PDT[11]. A critical question is what causes the incomplete response and complications and how can we improve clinical outcome?

We are convinced that light delivery based on *in situ* dosimetry during clinical PDT plays a vital role in preventing under- or over-treatment. The therapeutic effect following PDT depends on a combination of parameters that include drug dose, drug-light interval, and light fluence (rate). These parameters have been investigated in pre-clinical models and some stage I clinical trials optimizing PDT. It is our opinion that the influence of fluence rate on clinical PDT has been underestimated. Since the early nineteen eighties and in parallel with the development of PDT, several investigators carried out pioneering research in the field of *in vivo* light dosimetry where *in situ* light measurement methods were developed [12-15].
It was shown that the actual fluence rate in tissue does not only depend on the amount of light delivered, but also on the tissue optical properties and the geometry of the tissue, leading to a build up in fluence rate, especially in hollow organs[14]. Traditionally, the approach to light delivery in BE-PDT is to adjust the output power of the source to a value equal to the intended fluence rate multiplied by the surface area to be treated. This ignores not only the build up of fluence rate, but also the inter-patient variation in build up factor.

In a series of pre-clinical studies, Overholt *et al*[16,17] investigated this effect in normal canine esophagus and found significant variations in measured light fluence rate (S.D. ± 15%; n = 8). In a similar manner, we performed *in situ* light measurements during ALA-PDT of the BE[18]. Figure 1 shows the measured build-up in fluence rate and illustrates the dramatic inter- patient variations that occur during PDT of BE.

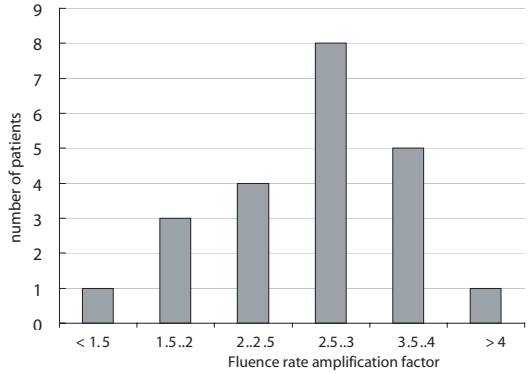

Figure 1(a) Histogram of the fluence rate build-up factor measured in situ during ALA-PDT of Barrett's esophagus that shows the delivered fluence is between 1.5 and 4 times higher than the calculated incident fluence[18].

We believe that these fluence rate variations have a critical impact on clinical response. Many studies have demonstrated the importance of fluence rate in the response of tissue to ALA-PDT. Previously we have shown a clear correlation between high fluence rate and reduced response to PDT[19]. In ALA-PDT of BE, we observed a similar correlation between high fluence rate amplification factors and incomplete response[8] (not statistically significant due to the small number of patients). In Photofrin-PDT, incomplete response and the risk of complications, particularly stricture formation, are important factors. In a recent study, Panjepour *et al* [20] investigated the relationship between the calculated light source output power and stricture formation. The authors varied the fluence from 115 J.cm^{-1} to 85 J.cm^{-1}. Overall strictures occurred on average in 23% of treated BE segments. No significant differences in the rate of stricture formation were found between treatment groups: Strictures (mild and severe) were observed in 26% of patients that received 85 J.cm^{-1} and in 22% that received 115 J.cm^{-1} (P = 0.544, Fisher's exact test). Strictures classified as severe also did not occur significantly more frequently in the highest fluence group (P = 0.677, Fisher's exact test). In our opinion, the variation in response (residual Barrett's and stricture formation) is much more likely to be a consequence of the variations in the delivered fluence. If we assume a distribution in actual fluence that is comparable to that shown in figure 1, the range in actual fluence is an order of magnitude greater than the range in the intended fluence. It is then not unreasonable to expect comparable incidence of stricture formation between treatment groups. We believe that light delivery based on *in situ* light dosimetry during Photofrin-PDT has the potential to reduce the risk of stricture formation and increase the complete response to Photofrin-PDT.

In situ light dosimetry is also critical for optimization of ALA-PDT in BE. The response of BE to a single treatment session is insufficient. This is due to the limitation on ALA dose that can be administered without toxicity induced side effects[2]. This has led investigators to perform repeat treatment sessions[7]. Another option to optimize PDT is light fractionation. We have shown increased efficacy of ALA-PDT using fractionated illumination with a 2 h dark interval between fractions[8, 21]. However, the choice of fluence for the first light fraction is critical, delivering a large fluence in the first light fraction (20 J.cm^{-2}) negates the increase in efficacy[22]. Clearly, variations in actual fluence between patients in BE make the prescription of the fluence of a particular light fraction impossible without proper *in situ* light dosimetry. We performed light fractionation during clinical ALA-PDT in a small group of patients[8] and observed a clear but not statistically significant increase in clinical response of BE over ALA-PDT with a single illumination. Critically the average fluence rate build up during the first light fraction was 2.51 ± 0.88 which resulted in an average actual fluence of 50.1 ± 17.5 J cm^{-2}. Reducing and standardizing the actual fluence using *in situ* light dosimetry is essential to enhance the response of BE to ALA-PDT.

To conclude, we believe, that utilizing *in vivo* light dosimetry, to deliver a fixed light fluence (rate) based on the *in situ* measured fluence rate would reduce the risk of stricture formation and increase complete response in Photofrin-PDT and allow standardized illumination protocols for ALA-PDT so that response can be optimized. The next critical step is to implement the technology necessary to base PDT dosimetry on the *in situ* measured fluence rate by varying the output power of the light source. It is clear that this implementation is best carried out by industry but remains the responsibility of clinicians within the PDT community to ensure that this occurs.

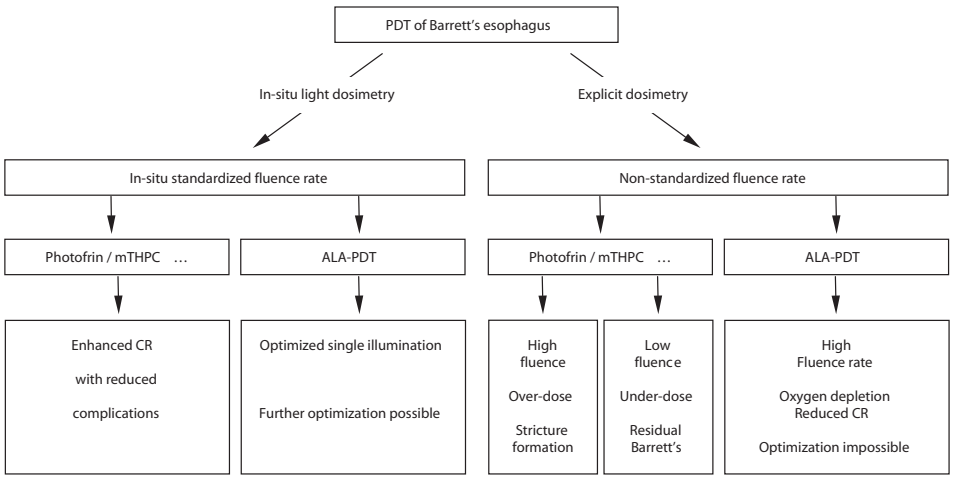

Figure 2. The consequences of not performing in situ light dosimetry during PDT of Barrett's esophagus compared to our proposed approach.

References

1. Siersema PD. Photodynamic therapy for Barrett's esophagus: Not yet ready for the premier league of endoscopic interventions. *Gastrointest Endosc.* 2005 **62**: 503-507.
2. Wolfsen HC and Carpe luz. Seize the light: endoprevention of esophageal adenocarcinoma when using photodynamic therapy with porfimer sodium. *Gastrointest Endosc.* 2005 **62**: 499-503.
3. Overholt B, Panjehpour M, Tefftellar E and Rose M. Photodynamic therapy for treatment of early adenocarcinoma in Barrett's esophagus. *Gastrointest Endosc.* 1993 **39**: 73-6.
4. Barr H, Shepherd NA, Dix A, Roberts DJ, Tan WC and Krasner N. Eradication of high-grade dysplasia in columnar-lined (Barrett's) oesophagus by photodynamic therapy with endogenously generated protoporphyrin IX. *Lancet.* 1996 **348:** 561-2.
5. Ackroyd R, Brown NJ and Davis MF, et al. Photodynamic therapy for dysplastic Barrett's oesophagus: a prospective, double blind, randomised, placebo controlled trial.*Gut.* 2000 **47**: 612-7.
6. Kelty CJ, Ackroyd R, and Brown NJ, et al. Comparison of high- vs low-dose 5-aminolevulinic acid for photodynamic therapy of Barrett's esophagus. *Surg Endosc.* 2004 **18**: 452-8.
7. Kelty CJ, Ackroyd R andBrown NJ, et al. Endoscopic ablation of Barrett's oesophagus: a randomized-controlled trial of photodynamic therapy vs.argon plasma coagulation. *Aliment Pharmacol Ther.* 2004 **20**: 1289-96.
8. Hage M, Siersema PD and van Dekken H, et al. 5-aminolevulinic acid photodynamic therapy versus argon plasma coagulation for ablation of Barrett's oesophagus: a randomised trial. *Gut.* 2004 **53**: 785-90.
9. Overholt BF, Lightdale CJ and Wang KK, et al. Photodynamic therapy with porfimer sodium for ablation of high-grade dysplasia in Barrett's esophagus: international, partially blinded, randomized phase III trial. *Gastrointest Endosc.* 2005 **62**: 488-98.
10. Etienne J, Dorme N, Bourg-Heckly G, Raimbert P and Flejou JF. Photodynamic therapy with green light and m-tetrahydroxyphenyl chlorin for intramucosal adenocarcinoma and high-grade dysplasia in Barrett's esophagus. *Gastrointest Endosc*. 2004 **59**: 880-9.
11. Lovat LB, Jamieson NF, Novelli MR, Mosse CA, Selvasekar C, Mackenzie GD, Thorpe SM and Bown SG. Photodynamic therapy with m-tetrahydroxyphenyl chlorin for high-grade dysplasia and early cancer in Barrett's columnar lined esophagus. *Gastrointest Endosc*. 2005 **62**: 617-23.
12. Wilson BC, Muller PJ and Yanch JC. Instrumentation and light dosimetry for intra-operative photodynamic therapy (PDT) of malignant brain tumours. *Phys Med Biol*. 1986 **31**: 125-33.
13. van Gemert MJ, Jacques SL, Sterenborg HJ and Star WM. Skin optics. *IEEE Trans Biomed Eng.* 1989 **36**: 1146-54.
14. Star WM, Marijnissen JP and van Gemert MJ. Light dosimetry: status and prospects. *J Photochem Photobiol B.* 1987 **1**: 149-67.

15. Jacques SL. Laser-tissue interactions. Photochemical, photothermal, and photomechanical. *Surg Clin North Am.* 1992 **72**: 531-58.

16. Panjehpour M, Overholt BF, DeNovo RC, Sneed RE and Petersen MG. Centering balloon to improve esophageal photodynamic therapy. *Lasers Surg Med.* 1992 **12**: 631-638.

17. Panjehpour M, Overholt BF, DeNovo RC, Petersen MG and Sneed RE. Comparative study between pulsed and continuous wave lasers for Photofrin photodynamic therapy. *Lasers Surg Med.* 1993 **13**: 296-304.

18. van Veen RL, Aalders MC, Pasma KL, Siersema PD, Haringsma J, van de Vrie W, Gabeler EE, Robinson DJ and Sterenborg HJ. In situ light dosimetry during photodynamic therapy of Barrett's esophagus with 5-aminolevulinic acid. *Lasers Surg Med.* 2002 **31**: 299-304.

19. Robinson DJ, de Bruijn HS, van der Veen N, Stringer MR, Brown SB and Star WM. Fluorescence photobleaching of ALA-induced protoporphyrin IX during photodynamic therapy of normal hairless mouse skin: the effect of light dose and irradiance and the resulting biological effect. *Photochem. Photobiol.* 1998 **67** 141-149.

20. Panjehpour M, Overholt BF, Phan MN and Haydek JM. Optimization of light dosimetry for photodynamic therapy of Barrett's esophagus: efficacy vs. incidence of stricture after treatment. *Gastrointest Endosc*. 2005 **61**: 13-8.

21. de Bruijn HS, van der Veen N, Robinson DJ and Star WM. Improvement of 5-aminolevulinic acid based photodynamic therapy in vivo using light fractionation with 75 minute interval. *Cancer Res.* 1999 **59**: 901-904.

22. Robinson DJ, de Bruijn HS, Star WM and Sterenborg HJ. Dose and timing of the first light fraction in two-fold illumination schemes for topical ALA-mediated photodynamic therapy of hairless mouse skin. *Photochem Photobiol.* 2003 **77**: 319-23.

7.

Diffuse reflectance spectroscopy from 500 to 1060 nm using correction for inhomogeneously distributed absorbers

Adapted from:

R.L.P. van Veen, W. Verkruijsse, and H.J.C.M. Sterenborg. Diffuse reflectance spectroscopy from 500 to 1060 nm by correction for inhomogenously distributed absorbers.
Opt Lett. 2002: (27): **246-248.**

Abstract

Diffuse reflectance spectroscopy for the measurement of absorption and scattering coefficients of biological tissue produces reliable results for wavelengths between 650 and 1050 nm. Implicitly, this approach assumes homogeneously distributed absorbers. In the present paper a correction factor is introduced for non-homogeneous distribution of blood concentrated in discrete cylindrical vessels. This extends the applicability of diffusion theory to lower wavelengths. We present measurements of in vivo optical properties in the wavelength range from 500-1060 nm.

Introduction, method, results and discussion

Detailed knowledge of tissue optical properties is essential to optimise optical diagnostic methods in medicine and as well as therapeutic laser applications. The photon propagation in turbid biological tissues can be described using diffusion theory. Farrell *et al.* adapted the diffusion approximation with extrapolated boundary conditions to describe steady state spatially resolved diffuse reflectance measurements[1-2]. In earlier work we used spatially resolved diffuse reflectance spectroscopy for the non-invasive determination of *in vivo* human tissue optical properties and absolute chromophore concentrations based on this analysis[3]. Rather than calculating optical properties for each of the wavelengths separately, the analysis considered the whole data set and calculated the absorption and reduced scattering spectra over the entire wavelength range. As a constraint in the analysis we assumed Lorentz-Mie scattering:

$$\mu_s' = \mu_s'(\lambda_0) \cdot \left(\frac{\lambda}{\lambda_0} \right)^{-b} \qquad \text{Eq.1}$$

Where b is a constant and is related to the size of the scattering particles[4]. In the wavelength range from 650 to 1050 nm the resulting absorption spectrum appeared to be equal to the sum of the specific absorption of 4 individual absorbers i.e. haemoglobin, oxy-haemoglobin, fat and water[3]. This approach assumes that all absorbers are distributed homogeneously. Other researchers have found similar results[5-7]. Extrapolated to wavelengths below 650 nm the sum of the absorption of these 4 basic components usually overestimates the absorption as calculated from the reflectance at these wavelengths by an order of magnitude. A condition for the validity of the diffusion approximation is that scattering dominates over absorption: $\mu_a << [(\mu_s(1-g)]$. Looking at the extrapolated optical properties it is tempting to attribute this discrepancy to a breakdown of diffusion theory in the lower wavelength range[8]. However, the values of the optical properties measured in this range do not justify this conclusion.

Investigators evaluating near infrared spectroscopy for non-invasive measurement of blood oxygenation encountered a comparable problem. When using the lower wavelengths in the NIR range incorrect values for the blood- oxygenation and volume resulted. This problem has been attributed to the fact that blood is not a homogeneously distributed absorber, but a strong absorber concentrated in a small fraction of the volume, i.e. the blood vessels. In case of sufficiently large vessel radius and strong absorption less light reaches the centre of the blood vessel. Hence, the measured the absorption coefficient will be smaller than expected on the basis of the same amount of homogeneously distributed blood in the tissue. Correction factors have been either derived analytically or based on Monte Carlo simulations using randomly distributed cylindrical vessels with various radii [9-11]. Another field of study where a similar problem was encountered is laser treatment of port-wine stains. Modelling port-wine stain colour (i.e. the wavelength region from 450-700 nm) required a

wavelength dependent correction factor for the blood volume that accounted for the effect of blood being concentrated in vessels[12-13]. The analytical formula for this correction factor was based on straightforward geometrical optics. Figure 1 shows the influence of increasing vessel diameter on the effective absorption coefficient.

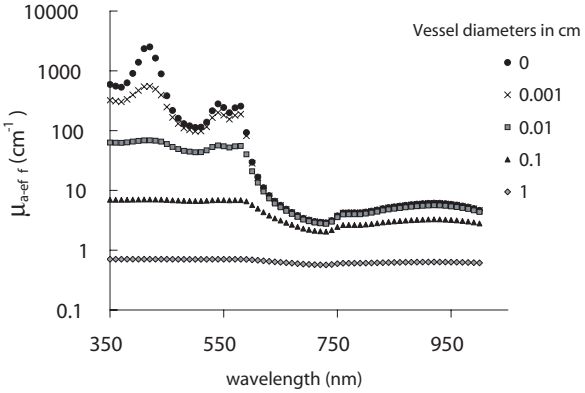

Figure 1. Effective absorption by blood distributed in discrete vessels for various vessel diameters (diffusely irradiated).

Figure 2 summarises the various correction factors found in the literature as a function of the vessel optical density ($\mu_{a,bl} \cdot R_{vessel}$). All are very close to each other, except the one by Liu *et al*, who were the first to tackle this problem[11]. We hypothesise that incorporation of the correction for in-homogeneously distributed absorbers into the spatially resolved diffuse steady state diffuse reflectance model will extend the validity of this approach to lower wavelengths. In the present paper we present experimental results that support this concept.

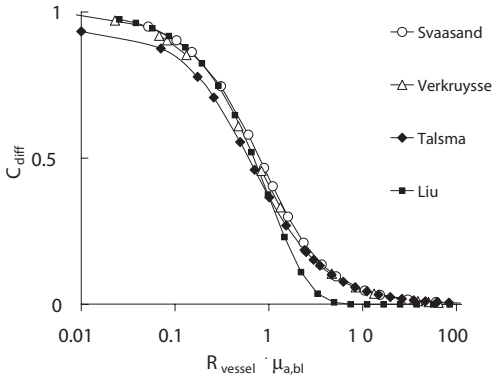

Figure 2. The different correction factors for in-homogeneously distributed absorbers. The first two depend only on the product $R_{vessel} \cdot \mu_{a,bl}$ and have considered the influence of scattering negligible. Talsma et al incorporated scattering by blood (μ_s'=2.54 mm-1). For Liu's et al equation we have set the absorption of the surrounding tissue to zero.

Since our calculation of optical properties from a set of diffuse reflectance measurements employs a least-squares minimisation routine that utilises the correction factor frequently we chose to use the correction factor as proposed in ref. (13) Eq. 2, as it is the simplest analytical expression available:

$$C_{diff}(\lambda) = \left(\frac{1 - e^{-2 \cdot \mu_{a,bl}(\lambda) \cdot R_{vessel}}}{2 \cdot R_{vessel} \cdot \mu_{a,bl}(\lambda)} \right) \qquad \text{Eq.2}$$

Where $\mu_{a,bl}(\lambda)$ stands for the absorption coefficient of whole blood, and R_{vessel} for the vessel radius. The effective absorption coefficient of the tissue we use in our analysis consists of two parts, the in-homogeneously and the homogeneously distributed contributions

$$\mu_a'(\lambda) = C_{diff}(\lambda) \upsilon \left(S \mu_{aHbO_2}(\lambda) + (1 - S) \mu_{aHb}(\lambda) \right) + \sum_i c_i \mu_{ai}(\lambda) \qquad \text{Eq.3}$$

Where $\mu_a'(\lambda)$ stands for the effective absorption coefficient, $\mu_{aHbO2}(\lambda)$ for the absorption coefficient of fully oxygenated whole blood, $\mu_{aHb}(\lambda)$ for the absorption coefficient of fully de-oxygenated whole blood, υ the blood volume fraction, S the oxygen saturation of the blood, $C_{diff}(\lambda)$ the correction factor for blood vessel exposed to diffuse light and c_i and $\mu_{ai}(\lambda)$ the volume fractions and absorption coefficients of the homogeneously distributed absorbers. Note that using this approach we obtain an estimate of the volume fractions of the homogeneously distributed absorbers, the blood volume fraction and the oxygenation, but also of the vascular radius R. As an additional fitting constraint we force all absorbing chromophore volume fractions to add up to 100%. This constraint increased the stability of the fit. Figure 3 shows the results of two *in vivo* measurements. The μ_a' residue is defined as the relative difference between measurement and model. For comparison we calculated μ_a without correction factor based on reflectance measurements between 650 and 1050 nm and extrapolated to the shorter wavelengths[3]. The μ_a' residue stays within ±5% down to 500nm, whereas for the classical approach the residues exceed 100% below 600 nm (not shown). For wavelengths below 500nm the signal to noise ratio decreases due to low light source output and low grating efficiency. Table 1 summarises the results of several tissue types resulting from this approach .The variances of the fitted values were derived by calculating the covariance matrix and are an indication of how precise these parameters are defined by the given data-set. Not shown are the covariances. In general these were roughly equal to the variances. In the red and near infrared wavelength range the resulting absorption spectra are in good agreement with those found by others[5-7]. The measurement on the wrist was taken deliberately on the visible veins in the skin.

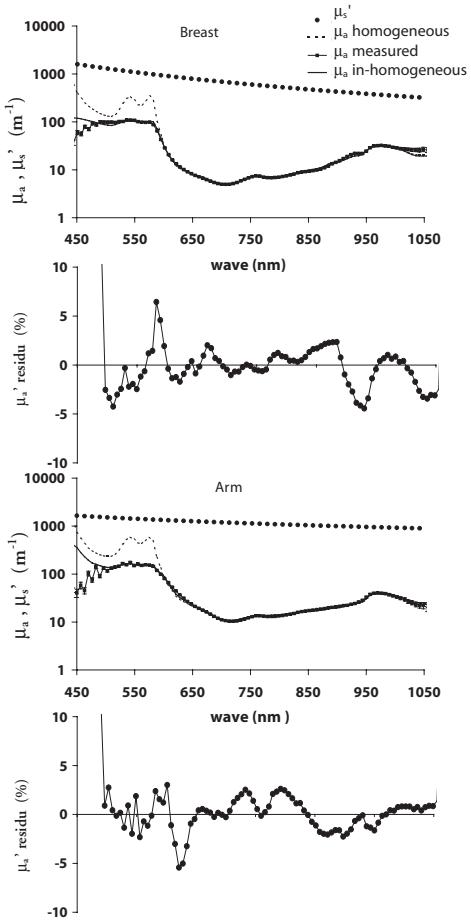

Figure 3. The results of fitting the absorbing components on the measured absorption spectra (solid squares) according to the homogeneous (dashed line), and in-homogeneous model Eq. 3 (solid black) respectively. The relative residue $\mu_a' = ([\mu_{a,model}-\mu_{a,meas}]/\mu_{a,model})$ *is depicted underneath. The reduced scattering spectra (filled circles) can be seen above the absorption spectra and are the result of fitting* $\mu_s'(\lambda_0)$ *and b Eq.1 on the reflectance spectra.*

The vascular diameter found here seems to underestimate the actual diameter. A strong and significant correlation between the blood volume fraction and the vessel radius was found (Spearman's rank correlation coefficient 0.854 (0.521 - 0.961) p=0.007).

Based on the preliminary data presented here we conclude that our analysis is feasible down to 500 nm and proves to be beneficial for expanding the wavelength range for applying diffuse reflectance spectroscopy. We believe that the range may even be extended to lower wavelengths when lamp output power and grating efficiency is adapted for lower wavelength regions. The concept of an effective absorption coefficient can easily be implemented in time- and frequency domain techniques. We believe the utilisation of this concept may have several advantages. It may provide accurate tissue optical properties for

wavelengths below 650 nm and consequently may enable the quantitative determination of tissue absorbers like cytochrome, bilirubin, or drugs that show absorption outside the NIR range. Moreover, the technique may enable monitoring of dynamic processes that involve the changes in vessel diameter for instance resulting from blood pressure changes, erythema or the more long-term ones like occurring as a result of portwine stain treatment. The accuracy of the parameter R_{vessel} we obtain from our measurements strongly depends on its relation to the actual size of the vessels. Svaasands derivation of the correction factor considers vessels with a circular cross section of a single diameter only. In tissue there will be variable sizes and shapes, which will be different at different depths in the tissue. Based on the optical properties we determined and accounting for the fact that the wavelength range below 600nm has the largest impact on the value of R_{vessel}, we expect R_{vessel} to refer to blood vessels in the upper 1 mm of the skin.

Table1. Contributions of the absorbing constitutes, and the tissue oxygenation levels of several tissue types[a]

Position	Blood [%]	Blood Oxygenation [%]	Water [%]	Fat [%]	Vessel Radius [µm]	μ_s' @ 1000 nm [m^{-1}]	Slope [-]
Forearm	2.0 (0.2)	63.1 (4.7)	59.7 (9.6)	33.3 (29.7)	36. 5 (0.5)	963. 5	- 1.06
Forearm	2.9 (0.2)	64.8 (3.7)	58.7 (9.2)	33.5 (30.7)	61. 8 (0.6)	766. 8	- 1.20
Forehead	1.6 (0.2)	75.1 (6.2)	60.4 (12.2)	38.1 (32.4)	20 .2 (0.5)	931. 8	- 1.30
Biceps	1.0 (0.6)	87.4 (18.2)	58.1 (8.6)	40.9 (29.1)	23.4 (1.3)	925. 5	- 0.72
Forear	1.0 (0.5)	70.1 (8.0)	55.9 (7.9)	43.2 (23.4)	13. 2 (0.8)	871. 3	- 0.92
Biceps	0.6 (0.3)	64.2 (11.0)	57.3 (7.2)	42.1 (18.6)	12.0 (0.9)	918. 3	- 1.27
Wrist	11.5 (1.9)	71.8 (3.6)	88.6 (25.4)	0.0 (96.6)	101.1 (0.8)	220. 4	- 0.18
Biceps	0.9 (0.6)	73.3 (12.6)	56.1 (8.6)	43.0 (27.4)	22.3 (1.9)	1073. 0	- 0.85
Biceps	1.4 (0.1)	86.0 (4.6)	35.8 (6.5)	62.9 (22.6)	30.1 (0.5)	692. 8	- 1.18
Chest (M)	2.0 (0.2)	92.1 (3.8)	60.4 (8.9)	37.6 (25.4)	71. 5 (1.6)	433. 6	- 2.84
Breast (F)	1.2 (0.1)	87.4 (3.5)	51.2 (5.2)	47.6 (14.3)	30 .7 (0.7)	344. 8	- 1.90

[a] *The variances of vessel radius Rvessel are relatively small. On the outmost right columns the scattering fit parameter i.e. slope of the scattering curve (LN (μ_s') versus LN (λ)), and the scattering coefficient (μ_s' at λ_0 =1000 nm) according to Eq. 1. Tissue scattering and absorption spectra can accurately be described using the parameters mentioned. Values in parenthesis indicate the variance of the parameter value calculated from the covariance matrix.*

References

1. Farrell TJ, Patterson MS and Wilson BA diffusion theory model of spatially resolved, steady-state diffuse reflectance for the noninvasive determination of tissue optical properties in vivo. *Med Phys.* 1992 **19**(**4**): 879-88.

2. Kienle A and Patterson MS. Improved solutions of the steady-state and the time-resolved diffusion equations for reflectance from a semi-infinite turbid medium. *J Opt Soc Am A Opt Image Sci Vis.* 1997 **14**(**1**): 246-54.

3. Doornbos RM, Lang R, Aalders MC, Cross FW and Sterenborg HJ. The determination of in vivo human tissue optical properties and absolute chromophore concentrations using spatially resolved steady-state diffuse reflectance spectroscopy. *Phys Med Biol.* 1999 **44**(**4**): 967-81.

4. Nilsson AMK, Sturesson C, Liu DL and Andersson-Engels S. Changes in Spectral Shape of Tissue Optical Properties in Conjunction with Laser-Induced Thermotherapy. *Appl Opt.* 1998 **37**(7): 1256-1267.

5. Dögnitz N. and Wagnières G. Determination of tissue optical properties by steady-state spatial frequency-domain reflectometry *Lasers Med. Sci.* 1998 **13**: 55–65.

6. Torricelli A, Pifferi A, Taroni P, Giambattistelli E. and Cubeddu R. *In vivo* optical characterization of human tissues from 610 to 1010 nm by time-resolved reflectance spectroscopy. *Phys Med Biol.* 2001 46(8): 2227-37.

7. Cubeddu R, Pifferi A, Taroni P, Torricelli A and Valentini G. Noninvasive absorption and scattering spectroscopy of bulk diffusive media: An application to the optical characterization of human breast. *Appl Phys Lett.* 1999 **74**: 874-876.

8. Furutsu K. and Yamada Y. Diffusion approximation for a dissipative random medium and the applications. *Phys Rev E*. 1994 **50**: 3634-3640.

9. Firbank M, Okada E and Delpy DT. Investigation of the effect of discrete absorbers upon the measurement of blood volume with near-infrared spectroscopy. *Phys Med Biol.* **42**(**3**): 465-77.

10. Talsma A, Chance B, and Graaff R. Corrections for inhomogeneities in biological tissue caused by blood vessels. *J Opt Soc Am A Opt Image Sci Vis.* 2001 **18**(**4**): 932-9.

11. Liu H, Chance B, Hielscher AH, Jacques SL and Tittel FK. Influence of blood vessels on the measurement of hemoglobin oxygenation as determined by time-resolved reflectance spectroscopy. *Med Phys.* 1995 **22**(**8**): 1209-17.

12. Verkruysse W, Lucassen GW, de Boer JF, Smithies DJ, Nelson JS and van Gemert MJ. Modelling light distributions of homogeneous versus discrete absorbers in light irradiated turbid media. *Phys Med Biol.* 1997 **42**(**1**): 51-65.

13. Svaasand LO, Fiskerstrand EJ, Kopstad G, Norvang LT, Svaasand EK, Nelson JS and Berns MW. Therapeutic response during pulsed laser treatment of port-wine stains: Dependence on vessel diameter and depth in dermis. *Lasers Med. Sci.* 1995 **10**: 235-243.

8.

Determination of VIS- NIR absorption coefficients of mammalian fat, using time- and spatially resolved diffuse reflectance and transmission spectroscopy

Adapted from:

R.L.P. van Veen, H.J.C.M. Sterenborg, A. Pifferi, A. Torricelli, Chikoidze E. and R. Cubeddu, Determination of VIS- NIR absorption coefficients of mammalian fat, with time- and spatially resolved diffuse reflectance and transmission spectroscopy. **J Biomed Opt. 2005: 10: 054004.**

Abstract

In vivo optical spectroscopy and the determination of tissue absorption and scattering properties have a central role in the development of novel optical diagnostic and therapeutic modalities in medicine. A number of techniques are available for the optical characterisation of tissue in the visible-near infrared region of the spectrum. An important consideration for many of these techniques is the reliability of the absorption spectrum of the various constituents of tissue.

The availability of accurate absorption spectra in the range 600 – 1100 nm may allow for the determination of the concentration of key tissue constituents such as oxy- and deoxy-haemoglobin, water and lipids. The objective of the current study is the determination of a reliable absorption spectrum of lipid(s) that can be used for component analysis of *in vivo* spectra. We report the absorption spectrum of a clear purified oil obtained from pig lard. In the liquid phase above 36 °C the oil is transparent and thus suitable for collimated transmission measurements. At room temperature the oil is a solid grease that is highly scattering. The absorption and scattering properties in this solid phase are measured using time resolved and spatially resolved diffuse reflectance spectroscopy. Using these three independent measurement techniques we have determined an accurate estimate for the absorption spectrum of mammalian fat.

Introduction

Near infrared (NIR) spectroscopic imaging is a relatively new, non-invasive medical diagnostic technique, which may provide several advantages over other diagnostic methods. At present several groups are investigating different tomographic[1,2], multi-spectral trans-illumination optical imaging[3,4] or spectroscopic techniques[5]. These measurements are performed either by continuous wave, or by time/frequency resolved methods.
Contrast between diseased and normal tissues resulting from differences in tissue optical properties e.g. reduced scattering and absorption coefficients may be caused by differences (extra or intra) cellular refractive index distributions, variations in blood saturation, and variations in blood, water or lipid content. Recent work on NIR optical mammography suggests that malignant and benign tissue structures can be discriminated from normal tissue by their water lipid ratios or due to differences in total haemoglobin content and oxygenation. Tumours are associated with an increase in blood volume and a decrease in oxygenation due to tumour proliferation [6,7,8]. The absorption spectra obtained from these techniques are assumed/thought to be a linear combination of the absorption spectra of the chromophores present in the tissue. Spectral decomposition of the measured absorption spectra into its components can be used to quantify absolute tissue chromophore concentrations. Furthermore, tissue oxygenation and total haemoglobin content can be calculated from these quantities. It is therefore essential to have detailed knowledge of the intrinsic absorption spectra of these 4 components.
Oxy, de-oxy-haemoglobin[9] and water[10] are well quantified and routinely applied.
A representative tissue fat spectrum however has yet to be determined. The fat spectra used for spectral decomposition vary between investigators. Heusmann *et al.*[11] employ a non-specified vegetable oil for the component analysis of the female breast tissue, whereas others have used olive oil[12], raw pig lard[13], sun-flour oil[14], or soy bean oil[15].
Other investigators even assume a negligible absorption due to fat. These spectra are significantly different from each other in respect of their spectral shape and the magnitude of the main absorption peaks. This makes an absolute comparison and interpretation of results of each technique difficult. The reason for the absence of a definitive fat spectrum in the literature is that mammalian fat is not available as a pure clear liquid. In the present paper we report the absorption spectrum of clear oil obtained from mammalian pig lard. At room temperature this oil is a solid grease that displays strong scattering properties. Absorption and scattering properties of this solid grease were measured using time resolved and spatially resolved diffuse reflectance spectroscopy. At temperatures above 36 °C it is a clear liquid with minimal scattering properties. Hence, an independent measurement of the absorption spectrum can be made using collimated transmission measurements.

Materials and Methods

Lipid purification

5 kg of muscle and skin free pig chest plate lard was divided in pieces of 1 cm^3 and placed in water maintained at a temperature of 90 °C. A thin layer of oil formed on the surface of the mixture and was removed and placed in a separate container. This process was continued for a period of 6 hours until the oil separation process had stopped. The oil still contained water and other visible tissue structures. The container was then placed in an oven at 50 °C to homogenise the fluid and then placed in a refrigerator at 5 °C. After one hour the oil had solidified into a pure white solid lipid above a multi layered mixture of water and gelatinous substance. The lipid could then be separated manually from the mixture below. The solid oil was then heated once more to 80 °C and passed twice through filter paper (standard grade 91, 10µm, Whatman int. Ltd, England) while it remained in its liquid state. The filtered oil was heated again to 80 °C and poured onto a filter containing Sodium sulphate (Na_2SO_4 Anhydrous J.T. Baker BV, The Netherlands) to remove any remaining of water. Finally the oil was placed in a test tube and centrifuged (Gyro Vap) for 30 minutes at 1000 rpm at a constant temperature of 70 °C. Pure oil was removed using a pipette leaving some sediment at the base of the test tube. At the end of this process 250 ml of oil was obtained that was visually clear at temperatures above 36 °C.

Collimated transmission measurement:

The set-up used is shown schematically in figure 1. Light from a 100 W quartz tungsten halogen lamp is coupled into an optical fibre leading to a cuvette holder (Avantes, Eerbeek, The Netherlands) and collimated to a beam of approximately 2mm diameter. Three different quartz cuvettes (Anadis, Malden, The Netherlands) with path lengths of 10, 20 and 50 mm were used. Transmitted light was collected using an integrating sphere with a collection port much larger that the beam diameter (Oriel instruments, Stratford, USA). In this way divergence of the light beam within cuvettes of different path length did not affect the total amount of light collected. The detection fibre was positioned inside the integrating sphere behind a baffle and directed the collected light to the entrance slit position of an imaging spectrograph (Oriel, MS257) and was spectrally projected onto a 16-bit 256-1024 pixel CCD camera cooled to –30 °C (Andor DU420-OE, Belfast Northern Ireland UK). The 150 lines/mm grating in the spectrograph allows us to cover a wavelength range from 440 to 1100 nm with a spectral resolution of 0.65 nm.
The cuvette holder and integrating sphere were placed in an oven and optical fibres were passed between the rubber fitting of the oven door to the spectrograph.
Measurements were performed at constant temperatures of 37, 60 and 80 °C. In order to avoid possible temperature gradient effects the set-up was allowed to settle for at least 20 minutes at each temperature setting. For each cuvette path length three sequential transmission and background measurements were performed.

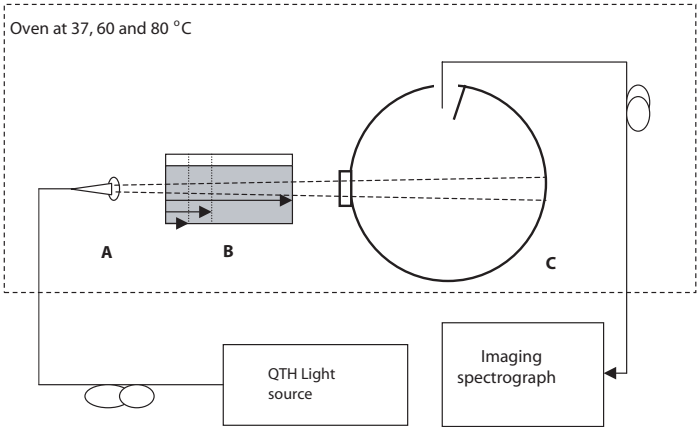

Figure 1. Schematic outlay of the transmission set-up. A) Collimating optics, B) Quartz cuvetts with lengths of 10, 20 or 50mm, C) Integrating sphere plus detection fibre. The dotted line indicates the oven used for constant temperatures.

The transmission data was averaged over the 3 sequential measurements and the background was subtracted. The absorption coefficients were calculated for 3 path length differences (50-10 mm, 50 –20 mm and 20-10 mm) according to equation 1.

$$\mu_{a,meas}(\lambda) = \frac{\left[\left(\frac{LN(I_{10}/I_{50})}{d_{50}-d_{10}}\right)+\left(\frac{LN(I_{20}/I_{50})}{d_{50}-d_{20}}\right)+\left(\frac{LN(I_{10}/I_{20})}{d_{20}-d_{10}}\right)\right]}{3} \qquad \text{Eq.1}$$

Where $I_{10,20,\text{and } 50}$ is the measured transmission intensity in CCD counts for the three cuvettes path lengths $d_{50,40,\text{ and } 10mm}$. The use of this method makes reference measurements i.e. empty cuvette or water obsolete, thus the absorption information originates solely from the transmission differences between the three path lengths and excludes all cuvette / oil boundary reflection effects. Secondly, the use of small path lengths and longer path lengths e.g. 10 and 40mm provides accurate spectral information in regions of low and high absorption coefficients respectively. Absorption coefficients were calculated for all 3 temperatures (37. 60, and 80 °C), to investigate possible influence of temperature on the absorption coefficient.

Spatially resolved Diffuse Reflectance Spectroscopy (DRS):

The measurement technique is based on a theoretical analysis developed by Farell *et al.*[16]. The illumination of the solid fat and the collection of the diffuse re-emitted light were performed by a multi-fiber probe. This black Perspex probe consists of 10 low OH medical grade fibers (400 µm core, length about 4 m) (CeramOptec GmbH, Bonn, Germany) in which the fibers are positioned at an average inter-fiber distances of 2 mm. The white light from a 100 W quartz tungsten halogen lamp is coupled into the

illumination fiber of the probe. The nine detection fibers in the probe direct the light to the entrance slit position of an imaging spectrograph (Oriel, MS257). The 150 lines/mm grating in the spectrograph allows us to cover a wavelength range from 600 to 1100 nm with a spectral resolution of 0.65 nm. A 16-bit 256-1024 pixel CCD camera cooled to -30 °C (Andor DU420-OE, Belfast Northern Ireland UK) detects the nine spectra originating at different distances from the illumination fiber. The solid fat was placed in a container and the sample dimensions were 8 by 8 by 5 cm, 3 measurements were taken at room temperature at 3 different positions on the sample.

Data processing and analyses of the data files were performed using Matlab™ software (Matlab, Mathworks Inc., MA, USA). Absorption and scattering spectra where obtained by fitting the diffusion equation, and assuming Lorentz-Mie- scattering according eq. 2 for all wavelengths.

$$\mu_s' = a \cdot \lambda^{-b} \qquad \text{Eq. 2}$$

Where b is a constant and is related to the size of the scattering particles.
Further details on the fit method can be found in[17,14].

Time resolved diffuse Reflectance Spectroscopy (TRS):

The measurement set-up consists in a fully automated system for time resolved reflectance spectroscopy continuously tunable in the 610-1050 nm range[13].
A synchronously-pumped mode-locked dye (DCM) laser was used as the excitation source from 610 to 700 nm, while an actively mode-locked Titanium-Sapphire laser provided light in the wavelength range of 705 to 1050 nm. A couple of 1 mm plastic-glass fibres (PCS1000W, Quartz et Silice, France) delivered light into the sample and collected the reflected photons at a relative distance of 1.5 cm. A double microchannel plate photomultiplier (R1564U with S1 photo-chatode, Hamamatsu, Japan) and a PC board for time-correlated single-photon counting (SPC134, Becker&Hickl, Germany) were used for detection. A small fraction of the incident beam was coupled to a 1 mm fibre (PCS1000W, Quartz et Silice, France) and fed directly to the photomultiplier to account for on line recording of the instrumental response function (IRF). Overall, the IRF was <120 ps and <180 ps FWHM in the red and near-infrared, respectively. Time-resolved reflectance curves were collected every 5 nm with an acquisition time of 4 seconds for each wavelength.

The reduced scattering and absorption spectra were constructed by plotting, versus wavelength, the values of μ_s' and μ_a, as obtained from fitting the experimental data with a standard solution of the diffusion approximation to the transport equation for a semi-infinite homogeneous medium[18] using the extrapolated boundary condition[19].
The diffusion coefficient D was taken to be independent of the absorption properties of the medium (i.e. $D = 1/(3\mu_s')$), in agreement with Furutsu and Yamada[20]. The theoretical curve was convoluted with the IRF and normalised to the area of the experimental curve.

The fitting range included all points with a number of counts higher than 80% of the peak value on the rising edge of the curve and 1% on the tail. The best fit was reached with a Levenberg-Marquardt algorithm[21] by varying both μ_s' and μ_a in order to minimise the reduced χ^2.

The exact temporal position of the IRF (t_0) was obtained fitting the experimental curves in the region of low absorption with the 3 free parameters μ_s', μ_a and t_o [22]. The average value of t_0 was then applied as a fixed parameter to all wavelengths.

In the range of measured values of the optical coefficients, with our set-up and the theoretical model we use, the accuracy in the absolute estimate of both μ_s' and μ_a is usually better than 10% [22,23].

Results

Figure 2 shows the results of the transmission measurements at 60 °C calculated according equation 1. The results for 37 °C were similar. Although the oil sample was visually clear some scattering could be observed as the light beam was visible from the side of the cuvette, indicating the presence of some remaining scattering particles.

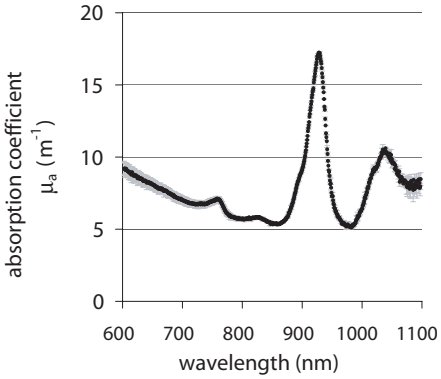

Figure 2. Example of absorption coefficients plus scattering contribution versus wavelength of liquid pig oil at 60°C, calculated according equation 1. Error bars represent the standard deviation over the average of the 3 different path lengths (10mm-20mm and 50mm).

As seen in figure 2 the absorption spectrum appears to be superimposed upon Mie-like scattering. An initial analysis revealed 6 major absorption peaks. Five peaks consisted of two nearly coinciding absorption bonds. The result at 80 °C clearly shows a much lower scattering contribution.

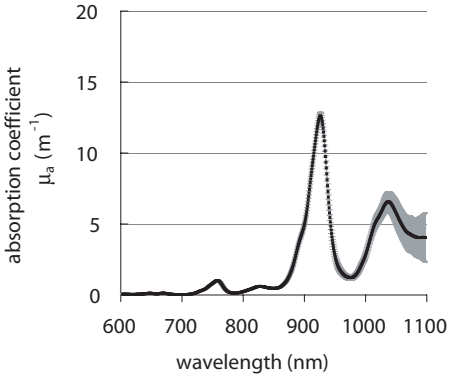

Figure 3. Absorption coefficient after correction for scattering contribution versus wavelength. The error bars represent the standard deviation over the 3 temperatures i.e. 37, 60 and 80 °C.

In order to eliminate the Mie-like scattering contribution from the absorption coefficient we've fitted 11 gaussian shaped absorption peaks plus a Mie-like scattering function through the transmission result according to equation 3 for all three temperatures separately.

$$\mu_{a.model} = A \cdot \exp\left[-B \cdot LN\left(\frac{\lambda}{\lambda_o}\right)\right] + \sum_i C_i \cdot \exp\left[\left(\frac{(\lambda_i - \lambda)}{\sigma_i}\right)^2\right] \qquad \text{Eq.3}$$

Where in the first term, the scattering contribution is defined by A and B, respectively related to scatter size and density and, λ_o the central fit wavelength. In the second term, the summation of the 11 absorption gaussians where C_i, represent the absorption magnitude, σ_i, center peak wavelength and σ_i bandwidth of each absorption band indicated with *i*. Fit constraints were non-negative fit parameters and absorption coefficient results. The scattering spectrum resulting from the fit was then subtracted from the original absorption spectrum results to obtain the absolute absorption coefficients. The average absorption coefficients at 37, 60 and 80 °C are shown in figure 3. Absorption spectra of all three temperatures coincide from 600 up to 980 nm, above 980 nm and higher the absorption coefficients of the measurement at 80 °C become up to 25% smaller compared to 37 and 60 °C. The relative error for each temperature, between the model and measurement was within 5% over the entire wavelength interval (600 up to 1100nm). Values found for the scatter slope (-*b*) ranged from 1.7 up to 2.6, indicating Lorentz-Mie scattering.

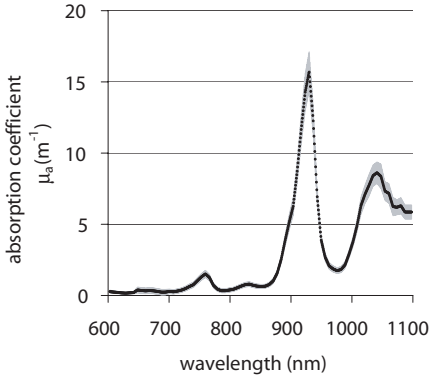

Figure 4. Absorption coefficient versus wavelength of pig oil at 15 °C in solid state resulting from the spatially-resolved measurements with a 0.65 nm resolution. The error bars represent the standard deviation over the 3 sequential measurements after repositioning.

Figure 4 shows the absorption (μ_a) spectrum of the solidified lipid sample obtained after averaging 3 relocated sequential spatially resolved DRS measurements performed at 15 °C. The main absorption peak is located at 930 nm (15.7 m^{-1}) with an overtone at 760 nm (1.47 m^{-1}). Reduced scattering properties decreased as function of wavelength (μ_s'=654 m^{-1} at 600 nm down to 370 m^{-1} at1087 nm).

Figure 5 shows the absorption (μ_a) spectrum of the purified lipid sample obtained averaging 3 consecutive spectral time resolved DRS acquisitions performed at 15 °C. The absorption spectrum shows two major peaks at 930 nm (12.8 m^{-1}), and at 760 nm (1.73 m^{-1}), while the peak around 1044 nm is beyond the tuning range of the instrumentation. The reduced scattering coefficient is a decreasing function of wavelength with values in the range 700 to 450 m^{-1}. As for the DRS, upon increasing the sample temperature from 0° to 25°C, as expected we have observed a progressive decrease of μ_s' (data not shown).

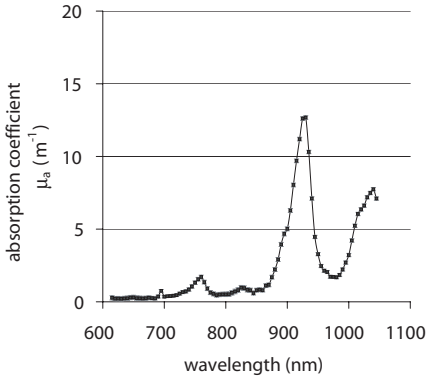

Figure 5. Absorption coefficient versus wavelength of pig oil at 15 °C in solid state resulting from the time-resolved measurements with a 5 nm resolution. The error bars represent the standard deviation over the 3 sequential measurements after repositioning.

The data presented in Figure 5 corresponds to the highest temperature at which the scattering coefficient is high enough to provide fully reliable results[22]. Up to this temperature no significant variations were observed in the absorption spectrum (data not shown).

In figure 6 the spectra of all three techniques are shown in log scale to illustrate spectral features at low absorption. Table 1 gives an overview on the main spectral absorption features as measured by all three techniques plus the average of all three methods.

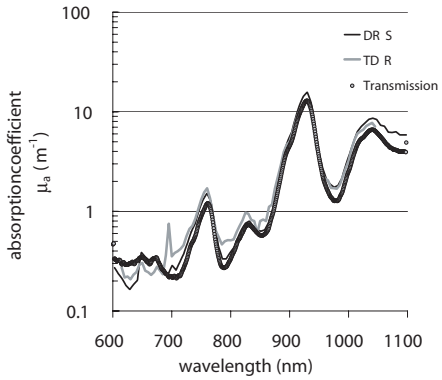

Figure 6. Absorption coefficient versus wavelength of mammalian fat in solid and liquid state resulting from the time/spatially-resolved and transmittance measurements.

Table 1. Main absorption peaks characteristics between 600 up to 1100 nm of mammalian fat for all three techniques. The average of all three techniques is given in the last column.

l [nm]	Transmittance	SD	DRS	SD	TR	SD	Average
670.4	0.45	0.1	0.34	0.20	0.25	0.26	0.35
760.2	1.28	0.21	0.50	0.25	1.70	0.10	1.49
830.7	0.80	0.17	0.80	0.17	0.95	0.07	0.85
929	13.10	0.26	15.69	1.42	12.7	0.36	13.80
1040	7.02	0.13	8.62	0.75	7.74	0.04	7.78

Discussion and conclusions:

In this paper we have presented the absorption spectrum of mammalian fat measured by three independent methods. Direct measurement on pig lard to obtain optical properties of mammalian fat was not feasible because this adipose tissue still contains blood and water. Transmission measurement of visually clear lard oil still contained some scattering, the result at 80 °C clearly shows a much lower scattering contribution, suggesting that the scattering observed is related to microscopic traces of solidification at the lower temperatures or changes in shape/mixture of fat partitions in the liquid fat rather than impurities. A maximal amount Mie-like scattering was subtracted from the

attenuation data as seen in figure 2 and 3 due the employed fit constraints. Despite the good fit results still some uncertainty remains regarding the absolute amount of scattering subtracted. The absorption coefficients determined at 80°C become smaller at wavelengths higher than 980 nm and may reflect temperature dependence of the absorption.

The results of the time and spatially resolved measurement reveal less spectral information at lower wavelengths. For DRS, this may indicate insufficient capacity to uncouple scattering from absorption especially for low absorption. Concerning the TRS data, the measurement performed to very low absorption (i.e. <700 nm), is possibly affected by the problem of pile-up of time-resolved photon distributions due to the long decay time associated with low μ_a. The data presented were obtained applying background subtraction at the experimental curves that can result in a slight overestimation of the absorption coefficient.

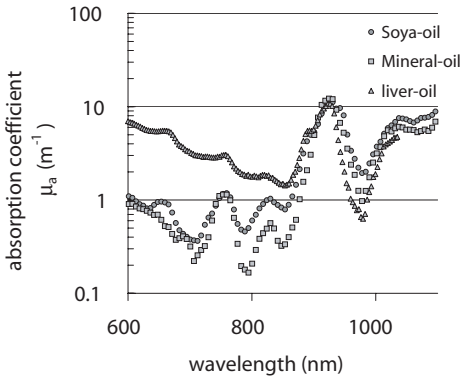

Figure 7. Absorption coefficient versus wavelength of pig lard oil (solid line), Soya oil (filled circle), mineral oil (filled squares) and Cod liver oil (filled triangles)

To demonstrate the differences in absorbing properties between the several types of oil we have measured the absorption of cod liver, mineral and soy oil. Measurement were performed using a standard transmission method, the results are depict in figure 7. All three spectra show a moderate scattering slope from approximately 600 up to 700 nm, and small differences in spectral shape and may contain chlorophyll. Furthermore differences in absorption is observed. Using one of these spectra in a component analysis of absorption spectra may therefore result in differences in absolute chromophore concentration. In summary we have determined the absorption spectrum of mammalian oil validated using three independent techniques. Incorporation of standard intrinsic absorption spectra enables for a more reliable comparison between techniques and methods used in NIR spectroscopy for the analysis of absolute tissue chromophore content.

References

1. Hebden JC, Veenstra H, Dehghani H, Hillman EM, Schweiger M, Arridge SR and Delpy DT. Three-dimensional time-resolved optical tomography of a conical breast phantom. *Appl Opt.* 2001 **40**: 3278-3287.

2. Pogue BW, Poplack SP, McBride TO, Wells WA, Osterman KS, Osterberg UL and Paulsen KD. Quantitative hemoglobin tomography with diffuse near-infrared spectroscopy: pilot results in the breast. *Radiology.* 2001 **218**: 261-6.

3. Pifferi A, Taroni P, Torricelli A, Messina F, Cubeddu R and Danesini G. Four-wavelength time-resolved optical mammography in the 680-980-nm range. *Opt Lett*. 2003 **28**: 1138-1140 .

4. Grosenick D, Moesta KT, Wabnitz H, Mucke J, Stroszczynski C, Macdonald R, Schlag PM and Rinneberg H. Time-domain optical mammography: initial clinical results on detection and characterization of breast tumors. *Appl Opt.* 2003 **42**: 3170-3186.

5. Shah N, Cerussi A, Eker C, Espinoza J, Butler J, Fishkin J, Hornung R and Tromberg B. Noninvasive functional optical spectroscopy of human breast tissue. *Proc Natl Acad Sci U S A.* 2001 **98**: 4420-4425.

6. Tromberg BJ, Coquoz O, Fishkin JB, PhamT, Anderson ER, Butler J, Cahn M, Gross JD, Venugopalan V and Pham D. Non-invasive measurements of breast tissue optical properties using frequency-domain photon migration. *Philos Trans R Soc Lond B Biol Sci*. 1997 **352**: 661-668.

7. Thomsen S and Tatman D. Physiological and pathological factors of human breast disease that can influence optical diagnosis. *Ann N Y Acad Sci.* 1998 **838**: 171-193.

8. Beauvoit B, Kitai T, and Chance B, Contribution of the mitochondrial compartment to the optical properties of the rat liver: a theoretical and practical approach. *Biophys J.* 1994 **67**: 2501-2510.

9. Matcher SJ, Elwell CE, Cooper CE, Cope M and Delpy DT. Performance Comparison of Several Published Tissue Near-Infrared Spectroscopy Algorithms. *Anal Biochem.* 1995 **227**: 54-68

10. Hale GM and Querry MR, Optical constants of water in the 200-nm to 200-micrometer wavelength region. *Appl Opt.* 1973 **12**: 555-563.

11. Heusmann H, Kolzer J and Mitic G. Characterization of female breast *in vivo* by time resolved and spectroscopic measurements in near infrared spectroscopy. *J Biomed Opt.* 1996 **1**: 425-434.

12. Quaresima V, Matcher SJ and Ferrari M. Identification and quantification of intrinsic optical contrast for near-infrared mammography. *Photochem Photobiol*. 1998 **67**: 4-14.

13. Torricelli A, Pifferi A, Taroni P, Giambattistelli E and Cubeddu R. *In vivo* optical characterization of human tissues from 610 to 1010 nm by time-resolved reflectance spectroscopy. *Phys Med Biol.* 2001 **46**: 2227-37.

14. van Veen RLP, Verkruijsse W and Sterenborg HJCM. Diffuse reflectance spectroscopy from 500 to 1060 nm by correction for inhomogenously distributed absorbers. *Opt Lett.* 2002 **27**: 246-248.

15. Cerussi AE, Jakubowski D, Shah N, Bevilacqua F, Lanning R, Berger AJ, Hsiang D, Butler J, Holcombe RF and Tromberg BJ. Spectroscopy enhances the information content of optical mammography. *J Biomed Opt.* 2002 **7:** 60-71.

16. Farrell TJ, Patterson MS and Wilson B. A diffusion theory model of spatially resolved, steady-state diffuse reflectance for the noninvasive determination of tissue optical properties *in vivo*. *Med Phys.* 1992 **19**: 879-888.

17. Doornbos RMP, Lang R, Cross FW and Sterenborg HJCM.The determination of *in vivo* human tissue optical properties and absolute chromophore concentrations using spatially resolved steady state diffuse reflectance spectroscopy. *Phys Med Biol.* 1999 **44**: 967-981.

18. Patterson MS, Chance B and Wilson BC. Time resolved reflectance and transmittance for the non invasive measurement of tissue optical properties. *Appl Opt.* 1989 **28**: 2331-2336.

19. Haskell RC, Svasaand LO, Tsay TT, Feng TC, McAdams MS and Tromberg BJ. Boundary conditions for the diffusion equation in radiative transfer. *J Opt Soc Am A.* 1994 **11**: 2727-2741.

20. Furutsu K and Yamada Y. Diffusion approximation for a dissipative random medium and the applications. *Phys Rev E.* 1994 **50**: 3634-3640.

21. Press WH, Teukolsky SA, Vetterling WT and Flannery BP. Numerical recipes in C: The art of scientific computing. 1992 (New york Cambridge University Press).

22. Cubeddu R., Pifferi A, Taroni P, Torricelli A and Valentini G. Experimental test of theoretical models for time-resolved reflectance. *Med. Phys.* 1996 **23**: 1625-1633.

23. Cubeddu R, Musolino M, Pifferi A, Taroni P and Valentini G. Time-resolved reflectance: a systematic study for the application to the optical characterisation of tissue. *IEEE J Quantum Electron* 1994 **30**: 2421-2430.

9.

Intraoperatively assessed optical properties of malignant and healthy breast tissue used to determine the optimum wavelength of contrast for optical mammography

Adapted from:

R.L.P. van Veen, H.J.C.M. Sterenborg, A.W.K.S. Marinelli, and M. Menke-Pluymers. Intra-operatively assessed optical properties of malignant and healthy breast tissue, to determine the optimum wavelength of contrast for optical mammography. **J Biomed Opt. 2004: (6):1129-1136**

Abstract.

We use spatially resolved diffuse remittance spectroscopy (DRS) for the measurement of absorption (μ_a) and reduced scattering (μ_s') coefficients of normal and malignant breast tissue *in vivo* during surgery. Prior to these measurements, the linearity of the measurement technique was evaluated on liquid optical phantoms. In addition, the reproducibility of *in vivo* tissue measurements was determined on a healthy volunteer.

We present results of the in-vivo measurement of optical properties in the wavelength range from 600 to 1100 nm performed during radical mastectomy. A total of 24 patients were included in the study. Both the absorption and reduced scattering properties show large variations. Significant differences in optical properties between normal (glandular plus lipid rich tissue) and tumour tissues are present in 74% of all patients. However, in some cases the tumour showed lower values than normal tissue, and in other cases this was the other way around. Thus, a general trend in optical properties is not observed. However, the average absorption contrast of all patients as a function of wavelength reveals an optimal contrast peak at 650 nm. We believe that this relates to a difference in vascular saturation between tumour and adjacent normal tissue.

1 Introduction

Breast cancer is the most widespread non-skin malignancy among women within the United States and most European countries. In Europe, annual mortality rates are about 70,000.

The current standard breast cancer screening tools are palpation and x-ray mammography. However, the latter technique is associated with insufficient specificity, resulting in a large number of false positives. This leads to many unnecessary biopsies and surgical procedures. X-ray mammography depends on the use of ionising radiation and is of limited use for young women and women with radiographic dense breasts. Furthermore, the use of ionising radiation comprises the risk of cancer induction. Near-infrared optical imaging is a relatively new non-ionising and non-invasive quantitative technique for the detection of breast cancer. Multispectral nearinfrared (NIR) imaging and spectroscopy might provide several advantages, such as low cost compared to CT and MRI. More important, however, is that optical imaging may provide information complementary to currently employed techniques, such as tissue oxygenation levels, total haemoglobin, water, and lipid content, that may improve the contrast between normal, benign, and malignant tissue structures. Currently, several groups are investigating different optical techniques, e.g., tomographic,[1–7] multispectral transillumination,[8–11] optical imaging, or functional spectroscopy techniques,[12–15] either continuous wave, or by time- or frequency-resolved techniques. Spectra or images result from differences in optical properties, i.e., reduced scattering and absorption coefficients, respectively. These result from variations in (extra) cellular refractive indices and oxy-haemoglobin, deoxy-haemoglobin (oxygenation), water, and lipid chromophore content, respectively. There is evidence in the literature that malignant and benign tissue structures can be discriminated from adjacent normal tissue by their water/lipid ratios, or due to differences in total haemoglobin content and oxygenation, e.g., tumours are associated with an increase in blood volume and a decrease in oxygenation proliferaty.[16,17] Spectral information on reduced scattering coefficients may provide information of scatter centre size and density, and is related to the tissue composition and cellular structure. For contrast optimisation it is therefore necessary to have detailed spectral knowledge of in-vivo optical properties to select the optimal detection wavelengths. As tissue optical properties are strongly influenced by tissue physiology, it is therefore imperative to perform these measurements *in vivo*. The aim of this study was to determine intrinsic in-vivo optical properties of various breast tissue types, e.g., normal glandular tissue, subcutaneous fat, skin, and different malignant tissue pathologies. To do these measurements *in vivo* as close to the target volume as possible, we have performed these measurements intra-operatively. For this we used an optical measurement technique known as spatially resolved diffuse reflectance spectroscopy (DRS). This is a relatively simple technique that allows for high-resolution measurement optical properties over a broad wavelength bandwidth.[18,19]

Prior to the clinical study, the system linearity was checked by means of liquid tissue phantoms. Furthermore, we determined the reproducibility of the method by means of a series of repeated measurements on a single volunteer.

2 Materials and Methods

2.1 Experimental Set-up

The set-up used is shown schematically in figure 1. The illumination of the tissue and the collection of the diffuse re-emitted light are performed by a multi-fibre probe. This black Perspex probe consists of 10 low hydroxyl (OH^-) medical graded fibres (400-μm core, length approximately 4 m) (CeramOptec GmbH, Bonn, Germany), in which the fibres are positioned at average inter-fibre distances of 2 mm (2 up to 18 mm). The white light from a 100-W quartz tungsten halogen lamp is coupled into the illumination fibre of the probe. Total light output power of the source fibre was 20 mW. The nine detection fibres in the probe direct the light to the entrance slit position of an imaging spectrograph (Oriel, MS257). The 150-lines/mm grating in the spectrograph allows us to cover a wavelength range from 440 to 1100 nm. A 16-bit 256 to 1024 pixel charge-coupled device (CCD) camera cooled to -30 °C

(Andor DU420-OE, Belfast, Northern Ireland) detects the nine reflectance spectra originating at different distances from the illumination fibre.

2.2 Data Processing

Data processing and analysis of the data files were performed using custom software written in Matlab™ (Matlab, Mathworks Incorporated, Massachusetts). The photon propagation in turbid biological tissues can be described using diffusion theory. Farrell, Patterson, and Wilson[20] adapted the diffusion approximation with extrapolated boundary conditions to describe steady-state spatially resolved diffuse reflectance measurements, more recently improved by Kienle and Patterson.[21] In earlier work[19] we used spatially resolved diffuse reflectance spectroscopy for the non-invasive determination of *in vivo* human tissue optical properties and absolute chromophore concentrations based on this analysis. Rather than calculating optical properties for each of the wavelengths separately, this analysis[18] considered the whole data-set and calculated the absorption and reduced scattering spectra over the entire wavelength range. As a constraint in the analysis, we assumed Lorentz-Mie scattering ($a \cdot \lambda^{-b}$). The diffusion approximation introduces some assumptions into the analysis. The light has to be diffuse, so scattering should dominate absorption. Furthermore, the distance between the source and detector fibre should exceed a minimum distance of approximately $r > 1/\mu_s'$. Based on preliminary results, it was concluded that to satisfy this constraint, the first three fibres had to be excluded from the analysis, consequently the fibre closest to the source was located at a distance of 8 mm.

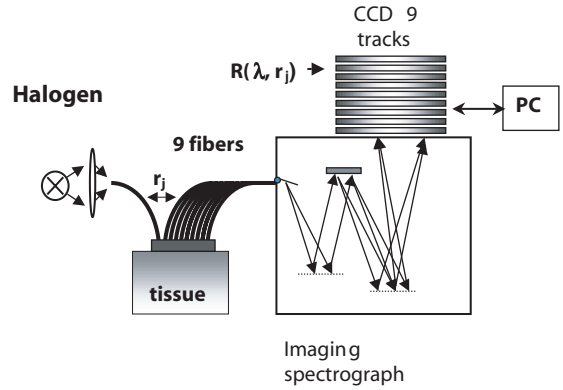

Figure 1. Basic layout of the diffuse reflectance spectroscopy set-up.

2.3 Phantom Measurements

Prior to the clinical measurements, the linearity of the technique was evaluated on homogeneous liquid optical phantoms[22] using intralipid (Intralipid 20% Fresenius Kabi, Hertogenbosch, Netherlands) and Evans Blue (EB) (ACROS organics, Geel, Belgium). First, the reduced scattering coefficient of the solution was kept constant while increasing the absorption coefficient from 2 m^{-1} up to 10000 m^{-1}. Second, we varied the reduced scattering coefficient while keeping the absorption at a fixed value of 33 m^{-1}.
During the measurement, the probe was mechanically held at a fixed position on the phantom surface. The probe was repositioned after each measurement. For each phantom, three measurements were made. Prior to these measurements, the specific absorption coefficient of EB was determined at 630 nm by means of collimated transmission measurements in a scattering-free solution.

2.4 Volunteer Study

To investigate reproducibility of in-vivo measurements, DRS measurements were performed on a single healthy volunteer (age 26) at ten different locations covering all quadrants in the vicinity of the aureole (n=5) and the border of the breast (n=5). The fibre optic probe was positioned manually at the measurement site. On each of the ten locations, three sequential measurements were performed without repositioning the probe.

2.5 Patients

In this study, 24 patients were enrolled with tumour dimensions exceeding 10 mm. The procedure was performed according to a protocol approved by the local medical ethics committee and with the patient's written informed consent. Histologically confirmed tumours were classified as either 1. benign/reactive, 2. ductal carcinoma in situ (DCIS), or 3. infiltrated; the latter either being of the ductal or lobular adeno type.
During the procedure, the fibre optic probe was placed inside a sterile transparent PVC cover bag (Intercover, Inter-national Medical Products, Zutphen, Netherlands).

During the measurements, all possible interfering light sources such as the theatre lights were turned off and measurements were conducted under subdued light conditions, i.e., less than 50 lux. The fibre-optic probe was held in position manually and placed on the surgical margins of either the tumour or the normal tissue. At each specific tissue location, three sequential measurements were made. If possible, measurements on the same tissue type were taken at several different positions. The total measurement time for a single *in vivo* measurement was 4 sec. Additional surgery time as a result of these measurements was approximately 10 to 15 min. Measurements were performed *in vivo* during modified radical mastectomies with the tissue blood supply still intact. Time of DRS measurements during surgery was halfway through the mastectomy procedure, partially exposing the muscular pectoralis, subcutaneous fat, lipid-rich glandular tissue, and tumour site.
In a number of cases, tumours with depths boundaries not lower than 5 mm beneath the skin surface were measured transcutaneously.

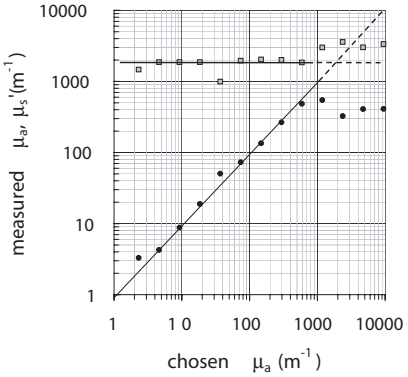

Figure 2. Absorption and reduced scattering coefficients as measured with DRS versus expected μa at constant reduced scattering coefficient ($\mu_{s'}$ = 2000 m^{-1}) at λ=630 nm. The dashed line indicates the region where the measured absorption starts to deviate from linearity.

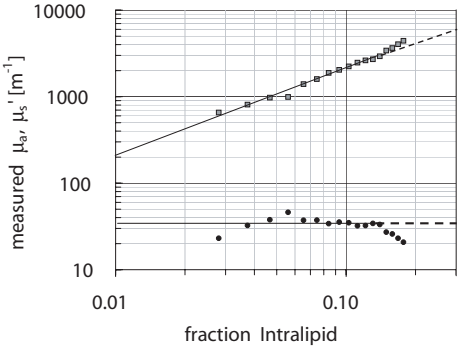

Figure 3. Scattering coefficients as measured with DRS versus fraction of Intralipid in the phantom solution. Absorption μ_a was kept constant at 33 m^{-1}. The dashed line indicates the region where the measured reduced scattering starts to deviate from linearity.

3 Results

3.1 Phantom Study

Figure 2 shows the results of DRS measurements on the optical phantoms with constant reduced scattering (~2000 m^{-1}) and increasing absorption up to 10000 m^{-1} at 630 nm. The solid straight line represents a linear regression fit through the log values of the data. The slope of the fit was 0.96 and is within the 95% confidence level interval (0.88 to 1.02) with a R^2 value of 0.98. The measured ma starts to deviate from the chosen μ_a for 590 $m^{-1} < \mu_a < 2$ m^{-1}, and coupling effects between μ_a and μ_s' are now observed. Figure 3 shows the results of DRS measurements on phantoms with constant absorption of 33 m^{-1} and increasing reduced scattering at 630 nm. The solid straight line represents a linear regression fit. The slope of the fitted linear regression was 0.83 and is within the 95% confidence level interval (0.64 to 1.01) with a R^2 value of 0.82. Both slopes are within 95% confidence interval, indicating the systems linear response for reduced scattering and absorption. The measured μ_s' starts to deviate from linearity for μ_s'>3000m^{-1}. The standard deviation originating from repositioning the probe three times is less than 3% for reduced scattering and absorption, respectively.

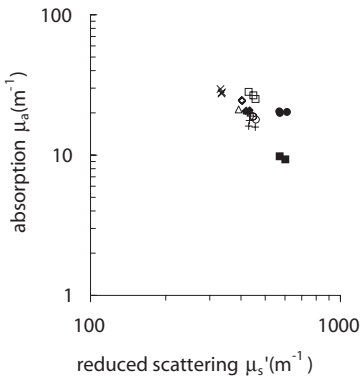

Figure 4. Absorption versus reduced scattering coefficients at 900 nm of healthy breast tissue measured on a volunteer. Each group of identical symbols represents three sequential measurements at the same location. Measurements were taken at ten different locations.

3.2 Volunteer

Figure 4 shows the absorption versus reduced scattering coefficients measured on the volunteer at 900 nm. We calculated the average (μ_a ,μ_s'), standard deviation (σ), and relative variation defined as σ/μ of the three sequential measurements at 900 nm for all ten locations (Table 1). Measurements on the same location appeared to reproduce within 4 and 2.6% for absorption and reduced scattering, respectively. Relocating the measurement probe over the ten different locations showed a much larger variability, i.e., and 27.2 and 18.6% standard deviation for absorption and reduced scattering, respectively.

This large difference suggests that the relative variations within one location reflect the reproducibility of the measurement technique, while the variations between the different locations are due to actual local variations in optical properties within the breast tissue.

Table 1. Analysis of the reproducibility of the measurements at 900 nm. Three repeated measurements on 10 locations show that the relative variations between measurements at that same location are roughly 7 times smaller than the relative variations between locations.

Location	μ_a [m^{-1}]	σ / μ. [%]	μ_s' [m^{-1}]	$/\mu$ [%]
1	20.6	1.2%	426	1.9%
2	26.7	5.8%	444	3.2%
3	18.5	2.9%	451	1.5%
4	28.4	3.9%	333	0.7%
5	20.7	2.7%	416	5.5%
6	28.0	11.7%	361	2.5%
7	9.6	3.5%	586	3.7%
8	20.3	1.3%	584	4.0%
9	16.5	5.9%	439	3.3%
10	24.5	1.0%	403	0.2%
Mean variation within location	4.0%		2.7%	
Relative variation between locations	27%		19%	

3.3 Patients

Intraoperative measurements were performed on 24 patients in total. For each patient, measurements on normal glandular breast tissue could be performed, measured at large distances from the tumour site. In addition, 18 sets of measurements on malignant tissue were made. In six patients, such measurements were not feasible due to either the small size of the tumour, i.e., <10 mm (N=2, inclusion errors) or the fact that the tumor was too deep below the resection surface (i.e., >10 mm). For the normal tissue measurements, the probe was positioned on locations that were visually identified as healthy. Measurements on the palpable tumours were performed at locations where the layer covering the tumour was the thinnest. Three tumours were located only 5 mm below the skin. These tumours were also measured transcutaneously. In total, 312 reliable spectra were recorded. Table 2 gives an overview of the total data-set. Patient age ranged from 37 to 88 years, of which five were premenopausal.

Table 2. Overview of the tissue types measured.

Tissue type measurement	Number of patients
Reactive alteration, hyperplasia	1
DCIS (ductal carcinoma in-situ)	2
Infiltrated lobular/ductal adeno carcinoma	15
Glandular/Fat	24
Tumor transcutaneous	3
Muscular pectoralis	10
Breast skin	9

An example of *in vivo* optical properties of normal and diseased breast tissue in the wavelength range from 600 to 1100 nm is shown in Fig. 5. The age of this patient was 47 and she was premenopausal. The tumour was an infiltrated ductal adeno carcinoma with an average size of 18 mm, located 6 mm underneath the resection surface. For this individual case, the reduced scattering properties did not show any significant differences between tumour and normal. However, a clear and significant difference is seen between the absorption coefficient of the tumour measurement and the measurement performed on normal lipid-rich glandular tissue. Another individual patient example is shown in Fig. 6.

Here absorption is plotted versus reduced scattering at 650 nm for each individual measurement. The age of the patient was 53 and she was postmenopausal. The tumour was a differentiated ductal carcinoma *in situ* after receiving chemotherapy.
A student's t-test shows significant differences in absorption between the means of the normal glandular and tumor tissue measurements ($p<0.05$).

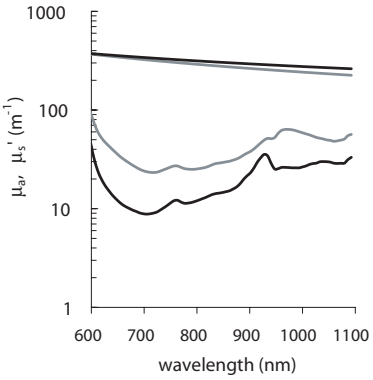

Figure 5. Example of the in-vivo reduced scattering and absorption spectra of normal (black) and malignant (grey) breast tissue versus wavelength in a single patient.

No significant differences in reduced scattering between both tissue types are present. In these two individual cases, the tumors are detectable in optical mammography based on the differences in absorption coefficients between normal and tumor. Such a simple criterion, however, would not be very successful in most other patients.

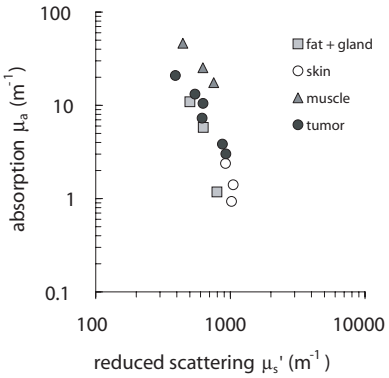

Figure 6. Example of the absorption plotted versus reduced scattering coefficients at 650 nm for a single patient. Each point represents a single measurement.

Tumor detection based on other criteria, i.e., the reduced scattering coefficient, or a combination of absorption, reduced scattering (optical penetration depth, albedo), and scatter power is illustrated in table 3.

Table 3. Fraction of tumors detected for different detection criteria.

Parameter (nm)	Detection Score (%)
Scatter power	26.1
μ_s' (650)	21.7
μ_s' (980)	26.7
μ_a (650)	39.1
μ_a (980)	52.2
optical penetration depth(650)	39.1
optical penetration depth(980)	56.5
1-albedo(650)	43.5
1-albedo(980)	39.1
all (650)	52.2
all (980)	69.9
all parameters combined	73.9

Here we list the detection score for different parameter or combination of parameters. The detection score is defined as the percentage of the 18 tumours that is detectable, whereas the detectability of each individual tumour is evaluated by performing a t-test on the means of the specific parameters for tumour and adjacent glandular tissue. In the case of multiple parameters, the tumour is assumed detectable when at least one of the t-tests shows a significant difference. The detection score was calculated from 600 to 1100 nm with a 20-nm interval. Table 3 shows that 74% are detectable at best for a combination of two wavelengths, i.e., 650 and 980 nm. This detection score is rather low, considering all the prior knowledge used.

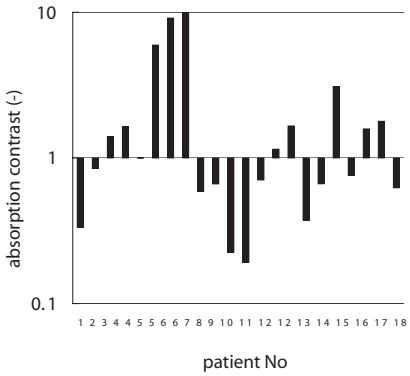

Figure 7. Absorption contrast between tumor and adjacent lipid-rich glandular tissue calculated for 18 patients at 650 nm.

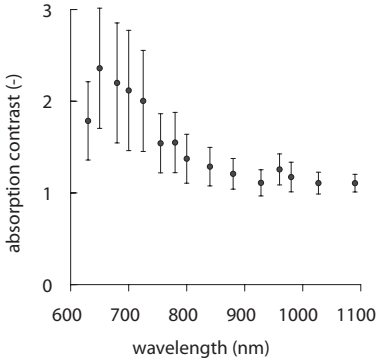

Figure 8. Average absorption contrast of all patients as a function of wavelength. The error bars represent the standard error of the mean.

Absorption contrast between tumour and adjacent normal (lipid-rich glandular) tissue was calculated for 18 patients by dividing the average of all tumour measurements by the average of all normal measurements in a single patient. Figure 7 shows the absorption contrast at 650 nm for 18 patients.

No systematic patterns could be observed, i.e., in some cases (12 out of 22), absorption was higher in tumour than in normal tissue, while in others the opposite was the case. Likewise for scattering, sometimes the tumour showed higher scattering than the adjacent normal glandular tissue, while sometimes it was lower. However, the average absorption contrast of all patients as a function of wavelength revealed a peak at 650 nm with a maximum of 2.4, as depicted in figure 8. The error bars given here represent the standard error of the mean, as the standard deviation was very high, as described earlier.
Reduced scattering did not reveal any spectral features in contrast, as seen in figure 9, and was on average a factor 1.08.

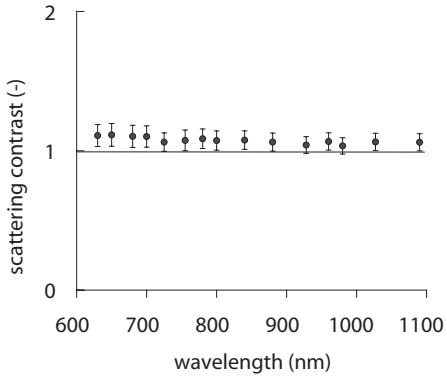

Figure. 9 Average reduced scattering contrast of all patients as a function of wavelength. The error bars represent the standard error of the mean.

In figure 10, the average optical properties of all patients and tissue types at 650 nm are shown, demonstrating overlap between the different tissue types due to the large standard deviations. However, figure 10 confirms the systematic differences between tumour and adjacent glandular tissue. Values for average Mie scatter power were 20.7 standard deviation (SD) 0.4 for lipid-rich glandular tissue, 21.4 SD 0.5 for muscle, 21.4 SD 0.8 for breast skin, 20.8 SD 0.4 for tumour, and 1.1 SD 0.9 for tumour transcutaneous.

4 Discussion

We present, to our knowledge; the first intraoperatively assessed in-vivo optical properties of normal and malignant female breast tissue in the wavelength region between 600 and 1100 nm. In this study large variations in optical properties were observed within subjects, and as even larger over the entire patient group. The DRS method was first tested on a series of homogeneous optical phantoms with the probe fixed on top of the surface. The derived $\mu s'$ were well linear with increasing intralipid concentration, and measured μa in good agreement with the predicted absorption, thus demonstrating the methods validity. The scattering properties of Intralipid measured by spatially resolved DRS are

comparable with those reported by van Staveren *et al.*,[22] e.g., 0.1 fraction of Intralipid 20% corresponds to a reduced scattering coefficient of ~2000 m^{-1}. In other studies, spatially resolved DRS was compared with time-resolved DRS by measurement on the same epoxy phantom[23] and pure mammalian lipid sample,[24] and results were in good agreement.

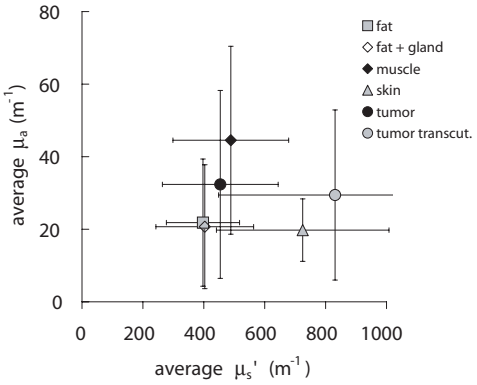

Figure 10. Average absorption coefficients versus average reduced scattering coefficients of all patients and tissue types at 650 nm. The error bars represent the standard deviation

The volunteer measurements showed variations on the order of 4% within a single location. It is unlikely that these variations are related to movement of the manually held fibre optic probe. The sampled volume is several millimetres in diameter, hence only a substantial (i.e., 1 mm or more) Movement is expected to cause a substantial change in the sample volumes. More important may be the effect of probe pressure. Increased pressure may push the main absorber, haemoglobin, out of the capillaries and could decrease water concentration due to interstitial water transport,[25] thus altering the optical properties. To a lesser extent, slight changes in probe angle may explain the variations. Repositioning the probe to other locations on the same breast showed even larger variations (27 and 19%), clearly demonstrating large variation in local optical properties.

The intraoperative measurements demonstrated large variations in optical properties, and no strong systematic differences between tumour and normal tissue were observed. Possible differences in optical properties observed may have been diluted to a certain extent because of the presence of a margin of normal tissue on top of the surgically exposed tumour. Measurements directly on the tumour were not possible, as the excision margins around the tumour are between 4 and 15 mm. In principle, the maximum information density of the measured signals is reached around 5 mm in depth, hence we rejected four cases where the resection margin was obviously more than 10 mm. This, however, was based on the surgeon's feeling during surgery and may not have been 100% accurate.

The manual positioning of the fibre optic probe, making good optical contact to the tissue and holding it steady during surgery proved to be cumbersome, especially in certain locations.

Although ambient lights were low, some spectra showed artefacts related to ambient light. This nearly always caused the fit procedure, which was used to transform reflection spectra to optical properties, to become unstable. This occurred in 129 out of the 441 measured spectra. Some of these cases were identifiable by the ambient light artefacts, but most were related to bad optical contact. We believe that some of the failures that produced an unstable fit were related to inhomogeneities in the tissue in the measurement volume, such as large blood vessels. The mathematical models used to analyse the data assume a homogenous medium. Volumes probed with the DRS technique are between 0.1 and 2 cm^3. Inhomogeneities within such a volume can easily occur, producing a mathematical incompatibility between measurement and model.

Many authors reported breast tissue optical properties either *ex vivo*[26–29] or *in vivo*,[30–32] all demonstrating a large variety in results. In part this can be accounted for by differences in methodology, e.g., *ex vivo* tissue samples suffer from blood loss and preparation may alter reduced scattering properties. Furthermore, the breast is an inhomogeneous organ consisting of different tissue types, and thus the measurement geometry potentially has a large impact on the *in vivo* optical properties obtained. In addition, physiological temporal variations such as age-depended breast parenchyma and menstrual cycle[33] have demonstrated to induce large variations in optical properties between pre- and postmenopausal subjects,[34,35] resulting from atrophy of glandular tissue and decrease in water content. Hormone replacement treatment (HRT) is of influence as well and is associated with epithelial proliferation in the ductal tracts and increased water content. Moreover, the different techniques used may be influenced differently by the inhomogeneities mentioned earlier. In the case of a small inhomogeneity that would not cause our fit algorithm to fail, our dc measurement would favour the areas of lowest optical properties, as these would have the largest contribution to the signals. Time resolved late gate measurements, on the other hand, could favour the areas with the largest scattering, as these photons would take longer.

The results of our transcutaneaous measurements coincide with previous work by Shah *et al.*[15] and Durduran *et al.*[31] Direct comparison of our intraoperatively measured values is not possible. Tomographically derived optical properties of normal glandular tissue presented by Jiang *et al.*[7] give higher scattering and lower absorption.

We found a moderately higher detectability in the region where blood absorption is large and near the water peak. The average contrast of all patients as a function of wavelength revealed an optimal contrast peak at 650 nm that can be related to a systematic difference in blood oxygenation between tumour and adjacent normal tissue. The ratio, as seen in figure 8, could be explained by a drop in blood saturation from 90% in normal tissue to 55% in and around the tumour. A similar trend in contrast between tumour and normal breast tissue has recently been demonstrated by Taroni *et al.*[36]

Although promising results are demonstrated in several ongoing trials, e.g., refs. [37] and [38], there is still unsatisfactory result with regard to the sensitivity for detection of fairly large tumours. These results are confirmed in the present study. Although the optical imaging

technique in itself may be very powerful, its diagnostic success relies on the presence of a contrast between tumour and normal. Based on the present findings, it is suggested that optimal contrast could be found around 650 nm, i.e., the wavelength region most sensitive to differences in tissue oxygenation.

5 Conclusion

The optical properties of different breast tissues are measured in the spectral range from 600 to 1100 nm, demonstrating large intra- and inter-patient variations. We believe that these variations are mainly due the heterogeneous nature of breast tissue, consequently this resulted in large differences in local optical properties partially masking possible differences between tumour and normal. Additional variations are introduced by tissue inhomogeneities and measurement artefacts, e.g., ambient light and probe tissue contact, e.g., misalignment of the sterile clear cover material and probe pressure. In 74% of the cases, the tumour could be distinguished from its surrounding normal tissue on the basis of significant difference of the average optical properties. However, no systematic differences are observed between tumour and normal tissue. In cases where significant differences are observed between tumour and adjacent normal tissue, we saw no systematic behaviour, i.e., scattering as well as absorption of tumour tissue could either be higher or lower than normal tissue. However, the average absorption contrast of all patients as a function of wavelength revealed an optimal contrast peak at 650 nm that can be related to a difference in tissue oxygenation between tumour and adjacent normal tissue.

References

1. Hebden JC, Veenstra H, Dehghani H, Hillman EM, Schweiger M, Arridge SR and Delpy DT. Three-dimensional time-resolved optical tomography of a conical breast phantom. *Appl Opt.* 2001 **40**: 3278-3287.

2. Pogue BW, Poplack SP, McBride TO, Wells WA, Osterman KS, Osterberg UL and Paulsen KD. Quantitative hemoglobin tomography with diffuse near-infrared spectroscopy: pilot results in the breast. *Radiology.* 2001 **218**: 261-266.

3. Zhu Q, Huang M, Chen N, Zarfos K, Jagjivan B, Kane M, Hedge P and Kurtzman SH. Ultrasound-guided optical tomographic imaging of malignant and benign breast lesions: initial clinical results of 19 cases. *Neoplasia.* 2003 **5**: 379-388.

4. Culver JP, Choe R, Holboke MJ, Zubkov L, Durduran T, Slemp A, Ntziachristos V, Chance B and Yodh AG. Three-dimensional diffuse optical tomography in the parallel plane transmission geometry: evaluation of a hybrid frequency domain/continuous wave clinical system for breast imaging. *Med Phys.* 2003 **30:** 235-247.

5. Li A, Miller EL, Kilmer ME, Brukilacchio TJ, Chaves T, Stott J, Zhang Q, Wu T, Chorlton M, Moore RH, Kopans DB and Boas DA. Tomographic optical breast imaging guided by three-dimensional mammography. *Appl Opt.* 2003 **42(25)**: 5181-5190.

6. Srinivasan S, Pogue BW, Jiang S, Dehghani H, Kogel C, Soho S, Gibson JJ, Tosteson TD, Poplack SP and Paulsen KD. Interpreting hemoglobin and water concentration, oxygen saturation, and scattering measured *in vivo* by near-infrared breast tomography. *Proc Natl Acad Sci U S A.* 2003 **100**: 12349-12354.

7. Jiang H, Iftimia NV, Xu Y, Eggert JA, Fajardo LL and Klove KL. Near-infrared optical imaging of the breast with model-based reconstruction. *Acad Radiol.* 2002 **9**: 186-194.

8. Pifferi A, Taroni P, Torricelli A, Messina F, Cubeddu R and Danesini G. Four-wavelength time-resolved optical mammography in the 680-980-nm range. *Opt Lett.* 2003 **28**: 1138-1140.

9. Grosenick D, Moesta KT, Wabnitz H, Mucke J, Stroszczynski C, Macdonald R, Schlag PM and Rinneberg H. Time-domain optical mammography: initial clinical results on detection and characterization of breast tumors. *Appl Opt.* 2003 **42**: 3170-3186.

10. Fantini S, Walker S, Franceschini MA, Kaschke M, Schlag PM and Moesta KT. Assesment of size, position and optical properties of breast tumors in vivo by nonivasive optical methods. *Appl Opt.* 1998 **37**: 1982-1989.

11. Franceschini MA, Moesta KT, Fantini S, Gaida G, Gratton E, Jess H, Mantulin WW, Seeber M, Schlag PM and Kaschke M. Frequency-domain techniques enhance optical mammography: initial clinical results. *Proc Natl Acad Sci U S A.* 1997 **94**: 6468-6473.

12. Tromberg BJ, Coquoz O, Fishkin JB, Pham T, Anderson ER, Butler J, Cahn M, Gross JD, Venugopalan V, and Pham D. Non-invasive measurements of breast tissue optical properties using frequency-domain photon migration. *Philos Trans R Soc Lond B Biol Sci.* 1997 **352**: 661-668.

13. Tromberg BJ, Shah N, Lanning R, Cerussi A, Espinoza J, Pham T, Svaasand L and Butler J. Non-invasive in vivo characterization of breast tumors using photon migration spectroscopy. *Neoplasia.* 2000 **2**: 26-40.

14. Cerussi AE, Jakubowski D, Shah N, Bevilacqua F, Lanning R, Berger AJ, Hsiang D, Butler J, Holcombe RF and Tromberg BJ. Spectroscopy enhances the information content of optical mammography. *J Biomed Opt.* 2002 **7**: 60-71.

15. Shah N, Cerussi A, Eker C, Espinoza J, Butler J, Fishkin J, Hornung R and Tromberg B. Noninvasive functional optical spectroscopy of human breast tissue. *Proc Natl Acad Sci U S A.* 2001 **98**: 4420-4425.

16. Thomsen S and Tatman D. Physiological and pathological factors of human breast disease that can influence optical diagnosis. *Ann N Y Acad Sci.* 1998 **838**: 171-193.

17. Beauvoit B, Kitai T and Chance B. Contribution of the mitochondrial compartment to the optical properties of the rat liver: a theoretical and practical approach *Biophys J.* 1994 **67**: 2501-2510.

18. van Veen RLP, Verkruijsse W and Sterenborg HJCM. Diffuse reflectance spectroscopy from 500 to 1060 nm by correction for inhomogenously distributed absorbers. *Opt Lett.* 2002 **27**: 246-248.

19. Doornbos RMP, Lang R, Cross FW, and Sterenborg HJCM. The determination of *in-vivo* human tissue optical properties and absolute chromophore concentrations using spatially resolved steady state diffuse reflectance spectroscopy. *Phys Med Biol.* 1999 **44**: 967-981.

20. Farrell TJ, Patterson MS, and Wilson B. A diffusion theory model of spatially resolved, steady-state diffuse reflectance for the noninvasive determination of tissue optical properties in vivo. *Med Phys.* 1992 **19**: 879-888.

21. Kienle A, Patterson MS. Improved solutions of the steady-state and the time-resolved diffusion equations for reflectance from a semi-infinite turbid medium. *J Opt Soc Am A.* 1997 **14**: 246-254.

22. van Staveren HJ, Moes CJM, van Marle J, Prahl SA and van Gemert MJC. Light scattering in Intralipid 10% in the wavelength region of 400-1100 nm. *Appl Opt.* 1991 **30**: 4507-4513.

23. Pifferi A, Torricelli A, Bassi A, Taroni P, Cubeddu R, Wabnitz H, Grosenick D, Möller M, Macdonald R, Swartling J, Svensson T, Andersson-Engels S, van Veen RLP, Sterenborg HJCM, Tualle JM, Tinet E, Avrillier S, Whelan M and Stamm H, Performance assessment of photon migration instruments: the Medphot protocol, in Biomedical Topical Meetings on CD-ROM (The Optical Society of America, Washington, DC, 2004), WD7.

24. van Veen RLP and Sterenborg HJCM, Pifferi A, Torricelli A and Cubeddu R. Determination of VIS-NIR absorption coefficients of mammalian fat, with time- and spatially resolved diffuse reflectance and transmission spectroscopy. In Biomedical Topical Meetings on CD-ROM (The Optical Society of America, Washington, DC, 2004), SF5.

25. Jiang S, Pogue BW, Paulsen KD, Kogel C and Poplack SP. In vivo near-infrared spectral detection of pressure-induced changes in breast tissue. *Opt Lett.* 2003 **28**: 1212-1214.

26. Troy TL, Page DL and Sevick -Muraca E.M. Optical properties of normal and diseased breast tissues: Prognosis for optical mammography. *J Biomed Opt.* 1996 **1**: 342-355.

27. Peters VG, Wyman DR, Patterson MS and Frank GL. Optical properties of normal and diseased human breast tissues in the visible and near infrared. *Phys Med Biol.* 1990 **35**: 1317-1334.

28. Ghosh N., Mohanty S., Majumder S. and Gupta P. Measurement of optical properties of normal and malignant human breast tissue. *Appl Opt.* 2001 **40**: 176-184.

29. Zacharakis G, Zolindaki A, Sakkalis V, Filippidis G, Papazoglou TG, Tsiftsis DD and Koumantakis E. In vitro optical characterization and discrimination of female breast tissue during near infrared femtosecond laser pulses propagation. *J Biomed Opt.* 2001 **6**: 446-449.

30. Heusmann H, Kolzer J and Mitic G. Characterization of female breast in vivo by time resolved and spectroscopic measurements in near infrared spectroscopy. *J Biomed Opt.* 1996 **1**: 425-434.

31. Durduran T, Choe R, Culver JP, Zubkov L, Holboke MJ, Giammarco J, Chance B and Yodh AG. Bulk optical properties of healthy female breast tissue. *Phys Med Biol.* 2002 **47**: 2847-2861.

32. Quaresima V, Matcher SJ and Ferrari M. Identification and quantification of intrinsic optical contrast for near-infrared mammography. *Photochem Photobiol.* 1998 **67**: 4-14.

33. Cubeddu R, D'Andrea C, Pifferi A, Taroni P, Torricelli A and Valentini G. Effects of the menstrual cycle on the red and near-infrared optical properties of the human breast. *Photochem Photobiol.* 2000 **72**: 383-391.

34. Chance B. Near-infrared (NIR) optical spectroscopy characterizes breast tissue hormonal and age status. *Acad Radiol.* 2001 **8**: 209-210.

35. Cerussi AE, Berger AJ, Bevilacqua F, Shah N, Jakubowski D, Butler J, Holcombe RF and Tromberg BJ. Sources of absorption and scattering contrast for near-infrared optical mammography. *Acad Radiol.* 2001 **8**: 211-218.

36. Taroni P, Pifferi A, Torricelli A, Spinelli L, Danesini GM and Cubeddu R. Do shorter wavelengths improve contrast in optical mammography? *Phys Med Biol.* 2004 **49**: 1203-1215.

37. Torricelli A, Spinelli L, Pifferi A, Taroni P, and Cubeddu R. Use of nonlinear perturbation approach for in-vivo breast lesion characterization by multi-wavelength time-resolved optical mammography. *Opt Express.* 2003 **11**: 853-867.

38. Grosenick D, Wabnitz H, Rinneberg H, Moesta KT and Schlag PM. Development of a time-domain optical mammograph and first in vivo applications. *Appl Opt.* 1999 **38**: 2927-2943.

10.

Optical biopsy of breast tissue using differential path-length spectroscopy

Adapted from:

R.L.P. van Veen, A. Amelink, M. Menke-Pluymers, C. van der Pol and H.J.C.M. Sterenborg. *In vivo* optical biopsy measurement of local optical properties of healthy and malignant breast tissue. **Phys Med Biol. 2005: 7;50(11): 2573-2581.**

Abstract

Differential path-length spectroscopy (DPS) was used to determine the local optical properties of breast tissue *in vivo*. DPS measurements were made on healthy and malignant breast tissue using a fibre-optic needle-probe, and were correlated to the histological outcome of core-needle biopsies taken from the same location as the measurements. DPS yields information on the local tissue blood content, the local blood oxygenation, the average micro-vessel diameter, the β-carotene concentration and the scatter-slope. Our data shows that malignant breast tissue is characterised by a significant decrease in tissue oxygenation and a higher blood content compared to normal breast tissue.

Introduction

Breast cancer is the most widespread non-skin malignancy among women within the United States and most European countries. In Europe, annual mortality rates are about 70.000. Early diagnosis of breast cancer is commonly believed to lead to better prognosis and relatively more breast conserving procedures compared to radical mastectomies. Current standard breast cancer screening tools are palpation and x-ray mammography. However, the latter technique is associated with insufficient specificity, resulting in a large number of false positives. This leads to many unnecessary biopsies and surgical procedures. Furthermore, X-ray mammography depends on the use of ionising radiation and is of limited use for young women and women with radiographic dense breasts. The use of ionising radiation comprises the risk of cancer induction as well. Optical imaging or spectroscopy in the visible (VIS) and near infrared (NIR) wavelength ranges are relatively new, non-ionising and non-invasive quantitative techniques that are currently world-wide under investigation for the detection of breast cancer, which may provide several advantages over commonly used techniques. Optical spectroscopy provides (compared to X-ray ultrasound or MRI) additional physiological information such as tissue oxygenation levels, total haemoglobin, water and lipid content, that may improve the contrast between normal, benign and malignant tissue structures. Currently, several groups are investigating different optical techniques, e.g. tomographic (Hebden *et al* 2001, Pogue *et al* 2001, Jiang *et al* 2002, Li *et al* 2003), multi spectral transillumination optical imaging (Pifferi *et al* 2003, Grossnick et al 2003, Fantini et al 1998), functional spectroscopy techniques (Tromberg *et al* 1997, Tromberg *et al* 2000, Cerussi *et al* 2002, Shah *et al* 2001), or optical biopsy (Bigio *et al* 2000). The contrast between cancerous and normal tissue types in all these techniques relies on differences in the optical properties, i.e. in the reduced scattering and absorption coefficients. For example, tumour absorption contrast could be associated with an increase in blood volume and an increase in oxygen consumption (Thomson *et al* 1998, Beauvoit *et al* 1994). Therefore, detailed knowledge of these optical and physiological properties is essential for further optimisation and innovation of non-invasive optical techniques.

In a previous study performed by our group (van Veen *et al* 2004), multi-fibre spatially resolved diffuse reflectance spectroscopy (DRS) was used to determine wavelengths of optimal tumour-to-normal contrast. In that study measurements were performed intra-operatively during modified radical mastectomies with the tissue blood supply still partially intact. However, the results demonstrated large intra- and inter-patient variations in the optical properties. Additionally, no systematic differences were observed between malignant and normal tissue, i.e. both the scattering and the absorption coefficient of malignant tissue could either be higher or lower than the surrounding healthy glandular lipid-rich tissue. It is assumed that these variations resulted mainly from the heterogeneous nature of breast tissue. The information probing volume of DRS is fairly large, between 0.1 and 2 cm^3 depending on the source-detector fibre distances.

Furthermore, it was assumed that the tissue in the probing volume is homogeneous so that semi-infinite diffusion theory models are valid. The DRS fitting algorithm was shown to be very sensitive to tissue inhomogeneities, such as the presence of large blood vessels. Finally, the large probing volume may have diluted the possible differences in optical properties by the presence of a margin of normal tissue on top of the surgically 'exposed' tumour site, making intrinsic tumour measurements not feasible.

To overcome the problems of our previous study, a technique that measures more locally is required. A novel diagnostic technique (Differential Path-length Spectroscopy, DPS) (Amelink *et al* 2004), developed recently in our group, was modified for this purpose. DPS is a minimally invasive technique able to determine intrinsic *in vivo* optical properties. The technique was successfully applied in the bronchial tree and demonstrated a lower capillary oxygenation and a larger average vessel diameter for malignant tissue compared to normal tissue (Amelink *et al* 2004).

For the present study a conventional biopsy needle was modified in such a way that biopsies could be taken from the exact same location as where the DPS measurements were performed. In this feasibility-study the DPS technique is applied to measure micro-vascular and scattering properties of normal and malignant breast tissue. DPS results were correlated to the histological outcome of the corresponding biopsies. The results for DPS optical biopsy measurements in n=12 patients are presented in this paper.

Methods

A detailed description of the DPS set-up and data analysis is given by Amelink *et al* (2004b); below the methodology will be described in brief.

Optical Biopsy needle:

The set-up consists of two optical fibres for the delivery and detection of light to and from the tissue, as shown in figure 1. Light from a Tungsten Halogen lamp (Ocean Optics, HL-2000-FHSA, Duiven, The Netherlands) is led through one arm of a 200 μm bifurcated optical fibre, which is coupled at its distal end to one arm (the delivery- and-collection (dc)-fibre) of a 600 μm bifurcated optical fibre-probe. Light reflected into the dc-fibre is coupled back into the 200 μm bifurcated fibre and analysed using a dual-channel spectrometer (Ocean Optics, SD2000). Light reflected back from the sample into the other arm of the 600 μm bifurcated fibre-optic probe (the collection (c) fibre) is led directly into the second channel of the dual-channel spectrometer. Both the delivery-and-collection (dc) and the collection (c) fibres were fixed with epoxy in a hollow metal tube having the exact same dimension as the original inner part of the biopsy needle (Bard Magnum Benelux, the Netherlands) as seen in figure 2.

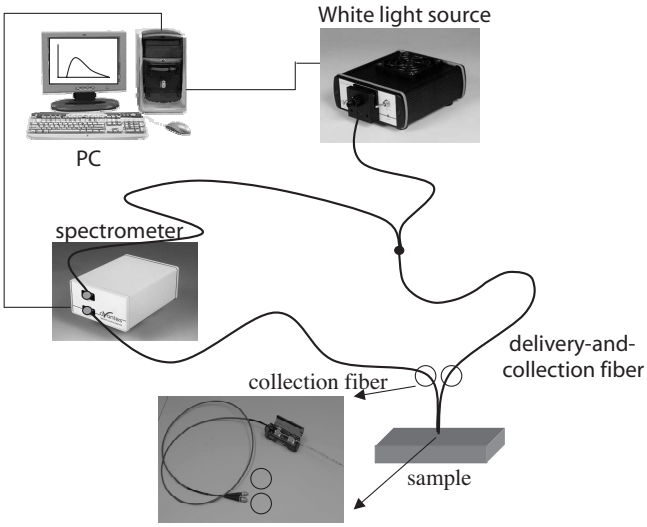

Figure 1. Schematic diagram of the portable DPS set-up.

The distal end of this fibre-optic needle-probe is polished at an angle of 30 degrees to minimise the collection of specularly reflected light at the probe-medium interface, and contacts the sample under investigation. The optical biopsy needle is sterilised by means of argon-plasma sterilisation. The intensity difference of the dc- and c-fibre collection signals is called the differential reflectance signal R(λ), and will be discussed in the data analysis section.

The biopsy gun (Bard Magnum) itself was modified in such a way that it could house the mantled fibre-optic needle-probe without any bending of the fibres. Integration time for a single measurement was 20 msec., and real-time analysis provided absorbing chromophore concentrations and scattering properties within ~3 seconds.

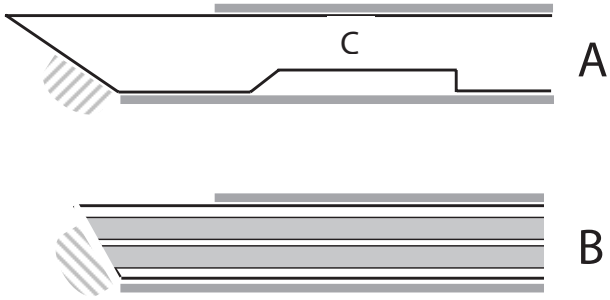

Figure 2. A) The original position of the inner and outer part of the biopsy needle, with "C" the biopsy sample gap. The shaded area is the region of interest that will be excised. First the inner part of the needle is shot forward, immediately followed by the tissue cutting outer part of the needle (dark grey). In B) the situation where the original inner-needle is replaced by the fibre-optic needle-probe for DPS measurements.

Patients:

12 Patients with superficial palpable tumours with dimensions exceeding 10mm and indicated for modified radical mastectomies were invited to participate in this study. All patients were older than 18 years and signed informed consent. The Medical Ethics Review Board of the Erasmus Medical Centre Rotterdam approved the study. For each patient between 4 and 6 biopsies were taken preferably, 3 from cancerous tissue and 2 from healthy breast tissue. Multiple measurements and biopsies were performed to take into account the breast tissue heterogeneity.

The biopsies were taken after anaesthetics and prior to surgery, and were only taken in that region of the breast that was selected for ablation. Surgeons guided the original biopsy needle manually to the palpable tumour mass. Once in position the fibre-optic needle replaced the original inner biopsy needle, and three sequential DPS measurements were made. After the DPS-measurements the biopsy needle was inserted again and a biopsy was taken at the exact same location as the DPS measurement as seen in figure 2. Additional surgery time to perform these measurements was approximately 10 to 15 minutes. The biopsies were fixed in formaline for subsequent pathological analysis.

Data analysis:

The shape of the DPS spectrum is a function of the scattering and absorption coefficient. DPS spectra resemble Mie-like scattering curves with superimposed absorption dips. For the analysis of the spectra, we assumed Lorentz-Mie scattering, i.e. $\mu_s'(\lambda) = a\lambda^{-b}$ where b is a constant related to the size of the scattering particles (Mourant *et al* 1997, Nilsson *et al* 1998). Furthermore, the main absorber in the measured wavelength range (350-1000 nm) is blood. Since blood is not distributed homogeneously throughout the tissue but concentrated in blood vessels, a correction has to be made in accordance with Verkruysse *et al* 1997 and van Veen *et al* 2002 . The complete model to which the DP spectra are fitted is given by Eq (1).

$$R(\lambda) = C_1'\lambda^{-b} \exp(-0.48(c^{beta}\cdot\varepsilon_a + (C_{cor}(\lambda)\,\rho\,[StO_2\,\mu_a^{HbO2}(\lambda) + (1-StO_2)\,\mu_a^{Hb}(\lambda)])) \quad \text{Eq.1}$$

Where ρ is the blood volume fraction, StO_2 the blood oxygenation, $\mu_a^{HbO2}(\lambda)$ the absorption coefficient of fully oxygenated whole blood, $\mu_a^{Hb}(\lambda)$ the absorption coefficient of fully de-oxygenated whole blood (Prahl *et al* 1999), C_1' a proportionality constant, c^{beta} the concentration of beta-carotene, ε_a the specific absorption coefficient of β-carotene (van der Poll *et al* 2003) and C_{cor} the correction factor which accounts for the inhomogeneous distribution of blood in tissue. For whole blood contained in an infinitely long cylinder, this correction factor is given by $C_{cor} = [(1-\exp(-\mu_{abl}(\lambda)D_{vessel}))/(\mu_{abl}(\lambda)D_{vessel})]$ with $\mu_{abl}(\lambda)$ the absorption coefficient of whole blood and D_{vessel} the vessel diameter. However, since this may not be an appropriate geometrical description for blood contained in the capillary network, the fitted vessel diameter may deviate from its absolute value.

A standard Labview™ linear chi squared minimisation procedure was used to determine the set of parameters describing the measurement in a statistically optimum way.

Results

A total of 12 patients with ages ranging from 48 to 84 were included. 50 Locations were measured with DPS and an average of 3 sequential DPS measurements with corresponding histology (n=10 cancerous and 40 normal breast tissue) were recorded.
In spite of attempts to take biopsies in the tumour mass, no tumour biopsies were obtained in 6 out of the 12 patients. All tumours were either lobular or ductal adeno-carcinomas.

Fitting the data to Eq. (1) yields values for StO_2, ρ, D_{vessel}, β-carotene and b. In case of low blood content present in the detection volume (ρ< 1%), the blood saturation StO_2 (i.e. oxy and de-oxy haemoglobin concentrations) and the vessel diameter D_{vessel} could not be fitted reliably. This was actually the case in 17 locations, once in cancerous tissue and 16 times in healthy breast tissue. Thus the blood saturation and vessel diameter were analysed for 33 locations, while the blood volume fraction, β-carotene concentration and scatter-slope were analysed for all 50 locations. Figure 3 shows a typical example of fit results for normal and malignant breast tissue.

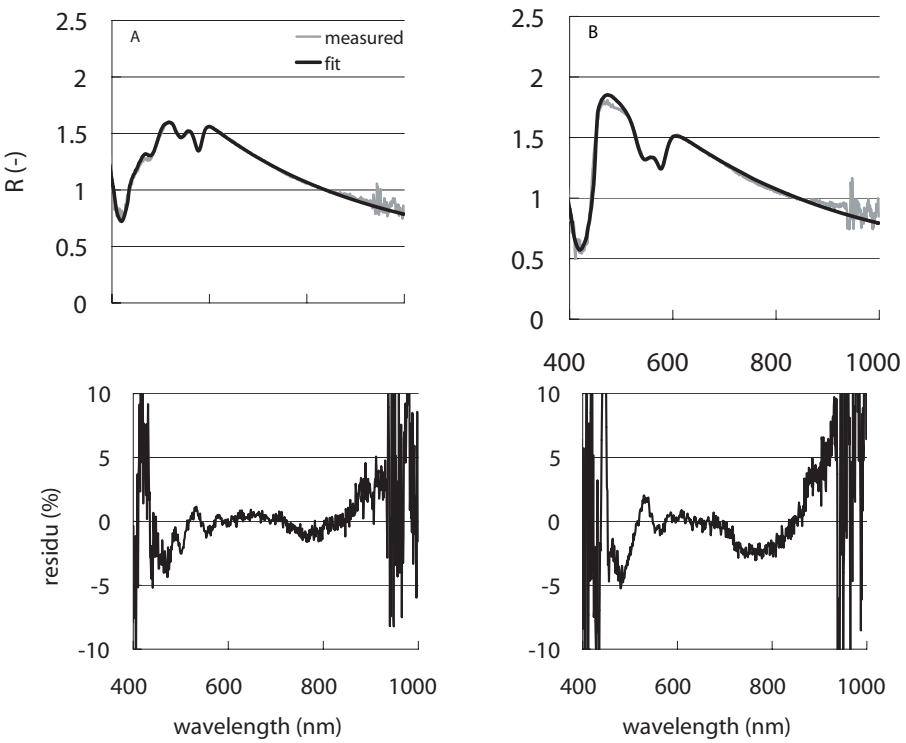

Figure 3. Examples of DPS spectra (grey line) and fits (black line) according to Eq. 1. A) Typical spectrum of normal glandular tissue (StO_2=96.5%, ρ=2.6%, D_{vessel}=7.6μm, beta-carotene concentration=113 μM and b=-1.73). The relative residu (Rbs_{model}-Rbs_{meas}/Rbs_{model}) is depicted underneath. The arrow indicates the location of the largest β-carotene peak @ 480nm. B) Spectrum of malignant breast tissue (StO_2=53.1%, ρ=4.1%, D_{vessel}=7.2μm, β-carotene concentration=4.3 μM and b=-1.37).

This particular patient suffered from a 29 mm infiltrating adeno-carcinoma. The noise above λ = 940 nm and below λ = 400 nm is caused by strong absorption in the fibres and a low efficiency of the CCD-array and the spectrometer grating. Spectral differences are clearly observed between the two spectra in the wavelength range 400 up to 600 nm. In this wavelength region blood and β-carotene absorption dominates the spectral shape of the differential reflectance signal. Comparing the spectra of figure 3 with the absorption spectra of Hb and HbO_2 it is clear that the malignant lesion has a much lower saturation than the normal glandular lipid-rich breast tissue. The accuracy of the model is demonstrated by the small relative residuals of the fit, i.e. within ±2% from 400 up to 900nm for both spectra. The spectral variation of the three sequential measurements at a single location is typically less than 5%, and variations in the extracted fit parameters are typically less than 10% of their values.

Due to the short photon path length (~0.48 mm) of photons contributing to the differential reflectance signal, DPS is not suitable at this stage to resolve the relatively small absorption by lipids at 928 nm and water at 980 nm, although the shape of the residuals spectra suggests some absorption artefacts due to water and fat in this wavelength region. Interestingly, the tumour location with the lowest saturation (StO_2 of 19%) showed a moderate absorption peak between 600 nm and 650 nm in addition to the blood absorption peak. The corresponding histology indicated the presence of necrosis.
A similar peak was observed in necrotic tissue in the bronchial tree.

Table 1 summarises the average values and standard deviations of 12 patients for the blood volume fraction ρ, the Mie-slope b, the blood oxygenation StO_2, the β-carotene concentration and the average blood vessel diameter D_{vessel}. Tissue types were either classified as malignant or healthy, further detailed classification was not realistic at these low numbers. The optical and physiological parameters extracted from all DPS measurements on each histological tissue type were averaged and tested on significant differences between the two groups. The differences in both the blood oxygenation StO_2 (Wilcoxon ranksum test: $p<0.003$) and blood content ρ ($p<0.02$) between malignant tissue and normal tissue were statistically significant. No significant differences were found for the β-carotene concentration, the average blood vessel diameter D_{vessel} and the scatter slope.

Table 1. Fit results. Average micro-vessel saturation (StO_2) and vessel diameter (D_{vessel}), blood content (ρ), β-carotene and scatter slope (b)

	Normal breast tisssue	Malignant breast tissue
St O_2 (%)	93 ± 7	65 ± 28§
	n=24	n= 9
D_{vessel} (µm)	18 18	26 14
	n=24	n= 9
ρ (%)	4.9 10	11 12§
	n=40	n=10
β-carotene (µm)	29 27	37 30
	n=40	n=10
b	-1.39 0.44	-1.25 0.29
	n=40	n=10

§ $p<0.05$

Discussion

Differential path-length spectroscopy was combined with large core-needle biopsy to measure optical properties in a small volume of healthy and malignant breast tissue. The results show a significant difference between malignant and healthy tissue in blood saturation and blood content. It is assumed that these phenomena are the results of tumour metabolism characterised by a high consumption of glucose resulting in a high oxygen consumption, and parasitisation of normal vasculature and angiogenesis by tumours (Vaupal *et al* 1989, 1991).

In a previous study we have intra-operatively assessed these properties in the wavelength range from 600 nm up to 1100nm using a spatially resolved continuous wave system. This system requires multiple fibers with large source-detector separations to satisfy the validity of the diffusion approximation. However, different tissue volumes are probed by different source detector fibre pairs. Due to inhomogeneities within these different sample volumes the diffusion approximation does not work adequately, leading to unstable fit and possible inaccurate results. In addition, the extracted optical properties represent average values over a relatively large tissue volume and any tissue type-specific optical properties are averaged out over the sample volume. Optical properties derived from time or frequency resolved techniques that employ a single source detector fiber geometry, represent a weighted average over various photon path trajectories. These photon trajectories, however, are wavelength dependent, and thus result in wavelength dependent sample volumes. Furthermore inhomogeneities within the sample volume cause the weights of these photon trajectories to be altered, complicating the interpretation of the measured signals in terms of optical properties.

Even when small source-detector separations are used, the average path length of the detected photons depends on the optical properties of the sample, which complicates the interpretation of the measured spectra and allows the interrogation depth to extend beyond the desired sample volume. (Bigio *et al* 2000, Zonios *et al* 1999).

Spatially resolved spectroscopy demonstrated large intra- and inter-patient variations. Such variations using DRS were confirmed by other groups (Durduran *et al* 2002, Cerussi *et al* 2002). In part, these variations can be accounted for by age, menstrual cycle and hormonal status dependence of the optical properties.

In contrast, the DPS interrogation depth is approximately 240 mm (roughly half the pathlenght), independent of the optical properties. This wavelength independence of the detected photon paths results in a straightforward interpretation of the measured signal in terms of optical properties (Amelink *et al* 2004)

In fact, theory and measurement give much better fits with the current DPS technique than in our previous study using DRS. Furthermore, the underlying motivation for this study is to find or delineate a tumour during large core needle biopsy (LCNB).
In order to find the boundary of a tumour, a sampling volume much smaller than the tumour volume is essential. However, for detection or (functional spectroscopic analysis) of tumours it may be favourable to sample over a volume of a similar size as the tumour in order to account for the heterogeneous tissue structure e.g. infiltrative growth pattern, lobular, glandular, lipid rich tissue etc.

Table 1 shows averages but also the standard deviations of the measured parameters, which are a measure of the biological variations that are encountered in breast tissue, even though formally standard deviations should not be used for non-normal distributions. We believe that these variations originate from the different tissue types present in the heterogeneous breast tissue, e.g. sclerotic, fibrotic, fat, lobular, glandular and connective tissue. In spite of this heterogeneity, tissue oxygenation and blood content are still significantly different between healthy and cancerous tissue types.

In 17 out of the 50 locations, the blood saturation StO_2 and the vessel diameter D_{vessel} could not be calculated reliably due to a low blood content in the detection volume (ρ<1%). Striking is that only 1 out of these 17 locations was a malignant location, strongly suggesting that a low blood content may indicate the presence of normal tissue.

No tumour biopsies were obtained in 6 out of the 12 patients, indicating the difficulty of manually guiding the biopsy needle to the tumour mass by palpation only. In total 23 locations (with blood content greater than 1%) were predicted by the clinical surgeon during the DPS procedure, to be cancerous, but merely 9 locations turned out to be histologically confirmed tumours. Interestingly, we found that in the other 14 locations the measured StO_2 levels were all higher than 90%. Out of the 9 confirmed tumour locations, only 2 locations exhibited saturation's over 90%. These initial results hint at the potential of DPS to discriminate between healthy and cancerous breast tissue, but this should be confirmed in a larger patient study.

A possible application of core-needle DPS may be to provide additional optical guidance during stereo-tactic LCNB procedures. LCNB alone cannot provide real-time characteristics of the tissue and the final diagnosis relies on pathological examination. Afterwards, imaging techniques and pathological examination reports will be correlated to determinate if the tissue samples were representative. DPS may serve as a supplementary tool for these procedures.

A second field of application may be in real-time optical guidance during surgery. For more than 90% of the women with breast cancer a surgical procedure is the first step in treatment. The majority of these patients have the option to choose for breast conserving therapy. During a lumpectomy it is difficult to predict tumour-free margins. Since pathological examination of the resection margins during the operation by frozen sections is time-consuming, postoperative pathological examination will give the final answer. A number of patients (15-30%) will have to undergo a re-resection if the tumour reaches the margins. Differential path-length spectroscopy may be helpful in performing lumpectomies with tumour free margins by providing real-time information on the pathological status of the tissue.

Conclusion

We have shown the feasibility of DPS combined with LCNB, to determine the local oxygenation, blood volume fraction, average blood vessel size, β-carotene concentration and scatter slope of malignant and healthy breast tissue. Our results show a significantly lower oxygenation and an increased blood content in malignant breast tissue compared to normal breast tissue. Although the data set for cancerous lesions is limited, the observed significant differences justify a prospective study using the same methodology during stereo tactic biopsy procedures in a large patient group. DPS may prove to be a supplementary tool to improve sensitivity and specificity of ultrasound, stereo-tactic or MRI guided Large Core Needle Biopsy (LCNB).

References

- Amelink A and Sterenborg HJ. Measurement of the local optical properties of turbid media by differential path-length spectroscopy. *Appl Opt.* 2004 **43**: 3048-54.
- Amelink A, Bard MP, Burgers SA and Sterenborg HJ. Single-scattering spectroscopy for the endoscopic analysis of particle size in superficial layers of turbid media. *Appl Opt.* 2003 **42**: 4095-101.
- Amelink A, Sterenborg HJ, Bard MP and Burgers SA. *In vivo* measurement of the local optical properties of tissue by use of differential path-length spectroscopy. *Opt Lett.* 2004b **29**: 1087-89.
- Bigio IJ, Bown SG, Briggs G, Kelley C, Lakhani S, Pickard D, Ripley P M, Rose I G and Saunders C. Diagnosis of breast cancer using elastic-scattering spectroscopy: preliminary clinical results. *J Biomed Opt.* 2000 **5**: 221-228.
- Cerussi AE, Jakubowski D, Shah N, Bevilacqua F, Lanning R, Berger AJ, Hsiang D, Butler J, Holcombe RF and Tromberg BJ. Spectroscopy enhances the information content of optical mammography. *J Biomed Opt.* 2002 **7**: 60-71.
- Durduran T, Choe R, Culver JP, Zubkov L, Holboke MJ, Giammarco J, Chance B and Yodh AG. Bulk optical properties of healthy female breast tissue. **Phys.Med Biol.** 2002 **47**: 2847-2861.
- Fantini S, Walker S, Franceschini MA, Kaschke M, Schlag PM and Moesta KT. Assesment of size, position and optical properties of breast tumors *in vivo* by nonivasive optical methods. *Appl Opt.* 1998 **37**: 1982-1989.
- Grosenick D, Moesta KT, Wabnitz H, Mucke J, Stroszczynski C, Macdonald R, Schlag PM and Rinneberg H. Time-domain optical mammography: initial clinical results on detection and characterization of breast tumors. *Appl Opt.* 2003 **42**: 3170-86.
- Hebden JC, Veenstra H, Dehghani H, Hillman EM, Schweiger M, Arridge SR and Delpy DT. Three-dimensional time-resolved optical tomography of a conical breast phantom. *Appl Opt.* 2001 **40**: 3278-85.
- Jiang H, Iftimia NV, Xu Y, Eggert JA, Fajardo LL and Klove KL. Near-infrared optical imaging of the breast with model-based reconstruction. *Acad Radiol.* 2002 **9**: 186-198.
- Li A, Miller EL, Kilmer ME, Brukilacchio TJ, Chaves T, Stott J, Zhang Q, Wu T, Chorlton M, Moore RH, Kopans DB and Boas DA. Tomographic optical breast imaging guided by three-dimensional mammography. *Appl Opt.* 2003 **42**: 5181-90.
- Mourant JR, Fuselier T, Boyer J, Johnson TM and Bigio IJ. Predictions and measurements of scattering and absorption over broad wavelength ranges in tissue phantoms. *Appl Opt.* 1997 **36**: 949–57.
- Nilsson AMK, Sturesson C, Liu DL and Andersson-Engels S. Changes in Spectral Shape of Tissue Optical Properties in Conjunction with Laser-Induced Thermotherapy. *Appl Opt.* 1998 **37:** 1256-67.
- Pifferi A, Taroni P, Torricelli A, Messina F, Cubeddu R and Danesini G. Four-wavelength time-resolved optical mammography in the 680-980-nm range. *Opt Lett.* 2003 **28**: 1138-1140.

- Pogue BW, Poplack SP, McBride TO, Wells WA, Osterman KS, Osterberg UL and Paulsen KD. Quantitative hemoglobin tomography with diffuse near-infrared spectroscopy: pilot results in the breast. *Radiology*. 2001 **218**: 261-66.
- Prahl S 1999 Optical Absorption of hemoglobin httt://omlc.ogi.edu/spectra/ hemoglobin
- Shah N, Cerussi A, Eker C, Espinoza J, Butler J, Fishkin J, Hornung R and Tromberg B. Noninvasive functional optical spectroscopy of human breast tissue. *Proc Natl Acad Sci.* 2001 **98**: 4420-25.
- Thomsen S and Tatman D. Physiological and pathological factors of human breast disease that can influence optical diagnosis. *Ann N Y Acad Sci.* 1998 **838**: 171-193.
- Tromberg BJ, Coquoz O, Fishkin JB, Pham T, Anderson ER, Butler J, Cahn M, Gross JD, Venugopalan V and Pham D. Non-invasive measurements of breast tissue optical properties using frequency-domain photon migration. *Philos Trans R Soc Lond B Biol Sci.* 1997 **352**: 661-668.
- Tromberg BJ, Shah N, Lanning R, Cerussi A, Espinoza J, Pham T, Svaasand L and Butler J. Non-invasive *in vivo* characterization of breast tumors using photon migration spectroscopy. *Neoplasia*. 2000 **2**: 26-40.
- van de Poll SW. Raman spectroscopy of atherosclerosis PhD thesis University of Leiden p. 2003 123 ISBN 90-9016109-0
- Vaupel PF, Kallinowski F and Okunieff P. Blood flow, oxygen and nutrient supply, and metabolic microenvironment of human tumors: a review. *Cancer Res.* 1989 **49**: 6449-65.
- Vaupel P, Schlenger K, Knoop C and Hockel M. Oxygenation of human tumors: evaluation of tissue oxygen distribution in breast cancers by computerized O_2 tension measurements. *Cancer Res.* 1991 **51**: 3316-22.
- van Veen RL, Verkruijsse W and Sterenborg HJCM. Diffuse reflectance spectroscopy from 500 to 1060 nm by correction for inhomogenously distributed absorbers. *Opt Lett.* 2002 **27**: 246-48.
- van Veen R L, Sterenborg HJ, Marinelli AW and Menke-Pluymers M. Intraoperatively assessed optical properties of malignant and healthy breast tissue used to determine the optimum wavelength of contrast for optical mammography. *J Biomed Opt.* 2004 **9**: 1129-36.
- Verkruysse W, Lucassen GW, de Boer JF, Smithies DJ, Nelson JS and van Gemert MJ. Modelling light distributions of homogeneous versus discrete absorbers in light irradiated turbid media. *Phys Med Biol.* 1997 **42**: 51-65.
- Zonios G, Perelman LT, Backman V, Manoharan R, Fitzmaurice M, van Dam J and Feld MS. Diffuse reflectance spectroscopy of human adenomatous colon polyps *in vivo*. *Appl Opt.* 1999 **38**: 6628-37.

11.

Summary and conclusions

The research presented in this thesis emanates from six separate clinical research projects investigating the *in vivo* measurement of light and the role of tissue optical properties in oncological applications of light. While the primary objectives of each of the individual projects were very diverse, the research presented here has a common thread centred on the *in vivo* measurement of light. The distribution of light within tissue is of vital importance in photodynamic therapy and is strongly dependent on the *in vivo* optical properties of tissue. Differences and variations in tissue optical properties are also of vital importance for optical diagnostics.

This thesis investigates the *in vivo* spatial and temporal variations in tissue optical properties and their importance for optical diagnostics and monitoring of therapy. We have developed dedicated light delivery and measurement devices, and performed clinical *in vivo* measurements during PDT, and during surgical and biopsy guided optical diagnostic procedures. The first sections of this thesis (chapters 2 – 5) concerns the role of intra-and inter-patient variations of tissue optical properties, their temporal behaviour, and the importance of *in vivo* light measurements in PDT. The second section (Chapters 6 – 10) describes the measurement of *in vivo* tissue optical properties and their relationship to optical diagnostics.

In **chapter two** we performed *in situ* light measurements during ALA-PDT of the Barrett's oesophagus. The approach to light delivery was to adjust the output power of the source to a value equal to the intended fluence rate multiplied by the surface area to be treated. This ignores the build up of fluence rate due to back scattering, which is dependent on the tissue optical properties.

The actual *in situ* measured fluence rates demonstrated dramatic inter-patients variations, and build-up factors of between 1.5 and 4 times higher than the intended fluence rate, were observed. In addition, significant intra-patient variations in measured fluence rate during PDT at the Barrett's surface were observed.

We conclude that inter-patient variations primarily originate from differences in optical properties. This phenomenon can be explained by the fact that in BE normal squamous epithelium often has a whitish colour whereas Barrett's columnar epithelium is more reddish-pink. Inter-patient differences in the surface ratio between normal and BE epithelium strongly influence the actual amount of therapeutic light delivered to the tissue, e.g. the less reddish BE epithelium the higher the actual fluence rate at the tissue surface. In addition, coughing and spasm of the oesophagus corresponded with large intra-patient variations in fluence rate as recorded during PDT, while smaller variations are possibly due to motion artefacts from respiration and heartbeat. The largest variation during treatment coincided with patient movement.

We postulate that the inter-patient variations in fluence (rate) could be of great consequence for the clinical outcome of PDT. Chapter 6 elaborates in detail on the consequences for ALA- and Photofrin-PDT for Barrett's oesophagus.

Chapter three reports on the development of a dedicated light delivery and measurement device for PDT in the nasopharyngeal cavity that enables an optimal and reproducible fluence rate distribution. The optical properties of tissue structures similar to those of the nasopharynx were determined on volunteers using spatially resolved diffuse reflectance spectroscopy (DRS). Tissue optical phantoms were prepared on the basis of these DRS results. The fluence rate distribution over the applicator surface in tissue optical phantoms was found to be homogeneous (SD/mean 3.8% and 18.3% respectively). However, the fluence rate distribution in five volunteers varied over the length of the applicator and was found to be less homogeneous compared to the phantom measurements (SD/mean ranging from 19% up to 52%). The maximal observed fluence rate build-up varied between subjects by a factor of 4.1 and 6.9. We concluded that these intra- and inter-subject variations originated from global and local differences in optical properties and nasopharyngeal geometry.

In **chapter four** the objective was to evaluate the performance of a dedicated light applicator for light delivery and fluence rate monitoring as described in chapter 3 during mTHPC (Foscan®) mediated photodynamic therapy of nasopharyngeal carcinomas.

We have performed 26 *in vivo* fluence rate measurements in total. Measured fluence rates varied between 70 mW cm^{-2} and 440 mW cm^{-2} at the middle of the applicator. We observed a significant systematic reduction in fluence rate during therapy in 20 out of 26 illuminations. These dynamic changes suggest a PDT-induced increase in blood content and a decrease in tissue oxygenation resulting in an increased absorption at 652 nm. Again, large intra-patient variations in fluence rate, for a given source output power of 100-mW cm^{-1}, emphasises the need for in-situ dosimetry.

For Malignant Pleural Mesothelioma (MPM)-PDT, light delivery based on *in situ* light dosimetry is essential due to the presence of vulnerable tissue structures such as the myocardium and oesophagus and the extremely complex treatment geometry.

In **chapter five** we performed *in situ* light dosimetry PDT of MPM. This facilitated the delivery of an integral and optimal light distribution over the inner thoracic surface. In spite of this approach, illumination of the sinus of the diaphragm remained difficult. For additional illumination of the sinus we developed a wedge shaped light applicator with incorporated light dosimetry. The wedge shaped applicator contains a cylindrical diffuser for light delivery and two isotropic detectors for simultaneous light dosimetry. These detectors were placed at strategic positions where the fluence rate is maximal or minimal (middle and edge).

We found that the normalised fluence rate distribution over the surface of the applicator demonstrated little change when submerged in four different optical phantoms, and enabled for a homogeneous additional illumination of the diaphragmal sinus.

Chapter six details the consequences of inter-patient variations in fluence rate build-up on the clinical response and complications following Photofrin and ALA-PDT for Barrett's oesophagus. We discuss potential reasons for non-or partial responders of ALA PDT and postulate that this is related to large variations in fluence rate amplification factors.

We also describe how the efficacy of fractionated ALA PDT is compromised by the uncontrolled variations in fluence rate amplification factor. Furthermore we conclude that the high incidence of strictures following Photofrin-PDT is directly related to the delivery of high light fluence.

In summary, *in vivo* measurement of the therapeutic light during PDT demonstrated large inter-patient variations that reflect global differences in optical properties. Comparable variations were also observed between healthy volunteers. Significant intra-patient variations in *in vivo* light measurements were demonstrated over the surface of the patient's treatment volume, which primarily results from the inhomogeneous distribution of optical properties. Furthermore these properties have shown to change during PDT.

As described above tissue optical properties are also central to the use of light for diagnostic purposes. Differences between the optical properties of normal and malignant tissue may allow tumours to be discriminated from normal tissue.

Chapter Seven describes a study on the inhomogeneous distribution of haemoglobin concentrated in discrete cylindrical vessels. Diffuse reflectance spectroscopy for measurement of absorption and scattering coefficients of biological tissue produced reliable results for wavelengths between 650 and 1050 nm. Implicitly, this approach assumes a homogeneous distribution of tissue absorbing constituents. A correction factor is introduced for inhomogeneous distribution of blood concentrated in discrete cylindrical vessels. This extended the applicability of diffusion theory to lower wavelengths. We present measurements of *in vivo* optical properties in the wavelength range from 500-1060 nm. The validity of this correction approach was confirmed by volunteer skin measurements.

We conclude that incorporation of this factor in the analysis extended the correct interpretation of the DRS measurements down to at least ~500nm, and provided correct information on the blood content and additionally information on the average vessel diameter within the sample volume.

Chapter eight details the measurement of an absorption spectrum of mammalian fat. The absorption spectra of haemoglobin and water were well defined and commonly applied in the component analysis of tissue; however, a reliable mammalian fat spectrum was previously not available. We have extracted mammalian fat from pig lard and purified it until it was an optically transparent liquid, suitable for transmission measurements. A transmission measurement method was developed that excluded all cuvette boundary reflection effects and allowed for accurate spectral information in regions of both low and high absorption coefficients. In addition, absorption and scattering properties of the pure fat in solid state were measured using time- and spatially resolved DRS. Using these three independent measurement techniques, we determined an accurate standard reference absorption spectrum of mammalian fat.

We conclude that incorporation of this fat absorption spectrum enables a more reliable and realistic tissue component analysis, and enables a better comparison between techniques and methods used in NIR spectroscopy. The spectrum is now used as a standard by many investigators (http://omlc.ogi.edu/spectra/).

Chapter nine describes the use of spatially resolved DRS to intra-operatively assess optical properties of histologically confirmed malignant and healthy breast tissue over a broad wavelength range (600 up to 1100 nm). The reproducibility of *in vivo* tissue measurements was first determined in a healthy volunteer. Three sequential measurements on the same breast location demonstrated variations of 4% for absorption and up to 2.6% for the reduced scattering. However, measurements on several locations on the same breast demonstrated dramatic spatial variations in optical properties, up to 18.6% and 27.2% for scattering and absorption, respectively. Subsequently the intrinsic optical properties of various types of tissue were measured intra-operatively, and demonstrated large intra- and inter-patient variations. We believe that these variations are mainly due to the heterogeneous nature of breast tissue. Consequently, this results in large differences in local optical properties.

The ratio between the average absorption of all patients of normal and malignant tissue as a function of wavelength revealed a peak at 650 nm, that most likely relates to a difference in tissue oxygenation between tumour and adjacent normal tissue, i.e. a decreased tumour oxygenation. However we note that variations in optical properties were in part introduced by the methodology, and by the fact that DRS measurements are highly sensitive to tissue inhomogeneities. We concluded that DRS measurements are sensitive to inhomogeneities due to the varying sampling volumes (~2mm^3 up to 2cm^3) resulting from different source detector fibre distances, and the fact that different wavelengths sample different tissue volumes.

To overcome the problems of spatially resolved DRS, a technique that measures within a very small volume (in the order of μm^3), which is much less sensitive to inhomogeneities was required. A diagnostic technique (Differential Path-length Spectroscopy, DPS) developed recently in our group, was modified for the determination of the local optical properties of breast tissue.

In **Chapter ten**, a conventional biopsy needle gun was modified in a way that biopsies could be taken from exactly the same location as where DPS measurements were performed. We demonstrate the feasibility of DPS combined with large core needle biopsy, to determine the local oxygenation, blood volume fraction, average blood vessel size, β-carotene concentration and scatter slope of malignant and healthy breast tissue. From the results we can conclude that malignant breast tissue exhibits a significantly lower oxygenation and an increased blood content compared to normal breast tissue.
The correction factor as described in chapter six was also of fundamental importance for the fit procedure of the *in vivo* DPS data for lower wavelengths.

We draw the following general conclusions from the research on *in vivo* light measurements presented in this thesis:

I. Optical properties vary between patients and in healthy subjects for similar tissue types.
II. Optical properties are distributed inhomogeneously within the treatment or diagnostic volume of interest.
III. Optical properties have shown to change during PDT.
IV. *In vivo* variations in tissue optical properties and in particular the absorption properties are primarily related to the total amount of blood and its oxygenation in region of interest.

Considering these four general conclusions with respect to their consequences for PDT and optical diagnosis, the following specific conclusions are drawn:

With respect to PDT:

- Light delivery based on a fixed source output power and surface area or volume could lead to clinically unacceptable complications and insufficient tumour response.
- Predefined light delivery planning based on the assumption that *in vivo* optical properties are static and homogeneously distributed within the treatment volume could lead to clinically unacceptable complications and insufficient tumour response.
- We postulate that performing light dosimetry during PDT basing the administered fluence (rate) on what is measured *in situ*, may significantly improve clinical response and reduce the incidence of complications.
- The concept of *in situ* based dosimetry should be taken in consideration for any specific application of PDT, especially for applications that involves cavity illuminations, e.g. bladder and the Barrett's oesophagus.

And with respect to optical diagnostics,

- Diffuse reflectance methods that employ the use of multiple wavelengths should take into account that for each of these wavelengths a different tissue volume is sampled as a result of tissue mediated differences in path length of the detected photons.
- Optical diagnostic methods that employ the use of multiple detection fibres at different source detector fibre distances should consider that for the same wavelength a different tissue volume is sampled.
- Diffuse reflectance models that assume a homogeneous distribution of optical properties used for the analysis of reflectance data harvested from a heterogeneous media, results in unstable modelling consequently, thus generating unreliable optical properties.

- The inhomogeneous distribution of haemoglobin concentrated in discrete cylindrical vessels can be corrected for. This correction is in our opinion of vital importance for the analysis of any future methods that employ diffuse reflectance data below 650nm.
- For functional optical diagnosis, the average optical properties of malignant tissue structures should dominate the average optical properties of the surrounding heterogeneous normal tissue.

In conclusion, the findings presented here should be taken into consideration when developing new optical diagnostic tools, theoretical models of light distribution, light delivery and dosimetry planning for PDT.

Samenvatting

Dit proefschrift richt zich op twee toepassingen van licht in de geneeskunde; de eerste is fotodynamische therapie (afgekort PDT, van het Engelse PhotoDynamic Therapy) en de tweede is optische diagnostiek middels diffuse reflectie spectroscopie. Voor beide toepassingen is de lichtverdeling in weefsel tijdens belichting met een lichtbron van vitaal belang. De verdeling van licht in weefsel is afhankelijk van de verstrooiende en absorberende eigenschappen van het weefsel, de zogenaamde optische eigenschappen. Het is voor fotodynamische therapie van groot belang deze eigenschappen te kennen, omdat hiermee bijvoorbeeld de indringdiepte van het therapeutische licht berekend kan worden en daarmee de te verwachten weefselschade. Ondanks veelbelovende preklinische resultaten, wordt fotodynamische therapie nog maar op beperkte schaal in de kliniek toegepast. Dit is het gevolg van de variabele resultaten en complicaties die optreden bij onjuiste toepassing van de methode. Optische diagnostiek maakt gebruikt van verschillen in optische eigenschappen tussen tumor, goedaardig en normaal weefsel om de weefseltypes te kunnen onderscheiden. Optische diagnostiek middels diffuse reflectie metingen heeft tot dusver relatief beperkte diagnostische waarde opgeleverd, waardoor ook deze toepassing van licht nog niet echt klinisch van de grond is gekomen.

De hypothese die het fundament van dit proefschrift is, is dat de onderliggende oorzaak van het beperkte klinische succes van beide optische methoden het gevolg is van het inhomogene en dynamische karakter van de optische eigenschappen weefsel *in vivo*. In dit proefschrift wordt deze hypothese getoetst middels onderzoek naar de ruimtelijke verdeling van optische eigenschappen (de zogenaamde lokale intra -patiënt variaties), verschillen tussen individuen (de zogenaamde globale inter-patiënt variaties) en het dynamische gedrag van optische eigenschappen door middel van *in vivo* licht metingen.

Het onderzoek gepresenteerd in dit proefschrift is ontsproten uit zes verschillende onderzoeks projecten over een periode van 7 jaar, waarin onderzoek werd verricht naar licht metingen *in vivo,* en de rol van optische eigenschappen in verschillende klinische toepassing van licht in de oncologie. Voor dit doel zijn specifieke licht applicatoren en meettechnieken ontwikkeld waarmee lichtmetingen zijn verricht tijdens fotodynamische therapie, chirurgie en biopsie procedures.

De eerste sectie van het proefschrift (hoofdstuk 2 –5) heeft betrekking op de invloed van intra- en inter- patiënt en dynamische variaties in optische eigenschappen op de lichtverdeling tijdens fotodynamische therapie, en de bijbehorende consequenties daarvan. Het tweede gedeelte (hoofdstuk 6 –10) beschrijft het kwantitatief meten van de *in vivo* optische eigenschappen en hun relatie tot optische diagnostiek.

In hoofdstuk twee zijn lichtmetingen verricht *in situ* tijdens fotodynamische therapie van de Barrett's slokdarm met de lichtgevoelige stof 5-ALA. De manier van lichttoediening in deze studie was gebaseerd op de klassieke aanpak waarbij een vaste lichtdosis per oppervlakte eenheid wordt aangeboden. Deze dosimetrische methode houdt geen rekening met de optische eigenschappen en hun dynamisch gedrag.

Door meervoudige diffuse reflecties aan het weefsel oppervlak, welke afhankelijk zijn van de verstrooiende en absorberende eigenschappen van het weefsel, zal de werkelijke diffuse lichtintensiteit aanzienlijk hoger zijn dan wat wordt aangeboden en bovendien sterk varieren.

De diffuse lichtintensiteit gemeten *in situ* vertoonde significante verschillen tussen individuele patiënten en lag een factor 1.5 tot 4 maal hoger dan de aangeboden lichtintensiteit. Daarnaast werden significante intra -patiënt variaties in diffuse lichtintensiteit waargenomen tijdens de behandeling.

Uit de waarnemingen konden de volgende conclusies worden getrokken: de oorzaak van deze dramatische inter patiënt verschillen zijn het resultaat van globale verschillen in optische eigenschappen. Het afwijkende barrett's epitheel is rood in vergelijking met het wittige normale plaveisel epitheel; naarmate er dus meer afwijkend barrett's epitheel in de slokdarm aanwezig is, zal deze meer absorberen en daardoor een lagere opbouw in diffuse lichtintensiteit vertonen. Dit heeft consequenties voor de hoeveelheid licht die aanwezig is voor absorptie door de lichtgevoelige stof.

Variaties binnen een patiënt gedurende therapie, i.e. intra patient variaties, correspondeerden met de door de therapie geïnduceerde spasmes en hoesten. De kleinere variaties waren het gevolg van ademhaling en hartslag.

Er wordt gepostuleerd dat deze substantiële inter-patient variaties grote consequenties kunnen hebben voor de klinische respons voor fotodynamische therapie. Hoofdstuk zes wijdt in detail uit over de gevolgen van deze variaties voor fotodynamische therapie van de Barrett's slokdarm.

Hoofdstuk drie beschrijft de ontwikkeling van een speciaal vormgegeven lichtapplicator met daarin lichtsensoren (isotrope detectoren), die zorgt voor een homogene en reproduceerbare licht distributie ten behoeve van PDT voor nasopharynx carcinomen. De licht distributie van de applicator is eerst getest in een optisch weefsel fantoom. Daarvoor zijn middels diffuse reflectie spectroscopie eerst de optische eigenschappen bepaald van weefsel structuren vergelijkbaar met die van het nasopharynx weefsel. Op basis van deze gemeten absorptie en verstrooiingscoëfficiënten werd het fantoom samengesteld. De resultaten demonstreerden een homogene lichtverdeling in lucht en in het weefsel fantoom (relatieve variaties waren 3.8% en 18.3% respectievelijk). Vervolgens is de lichtverdeling gemeten in de nasopharynx van vijf gezonde vrijwilligers. De resultaten van deze metingen vertoonden echter een beduidend minder homogene licht verdeling (relatieve variaties variërend tussen min. 19% en max. 52%, respectievelijk). De maximale opbouw in diffuse lichtintensiteit varieerde tussen vrijwilligers en was een factor 4.1 tot 6.9 hoger dan het berekende fluentie tempo in absentie van weefsel. Op grond van de gevonden resultaten kunnen we concluderen dat de geobserveerde variaties de oorzaak zijn van globale verschillen tussen de vrijwilligers, lokale variaties in optische eigenschappen en verschillen in nasopharynx geometrie.

In hoofdstuk vier wordt de in hoofdstuk drie beschreven applicator geëvalueerd tijdens fotodynamische therapy van nasopharynx carcinomen met de licht gevoelige stof mTHPC (Foscan®). In totaal zijn 26 lichtmetingen verricht *in vivo*. De diffuse lichtintensiteit aan het oppervlak van de applicator werd voor de behandeling ingesteld op een vaste waarde van ~100 mW cm^{-2}. De werkelijk gemeten diffuse lichtintensiteiten varieerden tussen 70 mW cm^{-2} and 440 mW cm^{-2} in het midden van de applicator. In 20 van de 26 metingen werd een significante daling van de diffuse lichtintensiteit waargenomen. Deze dynamische verandering suggereren een door de fotodynamische therapie veroorzaakte stijging in hoeveelheid bloed of een daling in de weefsel zuurstof saturatie van het bloed of een combinatie van beiden. Dit resulteert in een stijging van lichtabsorptie rond 652 nm en heeft als gevolg een lagere opbouw in diffuse lichtintensiteit. De grote variaties in gemeten lichtintensiteiten tussen patiënten en de waargenomen dynamische variaties gedurende de therapie bij een standaard laser bronvermogen benadrukken wederom het belang van *in vivo* licht dosimetrie voor fotodynamische therapie.

Voor fotodynamische therapie van asbest longkanker (kwaadaardig longslijmvlies tumoren, ook wel maligne pleuraal mesothelioma MPM genoemd) met de lichtgevoelige stof Foscan® is het van essentieel belang om de licht dosering te baseren op de diffuse lichtintensiteit en de diffuse licht dosis gemeten *in vivo*. Dit vanwege de vele gevoelige weefselstructuren zoals het hart en de slokdarm in de omgeving van het te behandelen gebied..

Hoofdstuk vijf beschrijft een studie naar *in vivo* licht dosimetrie tijdens fotodynamische therapie voor MPM. Tijdens deze procedure wordt eerst de long verwijderd waarna er een maximale chirurgische tumorresectie plaats vindt, welke gevolgd wordt door een adjuvante PDT sessie. Ondanks de optimale integrale belichting middels een sferische diffuser, welke op basis van de gemeten diffuse lichtintensiteit met vier isotrope detectoren in de thoraxholte wordt gepositioneerd, blijft het belichten van het diafragma-sinus moeilijk. Een wigvormige licht applicator met daarin isotrope detectoren is daarom ontwikkeld om een additionele lichtdosis af te leveren in de sinus.
De lichtapplicator bestaat uit een siliconen wig met daarin een cilindrische diffuser en twee isotrope detectoren op strategische locaties, namelijk in het midden (waar de lichtintensiteit het hoogst is) en aan het einde (waar deze het laagst is) van de applicator. De applicator is eerst getest in optische weefsel fantomen met verschillende optische eigenschappen om de diffuse lichtverdeling van de applicator te bepalen. Daarna is de applicator toegepast tijdens MPM-PDT. De genormaliseerde lichtverdeling over het oppervlak van de applicator demonstreerde weinig verschil tussen de verschillende fantomen. Tevens bleek de applicator tijdens PDT in staat te zijn een homogene additionele licht dosis af te leveren in het diafragma sinus.

Hoofdstuk zes behandelt in detail de gevolgen van de in hoofdstuk 2 gemeten inter-patiënt variaties in diffuse lichtopbouw voor PDT van de Barrett's slokdarm met betrekking tot de klinische respons en complicaties. We bespreken in dit hoofdstuk de potentiële oorzaken voor de absentie of gedeeltelijke respons van 5-ALA Barrett's PDT, en

poneren dat de gebrekkige klinische respons het gevolg is van de variaties in werkelijk afgeleverde diffuse lichtintensiteit en lichtdosis. Verder beschrijven we waarom de effectiviteit van gefractioneerde PDT met ALA gecompromitteerd wordt door de waargenomen variaties in de diffuse lichtintensiteit. Bij PDT met de potentere lichtgevoelige stof Photofrin komen complicaties zoals vernauwingen (stricturen) van de slokdarm ten gevolge van de therapie met grote regelmaat voor. We concluderen dat deze PDT-specifieke complicatie het directe gevolg is van een te hoge lichtintensiteit.

Samengevat: Het therapeutisch licht *in vivo* gemeten gedurende PDT demonstreerde substantiële variaties tussen patiënten bij een gelijkblijvend vermogen van de lichtbron. Deze variaties reflecteren de globale verschillen in optische eigenschappen tussen patiënten. Vergelijkbare verschillen werden waargenomen in gezonde vrijwilligers. Naast de inter-patiënt variaties, zijn ook significante lokale verschillen aan het oppervlak van het te behandelen oppervlak binnen een individu geobserveerd, de zogenaamde intra-patient variaties. De laatstgenoemde variaties zijn het resultaat van de inhomogene verdeling van optische eigenschappen en van de geometrie. De laatste belangrijke conclusie is dat de optische eigenschappen kunnen veranderen ten gevolge van de PDT.

Zoals eerder genoemd spelen weefsel optische eigenschappen ook een belangrijke rol in optische diagnostiek. Verschillen in optische eigenschappen kunnen worden gebruikt om tumor van normaal weefsel te onderscheiden.

Hoofdstuk zeven beschrijft een studie naar de invloed van de inhomogene distributie van hemoglobine (bloed) in cilindrische vaten op diffuse reflectie spectroscopty (DRS). De DRS methode wordt gebruikt om de absorptie- en verstrooiingscoëfficiënten te bepalen van weefsel, en levert betrouwbare resultaten op voor golflengtes tussen de 650 en 1050 nm. Het theoretische diffusiemodel waarmee de diffuse reflectie metingen wordt beschreven, heeft als aanname dat de absorptie homogeen verdeeld moet zijn.
Bloed absorbeert echter sterk beneden 650 nm en is ingesloten in discrete vaten. Hierdoor is de absorptie in weefsel dus niet homogeen verdeeld. Een correctie factor voor de inhomogene verdeling van bloed wordt geïntroduceerd en meegenomen in het diffusiemodel. Hiermee wordt het mogelijk de optische eigenschappen te bepalen tot 500nm. De betrouwbaarheid van de correctie methode werd gevalideerd en bevestigd op huid metingen van vrijwilligers. We concluderen dan ook dat het includeren van dit correctiemodel in de DRS analyse, de mogelijkheid bied om DRS data correct te interpreteren tot ~500nm in plaats van 650 nm. Tevens genereert het correctiemodel informatie over de exacte hoeveelheid bloed en extra informatie over de gemiddelde vaatdiameter binnen het gemeten volume.

Hoofdstuk acht beschrijft in detail de meting van het absorptiespectrum van dierlijk vet. Voor de component analyse van weefsel absorptie spectra worden de standaard en goed gedefinieerde absorptie spectra van bloed (100% zuurstof saturatie en volledige ge-desatureerd hemoglobine) en water gebruikt. Een betrouwbaar en goed gedefinieerd spectrum van humaan vet echter is hiervoor niet beschikbaar. Om dit spectrum te benaderen is puur dierlijk vet onttrokken uit varkens spek en gepurificeerd totdat het een

optisch transparante vloeistof werd waarmee klassieke transmissiemetingen mogelijk waren. Een transmissiemeetmethode is ontwikkeld die alle reflecties aan het oppervlak van het cuvet uitsluit, en het tevens mogelijk maakt om nauwkeurige spectrale metingen te verrichten in gebieden waar de absorptie hoog en laag is. Bij kamertemperatuur is het vet een solide, diffuus verstrooiende, niet transparante substantie. Er zijn daarom naast de transmissie metingen, twee diffuse reflectie methoden gebruikt om het absorptiespectrum van vet in vaste toestand te bepalen, namelijk ruimtelijke- en tijdsopgeloste diffuse reflectie spectroscopie. Met deze drie onafhankelijke methoden is een nauwkeurig referentie spectrum van dierlijk vet bepaald. Met dit spectrum is een betrouwbare componenten analyse van weefsel absorptie spectra mogelijk; tevens zorgt het gebruik van standaard referentie spectra voor een betere vergelijking tussen weefsel spectroscopische technieken en methodes. Het spectrum wordt nu als standaard referentie gebruikt door vele onderzoekers, en is beschikbaar op de database op de website van het Oregon Medical Laser Center (http://omlc.ogi.edu/spectra/).

Hoofdstuk negen beschrijft het gebruik van ruimtelijk opgeloste diffuse reflectie spectroscopie om tijdens chirurgie (intraoperatief) de optische eigenschappen van normaal borstweefsel en van borsttumoren te bepalen. Kennis omtrent deze eigenschappen is van essentieel belang voor o.a. optische mammografie. Metingen werden verricht in het golflengte gebied van 600 tot 1100 nm. Eerst is de reproduceerbaarheid van de methoden bepaald middels metingen op de borsthuid van een vrijwilligster. Drie opeenvolgende metingen op dezelfde borstlocatie resulteerde in een absorptie variatie van 4% en een 2.6% variatie in verstrooiing. Echter, metingen op verschillende locaties op dezelfde borst resulteerde in significante variaties in absorptie en verstrooiing tussen de locaties (18.6% and 27.2% voor respectievelijk verstrooiing en absorptie). Vervolgens zijn de intrinsieke optische eigenschappen bepaald van verschillende weefseltypen gedurende chirurgie, welke significante variaties in optische eigenschappen lieten zien. We suggereren dat deze variaties voornamelijk het gevolg zijn van heterogeniteiten in het weefsel, dwz de inhomogene verdeling van bloedvaten, klieren en vet. Dit resulteert in grote lokale variaties in optische eigenschappen. De ratio tussen gemiddelde absorptie van alle normaal en tumor weefsel spectra, liet een maximaal contrast zien rond de 650 nm. Het is zeer aannemelijk dat deze piek in contrast het directe gevolg is van verschillen in bloed zuurstofsaturatie tussen tumor en normaal borstweefsel. Rond 650 nm is het verschil in absorptie tussen zuurstofrijk en zuurstofarm bloed maximaal. Door het verhoogde metabolisme van de tumor zal door een verhoogd zuurstof gebruik de saturatie lager zijn.

De geobserveerde grote variaties in optische eigenschappen zijn echter niet alleen het gevolg van heterogeniteiten in het weefsel, maar zijn mede het gevolg van de DRS methodiek. Het theoretische DRS model is geldig mits er aan een paar aannames wordt voldaan; een ervan is dat het weefsel homogeen moet zijn. We concluderen dan ook dat DRS metingen zeer gevoelig zijn voor inhomogeniteiten, met als gevolg instabiele analyses. Het meetvolume verschilt voor iedere bron- detectie-fiberafstand (~2mm^3 tot 2cm^3), dwz een kleine afstand heeft weer een kleiner meetvolume.

Tevens is de locatie van het meetvolume weer afhankelijk van de golflengte, en is dus verschilend per golflengte voor een en dezelfde bron-detectie fiberafstand.

De bovengenoemde problemen van ruimtelijk oploste DRS compromitteert de validiteit van de methode. Het was daarom van belang om een techniek te gebruiken die in staat is de optische eigenschappen te bepalen over een heel klein meetvolume (orde van grote ~mm^3), en daardoor minder gevoelig is voor inhomogeniteiten. De recentelijk ontwikkelde techniek differentiële padlengte spectroscopie (DPS) is zo een techniek. De DPS methode is voor dit onderzoek gemodificeerd om de intrinsieke optische eigenschappen van borstweefsel te bepalen.

In hoofdstuk tien is een conventionele borst-biopteur aangepast zo dat DPS metingen konden worden verricht op exact dezelfde locatie als een weefsel monster (biopt) werd genomen. In deze studie zijn *in vivo* DPS metingen verricht en biopten genomen in normaal borstweefsel en in en rondom borsttumoren. Het is met deze techniek mogelijk gebleken om heel lokaal informatie te krijgen over de lokale bloed zuurstofsaturatie, de hoeveel bloed in het meetvolume, de gemiddelde vaatdiameter, de concentratie β-carotene, en informatie over de verstrooiing, voor zowel tumor als normaal weefsel.

Uit de resultaten kunnen we concluderen dat tumorweefsel een gemiddeld significant lagere bloed zuurstofsaturatie kent, en een verhoogd bloed volume in vergelijking met normaal borstweefsel. Het in hoofdstuk zes beschreven correctie model was tevens van fundamenteel belang voor de correcte analysevan DPS data bij de lagere golflengten.

Uit de resultaten van de in hoofdstuk 2 t/m 10 beschreven onderzoeken, worden de volgende algemene conclusies getrokken:

I. Optische eigenschappen variëren tussen patiënten en gezonde vrijwilligers voor vergelijkbare weefsel typen.
II. Optische eigenschappen zijn inhomogeen verdeeld binnen het klinisch relevante behandel of diagnostische weefsel volume.
III. Optische eigenschappen kunnen veranderen gedurende fotodynamische therapie.
IV. Variaties in optische eigenschappen en in het bijzonder de absorptie zijn primair gerelateerd aan de hoeveelheid bloed en saturatie in het behandel of diagnostisch volume.

Deze vier algemene conclusies in ogenschouw nemende, voor wat betreft de consequenties voor fotodynamische therapie en optische diagnostiek middel diffuse reflectie metingen, worden de volgende specifieke conclusies worden getrokken.

Met betrekking tot fotodynamische therapie:

- Licht dosimetrie op basis van een vast lichtbron vermogen en het te behandelen weefsel oppervlak/volume, kan leiden tot een inefficiënte tumor respons en ongewenste complicaties.
- Licht dosis planning op basis van de aanname dat de optische eigenschappen in het behandelvolume homogeen gedistribueerd, en gedurende therapie statisch zijn, kan leiden tot een inefficiënte tumor respons en klinisch onacceptabele complicaties.
- We postuleren dat lichtdosering op basis van de werkelijk *in situ* gemeten fluentie (tempo), kan leiden tot een significante verbetering in tumor respons en een drastische vermindering in complicaties.
- Het concept van *in situ* licht dosering op basis van de werkelijk gemeten fluentie, moet overwogen worden voor iedere PDT applicatie, en met name toepassing waarbij het behandelvolume zich in een holle ruimte bevindt, zoals de Barrett's slokdarm en de blaas.

Met betrekking tot optische diagnostiek:

- Diffuse reflectie methoden die gebruikt maken van meerdere golflengten moeten rekening houden met het feit dat voor iedere golflengte het detectievolume verschillend is, tengevolge van de weefseloptische eigenschappen waardoor voor iedere golflengte de padlengte van de gedetecteerde fotonen anders is.
- Diffuse reflectie methoden die gebruikt maken van meerdere bron detectie fiber afstanden, moeten rekening houden met het feit dat voor iedere afstand het detectievolume voor dezelfde golflengte verschillend is.
- Diffuse reflectie modellen, met als aanname een homogene distributie in optische eigenschappen, die gebruikt worden voor de analyse van data onttrokken uit een heterogeen medium, resulteren in een instabiele modellering en bijgevolg onbetrouwbare optische eigenschappen.
- Voor de inhomogene distributie van bloed in discrete cylindrische vaten, en daardoor de inhomogene distributie absorptie, kan worden gecorrigeerd. De in dit proefschrift beschreven correctieanalyse is van vitaal belang voor iedere optisch diagnostische toepassing die gebruikt maakt van diffuse reflectie onder de 650nm.

Curriculum vitae

Robert L.P. van Veen werd geboren op 7 april 1971 te Leidschendam in Zuid-Holland. Zijn techniek georiënteerde studietraject begon met het doorlopen van de LTS Elektrotechniek, de MTS Energie Techniek, en Technische Computerkunde en eindigde op de Technische Hogeschool in Rijswijk waar hij Technische Natuurkunde studeerde en in 1997 afstudeerde in specialisatierichting Fotonica. Stages werden o.a. gelopen op de Vrije Universiteit bij de vakgroep fysische chemie. Na zijn studie is hij gaan werken in de Daniel den Hoed kliniek in Rotterdam op de afdeling klinische fysica bij de subdivisie Fotodynamische Therapie onderleiding van Dr. W. Star. De werkzaamheden vonden plaats binnen het NKB project Photodynamic therapy for malignant mesothelioma, waarin o.a. onderzoek werd gedaan naar de optimalisatie van *in vivo* licht dosimetrie. Dr. ir. H.J.C.M. Sterenborg werd in 1998 de nieuwe projectleider van deze groep. Parallel aan het dosimetrisch onderzoek, werd vervolgens onderzoek verricht naar methoden voor het meten van optische weefsel eigenschappen binnen het kader van drie EU projecten LAIC, OPTIMAMM en MEDPHOT. Vanaf 2004 tot op heden verrichtte de auteur onderzoek naar de dosimetrie voor fotodynamische therapie voor nasopharynx carcinomen op een STW project.

De uit de bovengenoemde projecten ontsproten wetenschappelijke publicaties vormde de basis van dit proefschrift met als titel "*In vivo* optical measurements for diagnostics and monitoring of treatment" welke op 7 juni 2006 verdedigd zal worden aan de Erasmus Universiteit te Rotterdam ter verkrijging van de graad van doctor.

Scientific output.

First author:

1. R.L.P. van Veen, M.C. Aalders, K.L. Pasma, P.D. Siersema, J. Haringsma, W. van De Vrie, E.E. Gabeler, D.J. Robinson and H.J.C.M. Sterenborg. In situ light dosimetry during photodynamic therapy of Barrett's esophagus with 5-aminolevulinic acid. *Lasers Surg Med.* 2002: **31(5):** 299-304.
2. R.L.P. van Veen, J.H. Schouwink, W.M. Star, H.J. Sterenborg, J.R. van der Sijp, F.A. Stewart and P. Baas. Wedge-shaped applicator for additional light delivery and dosimetry in the diaphragmal sinus during photodynamic therapy for malignant pleural mesothelioma. *Phys Med Biol.* 2001: **46**(7): 1873-1883.
3. R.L.P. van Veen, W. Verkruijsse and H.J.C.M. Sterenborg. Diffuse reflectance spectroscopy from 500 to 1060 nm by correction for inhomogenously distributed absorbers. *Opt Lett.* 2002: (**27**): 246-248.
4. R.L.P. van Veen, H.J.C.M. Sterenborg, A. Pifferi, A. Torricelli, E.Chikoidze and R. Cubeddu. Determination of VIS- NIR absorption coefficients of mammalian fat, with time- and spatially resolved diffuse reflectance and transmission spectroscopy. *J Biomed Opt.* 2005: (**10**): 054004.
5. R.L.P. van Veen, H.J.C.M. Sterenborg, A.W.K.S. Marinelli and M. Menke-Pluymers. Intra-operatively assessed optical properties of malignant and healthy breast tissue, to determine the optimum wavelength of contrast for optical mammography. *J Biomed Opt.* 2004: (**6**): 1129-1136.
6. R.L.P. van Veen, A. Amelink, M. Menke-Pluymers, C. van der Pol and H.J.C.M. Sterenborg. In-vivo optical biopsy measurement of local optical properties of healthy and malignant breast tissue. *Phys Med Biol.* 2005: **7;50(11)**: 2573-2581.
7. R.L.P van Veen, H. Nyst, S. Rai Indrasari, M. Adham Yudharto, D.J. Robinson, I.B. Tan, C. Meewis, R. Peters, S. Spaniol, F.A. Stewart, P.C. Levendag and H.J.C.M. Sterenborg. In-vivo fluence rate measurements during Foscan® mediated Photodynamic Therapy of persistent and recurrent Nasopharyngeal Carcinomas using a dedicated light applicator (accepted for publication in *J Biomed Opt*)
8. R.L.P. van Veen, D.J. Robinson, P.D. Siersema and H.J.C.M. Sterenborg. The importance of dosimetry during photodynamic therapy (submitted as a letter to *Gastrointestinal Endoscopy.*)

Co author papers:

1. H.J.van Staveren, R.L.P. van Veen, O.C. Speelman, M.J. Witjes, W.M. Star and J.L. Roodenburg. Classification of clinical autofluorescence spectra of oral leukoplakia using an artificial neural network: a pilot study. *Oral Oncol.* 2000: **36(3)**: 286-293.

2. M Hage, P D Siersema, H van Dekken, E W Steyerberg, J Haringsma, W van de Vrie, T E Grool, R L P van Veen, H J C M Sterenborg, and E J Kuipers. 5-Aminolevulinic acid photodynamic therapy versus argon plasma coagulation for ablation of Barrett's oesophagus: a randomised trial. *Gut.* 2004: **53(6)**: 785-790.

3. H. Schouwink, E.T. Rutgers, J. van der Sijp, H. Oppelaar, N. van Zandwijk, R.L.P. van Veen, S. Burger, F.A. Stewart, F. Zoetmulder, and P. Baas. Intraoperative. Photodynamic Therapy after Pleuropneumonectomy in Patients With Malignant Pleural Mesothelioma - Dose Finding and Toxicity Results, *Chest*. 2001: **20(4)**: 1167-1174.

4. H. Schouwink, M. Ruevekamp, H. Oppelaar, R.L.P. van Veen, P. Baas, and F.A. Stewart. Photodynamic therapy for malignant mesothelioma: preclinical studies for optimization of treatment protocols. *Photochem Photobiol.* 2001: **3(4)**: 410-7.

5. A. Pifferi, A. Torricelli, A. Bassi, P. Taroni, R. Cubeddu, H. Wabnitz, D. Grosenick, M. Möller, R. Macdonald, J. Swartling, T. Svensson, S. Andersson-Engels, R.L.P. van Veen, H.J.C.M. Sterenborg, M. Whelan and H. Stamm. Performance assessment of photon migration instruments: the MedPhot protocol, *Appl Opt.* 2005: **10;44(11)**: 2104-14.

6. H. Nyst, R.L.P. van Veen, I,B. Tan, R. Peters, P.C. Levendag, H.J.C.M. Sterenborg and F.A. Stewart. Development of a dedicated light delivery and dosimetry device for photodynamic therapy of nasopharyngeal carcinomas: Phantoms and volunteers.(Submitted to *Lasers Surg. Med*)

Procedings:

1. R.L.P. van Veen and H.J.C.M. Sterenborg. Correction for in-homogeneously distributed absorbers in spatially resolved diffuse reflectance spectroscopy, *Proc. SPIE* 4431 192-194

2. R.L.P. van Veen, H. J. C. M. Sterenborg, A. Pifferi, A. Torricelli and R. Cubeddu, ''Determination of VIS- NIR absorption coefficients of mammalian fat, with time- and spatially resolved diffuse reflectance and transmission spectroscopy," in Biomedical Topical Meetings on CD-ROM, Paper SF5, Optical Society of America, Washington, DC 2004.

3. A. Pifferi, A. Torricelli, A. Bassi, P. Taroni, R. Cubeddu, H. Wabnitz, D. Grosenick, M. Möller, R. Macdonald, J. Swartling, T. Svensson, S. Andersson-Engels, R.L.P. van Veen, H.J.C.M. Sterenborg, M. Whelan and H. Stamm. Performance assessment of photon migration instruments: the MedPhot protocol, accepted for publication in Applied Optics. in Biomedical Topical Meetings on CD-ROM, Optical Society of America, Washington, DC 2004.

International Presentations:

1. R.L.P. van Veen and H.J.C.M. Sterenborg, A. Pifferi, A. Torricelli and R. Cubeddu, Determination of VIS- NIR absorption coefficients of mammalian fat, with time- and spatially resolved diffuse reflectance and transmission spectroscopy. Biomedical OpticsTopical Meetings, April 14-17, 2004, Miami Beach, Florida, USA.

2. R.L.P. van Veen, H.J.C.M. Sterenborg and A.W.K.S. Marinelli, In-vivo optical properties of breast tissue from 600 to 1100 nm using spatially resolved diffuse remittance spectroscopy. EFOMP European Congress on Medical Physics, Eindhoven, The Netherlands, 2003

3. R.L.P. van Veen and H.J.C.M. Sterenborg, Correction for inhomogeneously distributed absorbers in spatially resolved diffuse reflectance spectroscopy. European Conference on Biomedical Optics 2001, Munich, Germany, 2001.

4. R.L.P. Van Veen, M.C. Aalders, K.P. Pasma, P.D. Siersema PD, J. Haringsma, W. van de Vrie, E.E. Gabeler, D.J. Robinson and H.J. Sterenborg. In situ light dosimetry during photodynamic therapy of Barrett's esophagus with 5-aminolevulinic acid. 9th United European gastroenterology week, Amsterdam, 2001

4. R.L.P. van Veen, H. Nyst, S. Rai Indrasari, M. Adham Yudharto, D.J. Robinson, I.B. Tan, C. Meewis, R. Peters, S. Spaniol, P.C. Levendag and H.J.C.M. Sterenborg. Photodynamic therapy for recurrent cancer in the nasopharynx; development of a light application device and first clinical results, International Photodynamic Association (IPA) Munic Jun. 2005

5. R.L.P. van Veen on behalf of H. J. Nyst, S. Rai Indrasari, B. Hariwiyanto, M. Adham Yudharto, A. J. M. Balm, F. Stewart, R. Peters, S. Spaniol, J.M. Middeldorp, D.J. Robison, H.J.C.M. Sterenborg, P. C. Levendag and I.B. Tan. A Phase I/II Clinical Study: Foscan® mediated Photodynamic Therapy in patients with recurrent or persistent Nasopharyngeal Carcinoma, International Photodynamic Association (IPA) Munic. Jun. 2005

6. R.L.P. van Veen on behalf of R. Doornbos, M.C. Aalders, H.J.C.M Sterenborg. Spatially resolved diffuse reflectance spectroscopy *in vivo*. Fifth International Conference on Optics Within Life Sciences OWLS V, Crete, Oct. 1998

Dankwoord

Dit proefschrift is mede tot stand gekomen dankzij de wetenschappelijke adviezen, bijdragen, en steun van vele collega's, vrienden en familie. Vrienden en familie wil ik met name bedanken voor hun jarenlange steun, die absoluut noodzakelijk is gebleken om dit proefschrift te kunnen schrijven.

Voor wat betreft de persoonlijke dankwoorden beperk ik mij tot mijn directe collegae en vakbroeders.

Om te beginnen Dr. W.M. Star, beste Willem, mede dankzij jou is dit proefschrift tot stand gekomen, je leerde mij de basisvoorwaarden voor het verrichten van goed gefundeerd onderzoek. Het presenteren ervan in de vorm van artikelen bleek echter voor mij toch wat lastiger. Het eerste dosimetrie artikel was dan ook niet zonder jouw hulp tot stand gekomen.

Mijn copromotor Dr.ir. H.J.C.M. Sterenborg. Dick, van meet af aan had je een blindelings vertrouwen in mij, en stuurde mij zonder zorgen de hele wereld over. Jouw bijdrage is enorm geweest, je gaf me alle vrijheid en steun en leerde mij hoe je wetenschappelijk artikelen moest dichttimmeren en het koren van het kaf te scheiden. Ondanks dat ik je soms tot wanhoop dreef met mijn concept manuscripten met daarin typisch "vanveeniaanse" dwalingen, en geneuzel over details, slaagde je er steeds in, mij de rode draad te doen vinden. Dick, ik heb genoten van onze gesprekken over politiek, kunst en alles op persoonlijk vlak onder het genot van een biertje. Verder wens ik je veel succes toe.

Mijn collega's Ing. Riëtte de Bruijn en Ing. Angelique van der Ploeg van den Heuvel, ontzettend bedankt voor heel wat leuke jaren, steun en hulp in het lab. Mijn bewondering voor jullie professionaliteit is enorm. Riëtte, ik verwacht natuurlijk van jouw hand nog een dijk van een proefschrift.

Ing. Bastiaan Kruijt, beste Bastiaan, nogmaals ontzettend bedankt voor jouw briljante Labview dosimetrie programma en hulp. Ik wens je veel succes met je verdere onderzoek.

Dr. A. Amelink, Arjen dude, DPS is in ieder geval een onderdeel van mijn future geworden. Bedankt voor de vele waardevolle wetenschappelijke discussies, en je bijdrage in de totstandkoming van dit proefschrift.

Drs.Ing. O. Kaspers, beste Olaf, ik wil je bij deze veel succes toewensen met het afronden van je promotie onderzoek.

Dr. D.J. Robinson, Dear Dom, I would like to thank you for your significant scientific contribution in all manuscripts on PDT, and fruitful discussions on *in vivo* light dosimetry. Thank you for pulling me through these last difficult and busy months.

Dr. D. de Veld, Lieve Diana, ondanks al ons geruzie over TL verlichting…
Dr. D. mijn dank is groot, het was heerlijk om met jou, humor en verdriet in ons Daniel kantoor te mogen delen.

En tevens gaat mijn dank uit naar mijn kersverse collegae van het CDOT, Gerwin, Tom, Kees, Senada, Bas, Maarten, Diana en Peter.

Mijn promotor Prof. Dr. P.C. Levendag, Beste Peter, bedankt voor het mogelijk maken van deze promotie. Onze contacten waren kort maar krachtig.

Een stelling van Jeroen Rovers (bedankt voor een geweldige twee weken in het Royal London Hospital) luidt “Het gat tussen de kliniek en de prekliniek, is te dichten door erin te springen”
Bij deze wil ik enkele personen in het bijzonder bedanken die samen met mij deze sprong hebben gemaakt. Dr. M. Menke-Pluymers, beste Marian, ontzettend bedankt voor je enthousiasme en toewijding voor wat betreft de optische borstmetingen. Met veel plezier heb ik met jou aan deze studies mogen werken. Dr. P. Siersema en Dr. J. Haringsma, Peter, Jelle, het was altijd zeer plezierig om met jullie te werken aan de Barrett’s PDT studie. Mijn dank voor jullie contributie is groot.

Verder wil ik alle mensen verantwoordelijk voor de technische ondersteuning (MI, MEA, EMI) achter deze studies bedanken. Rob Peters, ondanks je grote werk druk, ontzettend bedankt voor het meedenken en ontwikkelen van de nasopharynx applicator, en de diafragmawig. Bob Visser van MEA en Edward Donkersloot van MI, heren ontzettend bedankt voor de instrumentele ondersteuning. Verder gaat mijn dank natuurlijk uit naar alle coauteurs voor hun bijdrage in de artikelen.

Buiten het Erasmus MC, is een groot gedeelte van het onderzoek verricht in het Antoni van Leeuwenhoek ziekenhuis, het AMC lasercentrum en de Polytechnico di Milano.

I would like to thank Prof.dr. R Cubeddu. Dr. A. Pifferi, Dr. A. Torricelli, and Dr. P. Taroni of the dipartimento di fisica of the Politechnico di Milano for their hospitality, kindness and collaboration during my research visits. I wish I had known about strutto.

Dr. P. Baas en Dr. F. Stewart, Beste Fiona en Paul ook zonder jullie was dit proefschrift nooit geschreven. Bedankt voor alle wetenschappelijke adviezen, prettige samenwerking, en wetenschappelijke contributie aan dit werk.

Dr I. Tan. Beste Bing, ik wil je ontzettend bedanken voor je wetenschappelijke bijdrage, maar zeker ook voor een geweldige tijd in Indonesië en op de OK in het AvL.
Mijn bewondering voor jouw onuitputtelijke inzet voor de PDT in het hoofd hals gebied, is zeer groot. Terima kasih pak Bing.

Dr. H. Nyst, beste Heike, ik kan niets anders zeggen dan dat samenwerken met jou in Indonesië en hier echt geweldig was. Jouw professionaliteit en doorzettingsvermogen in R.S. Dr. Sardjito deed mij regelmatig versteld staan. Ondanks alle stress, spanning, onbegrip en hitte in Yogja was het een bijzondere en heel leuke tijd. Veel succes met je proefschrift.

Verder bedank ik natuurlijk alle mensen van het AMC laser centrum. Beste Martin, Ton en Johan, ik heb het altijd geweldig gevonden om in het Lasercentrum mijn DRS onderzoek te kunnen doen, en me daarbij zeer gastvrij gevoeld. Joy bedankt voor je goede zorgen.

Dr.ing. M. Aalders, Maurice, er verschijnt nu mede dankzij jou een hele grote grijns op mijn gezicht.